2018

A model to predict concentrations and uncertainty for mercury species in lakes

Ashley Hendricks
Michigan Technological University, ashleyh@mtu.edu

A MODEL TO PREDICT CONCENTRATIONS AND UNCERTAINTY FOR MERCURY SPECIES IN LAKES

By

Ashley N. Hendricks

A THESIS

Submitted in partial fulfillment of the requirements for the degree of

MASTER OF SCIENCE

In Environmental Engineering

MICHIGAN TECHNOLOGICAL UNIVERSITY

2018

This thesis has been approved in partial fulfillment of the requirements for the Degree of MASTER OF SCIENCE in Environmental Engineering.

Department of Civil and Environmental Engineering

Thesis Advisor:	*Dr. Noel R. Urban*
Committee Member:	*Dr. Min Wang*
Committee Member:	*Dr. Cory P. McDonald*
Department Chair:	*Dr. Audra Morse*

Table of Contents

List of Figures v

List of Tables vii

Preface viii

Acknowledgements ix

Abstract x

1 Introduction 1

1.1 Mercury as a Problem 1

1.2 Introduction to Modeling Mercury 5

1.3 Mercury Cycling in Lakes 7

1.4 Approach for Model Validation 9

1.4.1 Motivation for Validation 9

1.4.2 Current State of Practice for Model Validation of Mercury Models 10

1.4.3 Bayesian Approach for Uncertainty Analysis of Models 10

1.5 Objectives 12

2 Methods 13

2.1 Coupling of a mercury model with a water quality model 13

2.2 Study Location 14

2.3 Seasonality and Water Quality Model 16

2.3.1 Water Balance 16

2.3.2 Heat Budget 17

2.3.3 Light Attenuation 19

2.3.4 Dissolved Organic Carbon Mass Balance 21

2.3.5 Chlorophyll Mass Balance 22

2.3.6 Corrections for Ice Cover 23

2.3.7 Thermocline Dispersion 23

2.4 Mercury Model 24

2.4.1 Lake Mass Balance 24

2.4.2 Air-Water Exchange 30

2.4.3 Deposition 32

2.4.4 Runoff Coefficients 32

2.4.5 Partitioning 33

2.5 Predictions for mercury concentrations in fish 34

2.6 Validation Methods 35
2.6.1 Calibration 35
2.6.2 Sensitivity Analysis 35
2.6.3 Uncertainty Analysis 36

3 Results 39

3.1 Water Quality Model Results 39
3.1.1 Water Balance 39
3.1.2 Heat Budget 40
3.1.3 DOC Mass Balance 42
3.1.4 Chlorophyll-a Mass Balance 43

3.2 Mercury Model Results 44
3.2.1 Lake Mercury Model Results 44
3.2.2 Predictions of Mercury in Fish 49

3.3 Sensitivity Analysis Results 50

3.4 Uncertainty Analysis Results 52

4 Discussion and Conclusions 56

4.1 Mercury Cycling in Torch Lake 56
4.1.1 In-Lake Cycling of Mercury in Torch Lake 56
4.1.2 Atmospheric and Watershed Loading to Torch Lake 60
4.1.3 Mining impacts on mercury cycling in Torch Lake 62

4.2 Seasonality of Mercury Cycling 63
4.2.1 Motives for Inclusion of Seasonality in the Model 63
4.2.2 Seasonal Parameterization in the Model 63
4.2.3 Seasonality Observed in Torch Lake's Mercury Cycle 65
4.2.4 Disadvantages of Including Seasonality 69
4.2.5 Recommendations for Improving Seasonality in the Model 70

4.3 Approaches for Model Validation 70

4.4 Future Work 71

5 Reference List 73

6 Appendix 92

List of Figures

Figure 1.1. Diagram of the global mercury cycle. 1

Figure 1.2. Map contrasting the land cover type for the Upper Peninsula of Michigan to southern Michigan (USGS 2014).....2

Figure 1.3. A map of the United States indicating states with fish consumption advisories (U.S. EPA 2013; Esri 2012).....3

Figure 1.4. Map of the lakes sampled in the Upper Peninsula of Michigan for Mercury (State of Michigan 2005; Wisconsin Department of Natural Resources 2017 Kerfoot et al. 2017; Priyadarshini 2017).....4

Figure 1.5. Diagram of the lake mercury cycle. 7

Figure 2.1. Map of the study location. 15

Figure 2.2. Diagram of in-lake mercury cycling used to parameterize the model.....26

Figure 3.1. Water balance over one year. Values represent ten-year averages. 39

Figure 3.2. Measured and modeled temperatures in water and air for Torch Lake. Measured values were taken from GLEC 2003, Weather Underground historical data for Lake Linden, MI and MDEQ 2018. 40

Figure 3.3. Modeled inflow temperatures for the Trap Rock River compared to temperatures in the Sturgeon River.....41

Figure 3.4. Annual DOC measured and modeled concentrations in Torch Lake. 42

Figure 3.5. Chlorophyll A Concentrations for Torch Lake over a year duration. 43

Figure 3.6. Annual divalent, methyl, and elemental mercury concentrations predicted for Torch Lake. 44

Figure 3.7. Comparison of total mercury concentrations modeled and measured in Torch Lake.....45

Figure 3.8. Comparison of modeled and measured total and methyl concentrations in sediment as dry weight.....46

Figure 3.9. Modeled (on the left in green) and measured (on the right in white) concentrations in Torch Lake.....49

Figure 3.10. Sensitivity analysis results for the resultant change in mercury concentrations from changing the values of the model parameters. 51

Figure 3.11. Trace plots of the parameter value as a function of the iterations after the warm-up period for oxidation in the sediments (a) and methylation in the water column (b). 54

Figure 3.12. Posterior mean and model values compared. Error bars around the model value indicate the range of values reported in literature. Error bars around the posterior mean indicate the 2.5^{th} and 97.5^{th} percentiles about the posterior mean. 55

Figure 4.1. Magnitude of the process rates (g yr^{-1}) for the mass balance of total mercury. 56

Figure 4.2. Magnitude of the process rates (g yr^{-1}) for the mass balance of methyl mercury. 57

Figure 4.3. Magnitude of the process rates (g yr^{-1}) for the mass balance of elemental mercury. 58

Figure 4.4. Magnitude of the process rates (g yr^{-1}) for the transformation processes of the three mercury species in the overall mass balance of mercury in the lake and sediments.....59

Figure 4.5. Seasonality in the process rates for elemental mercury in the epilimnion. Production of methyl mercury is represented by solid lines and losses by dashed lines. 66

Figure 4.6. Seasonality in the process rates for methyl mercury in the epilimnion. Production of methyl mercury is represented by solid lines and losses by dashed lines. 67

Figure 4.7. Runoff averaged over a ten-year span and modeled mercury concentrations in watershed runoff compared with measurements (GLEC, 2003; U.S. Geological Survey, 2015). 68

Figure 4.8. Annual total mercury runoff from the watershed to the lake (per watershed area) compared with runoff. 69

Figure 6.1. Trace plots for model parameters reduction and oxidation in the water and sediments as a function of the number of iterations. 114

Figure 6.2. Trace plots for model parameters methylation and demethylation in water and sediments as a function of the number of iterations. 115

List of Tables

Table 2.1. Indices for the area and the volume of the lake compartments. 14

Table 2.2. Defined indices for matrices in mercury mass balance equation.....25

Table 2.3. Parameterization and description of process matrices, K 27

Table 2.4. Parameterization and description of loading matrices, W 28

Table 2.5. Mercury Bioaccumulation Factors (BAF) in fish 34

Table 3.1. Modeled lake mercury concentrations compared with measurements in northern Wisconsin lakes. 47

Table 3.2. Model process rates (g yr^{-1}) summed annually for Torch Lake.....48

Table 3.3. Posterior means of the model parameters (day^{-1}) and convergence diagnostics. 52

Table 3.4. Convergence diagnostics of the predicted mercury concentrations.....53

Table 4.1. Comparison of deposition rates (μg m^{-2} yr^{-1}) to the watershed and lake surface for methyl and total mercury.....61

Table 4.2. Comparison of dry deposition rates (μg m^{-2} yr^{-1}) to the watershed and lake surface for inorganic mercury. 61

Table 6.1. Model parameter values, description, units, and references. 92

Table 6.2. Sensitivity results for all parameters expressed as the percent change in mercury concentrations. 109

Preface

This thesis is written in the intention for publication. Portions of the thesis have already been published in Perlinger et al. (2018) and Kerfoot et al. (2018).

Acknowledgements

I would like to acknowledge my advisor, Dr. Noel Urban, for sparking my interest in research and for all the feedback and advice over the years. Thank you to my committee, Dr. Min Wang and Dr. Cory McDonald, for the helpful input and comments on my thesis and research. I also appreciate all the assistance from everyone in the ASEP's team and everyone in my research group: Dr. Noel Urban, Dr. Judith Perlinger, Mugdha Priyadarshini, Emily Shaw, Tanvir Khan, Ashley Lingle, Hang Wang, Hongyi Lin, Ankita Mandelia, Emily Sokol, Meredith Brehob, Alan Labisch, Rachel Stern, and Abigail Kanasty. Also, thank you to Michigan Technological University's Civil and Environmental Department and faculty.

Without my funding sources, this project would not have been possible. My funding came from Michigan Technological University's Student Undergraduate Research Fellowship, University of Michigan's Michigan Space Grant Consortium, the International Association of Great Lakes Research's Dolan Scholarship, and the National Science Foundation Coupled-Natural-Human Systems Award (#1313755).

I also would like to thank my family and my friends. Without their support and help, I would not be where I am here today.

Abstract

To increase understanding of mercury cycling, a seasonal mass balance model was developed to predict mercury concentrations in lakes and fish. Results indicate that seasonality in mercury cycling is significant and is important for a northern latitude lake. Models, when validated, have the potential to be used as an alternative to measurements; models are relatively inexpensive and are not as time intensive. Previously published mercury models have neglected to perform a thorough validation. Model validation allows for regulators to be able to make more informed, confident decisions when using models in water quality management. It is critical to quantify uncertainty; models are often over-parameterized and constrained by few measurements. As an approach, the Markov Chain Monte Carlo (MCMC) Bayesian method was used for uncertainty analysis. The uncertainty analysis provided a better means for calibration, helpful insight on the distribution of model parameter values, and the uncertainty in model predictions.

1 Introduction

1.1 Mercury as a Problem

Mercury contamination in lakes is both a local and a global issue. When in the atmosphere, mercury has a long residence time (a half of a year to a year) and can be transported for long distances (Perlinger et al. 2018); see Figure 1.1. Sources to the atmosphere of mercury include both natural processes (wild fires and volcanoes) and anthropogenic emissions; the majority is from anthropogenic emissions (Evers et al. 2011). Once in the atmosphere, it can be deposited to lakes and watersheds (and then can runoff to lakes) through atmospheric wet and dry deposition (Ambrose et al. 2005). This means that even the most remote lakes have some mercury in water and in fish (Landis and Keeler 2002). The main source of mercury to lakes is atmospheric deposition; however, just because a lake receives more atmospheric deposition does not mean it will necessarily have higher fish or lake mercury concentrations than a lake with less atmospheric deposition (Perlinger et al. 2018).

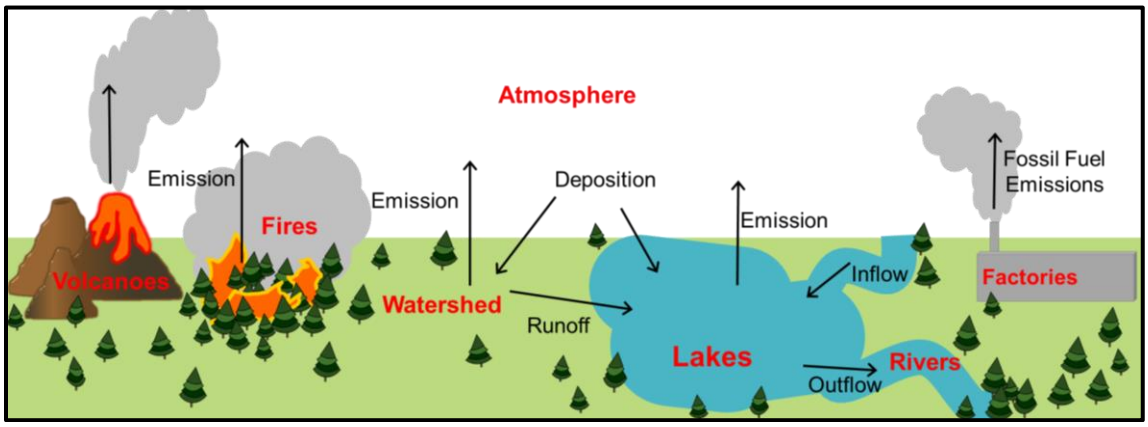

Figure 1.1. Diagram of the global mercury cycle.

The mercury cycle in lakes is complex; it is unclear what leads to elevated mercury concentrations in fish in some lakes and not in others. Although studies have determined characteristics that drive individual mercury processes in aqueous systems, the overall interplay of the processes is not predictable in each lake because of specific lake characteristics. These characteristics include photolysis (Amyot et al. 1994; Costa and Liss 1999), salinity (Lalonde et al. 2004), humic and fulvic acids (Alberts et al. 1974; Allard & Arsenie 1995; Chakraborty et al. 2015), or DOC (Amyot et al. 1997a,c).

The many factors contributing to observed differences in mercury between Michigan's Upper and Lower Peninsula lakes are an example of how difficult it can be to understand why mercury is elevated in some lakes but not in others. The Upper Peninsula of Michigan receives less atmospheric wet deposition of mercury than the Lower Peninsula, but total

mercury concentrations in fish (walleye, bass, and northern pike) are higher in the Upper Peninsula (Knauer et al., 2011; Kerfoot et al., 2018). Wet deposition measurements collected for 1994 to 2003 by Keeler and Dvonch (2005) showed deposition at a site located near Eagle Harbor of the Upper Peninsula to be smaller compared to two sites in the Lower Peninsula, Dexter (2.1 times larger) and Pellston (1.3 times larger). Elemental mercury evasion rates were found to be lower in the Upper Peninsula than Lower Peninsula based on differences in land cover types between the two regions (Denkenberger et al. 2012). The Lower Peninsula has more urban development, grasslands, and agriculture whereas the Upper Peninsula is dominated by forested areas (see Figure 1.2). The Upper Peninsula also has more wetlands and lakes that have higher DOC concentrations than lakes in the Lower Peninsula (Kerfoot et al., 2008; Michigan Department of Environmental Quality, 2013). Furthermore, the Upper Peninsula receives less sulfate wet deposition than the lower peninsula (Knauer et al., 2011). Lake DOC, sulfate concentrations, and the fraction of wetlands in a lake's watershed have been found to be correlated with and indicators of methylation and elevated mercury levels in fish (Brumbaugh et al. 2001; Balogh et al. 1998; Austin et al., 2016; Driscoll et al. 2007). In summary, the in-lake mercury cycling in Upper Peninsula lakes, in combination with elevated DOC and wetlands areas, apparently contributes to elevated mercury concentrations in fish in Upper Peninsula lakes despite lower atmospheric deposition of mercury.

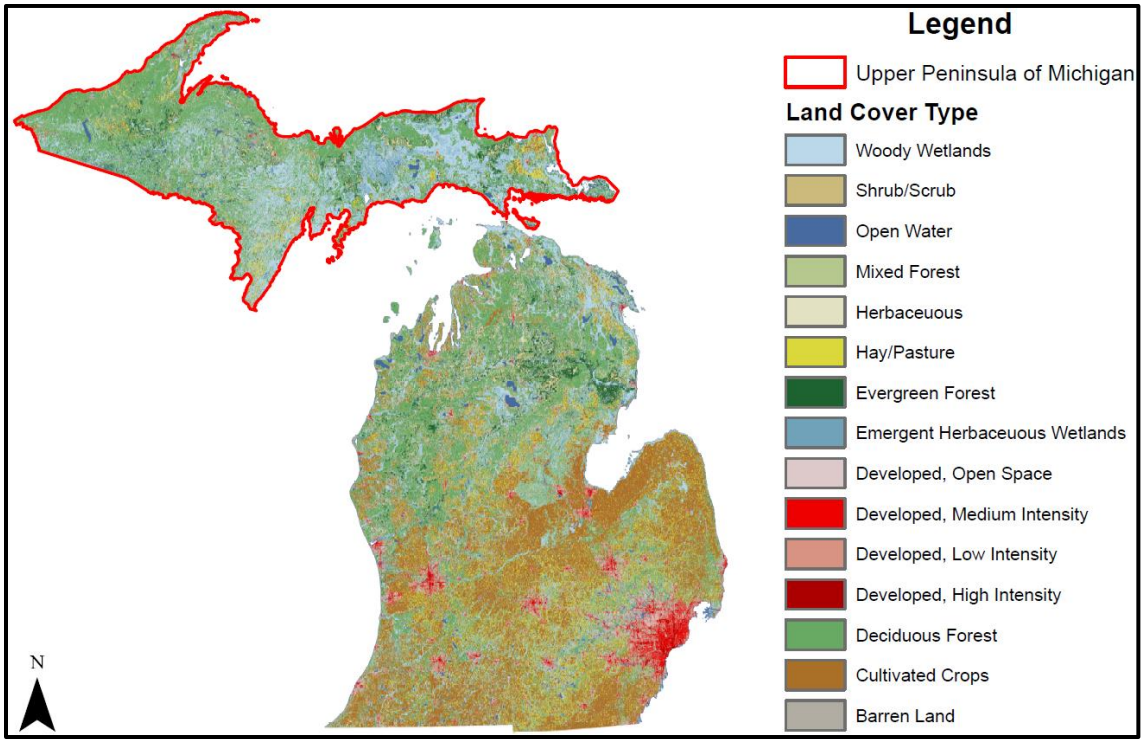

Figure 1.2. Map contrasting the land cover type for the Upper Peninsula of Michigan to southern Michigan (USGS 2014).

The variability of mercury concentrations among different lakes has prompted lake-specific fish consumption advisories to be set in addition to statewide advisories. As of 2011, all fifty states (including Michigan) have at least one advisory for mercury (see Figure 1.3); a total of 3,710 waterbodies in the United States have lakes under advisory for mercury (U.S. EPA 2013). Before the advisory can be set, an estimate of mercury concentrations in fish is needed. To measure fish mercury concentrations for each lake would be expensive and time consuming.

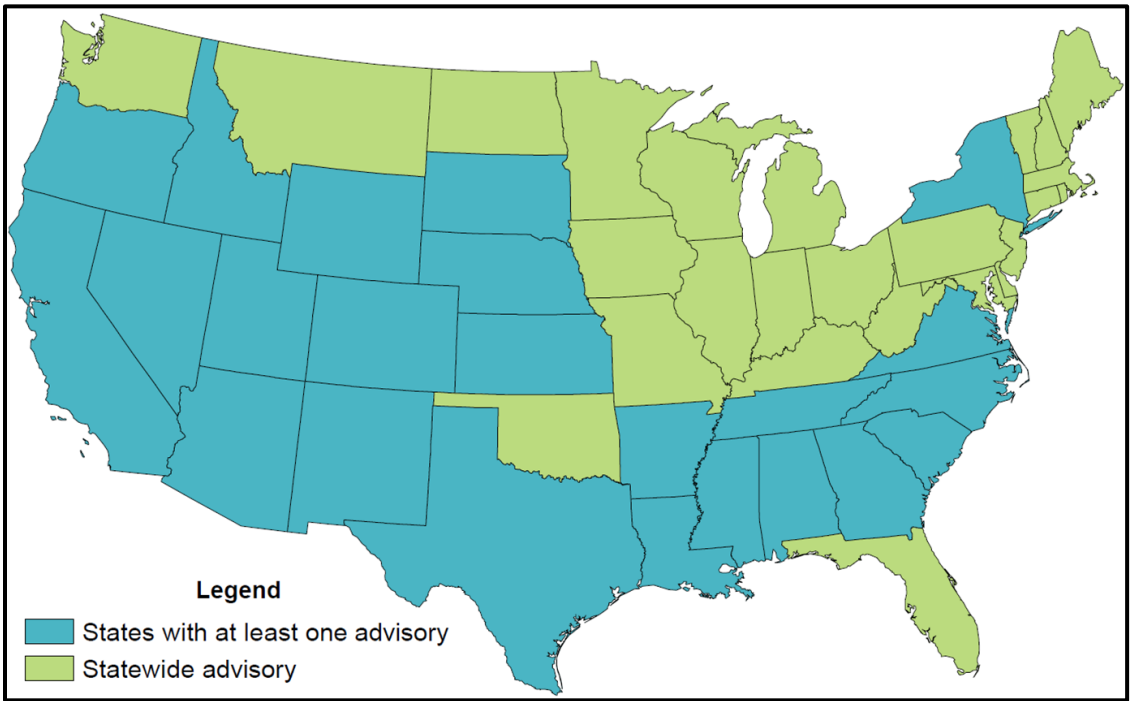

Figure 1.3. A map of the United States indicating states with fish consumption advisories (U.S. EPA 2013; Esri 2012).

Despite there being over 5,000 lakes larger than 0.01 km^2 in the UP (State of Michigan 2017), only 75 of the lakes have measurements for mercury concentrations in fish (Priyadarshini 2017). A map with the lakes with fish above the safe consumption limit is shown in Figure 1.4 below. A mechanistic approach for estimating these concentrations is to develop a mathematical, mass balance-based model for mercury cycling in lakes.

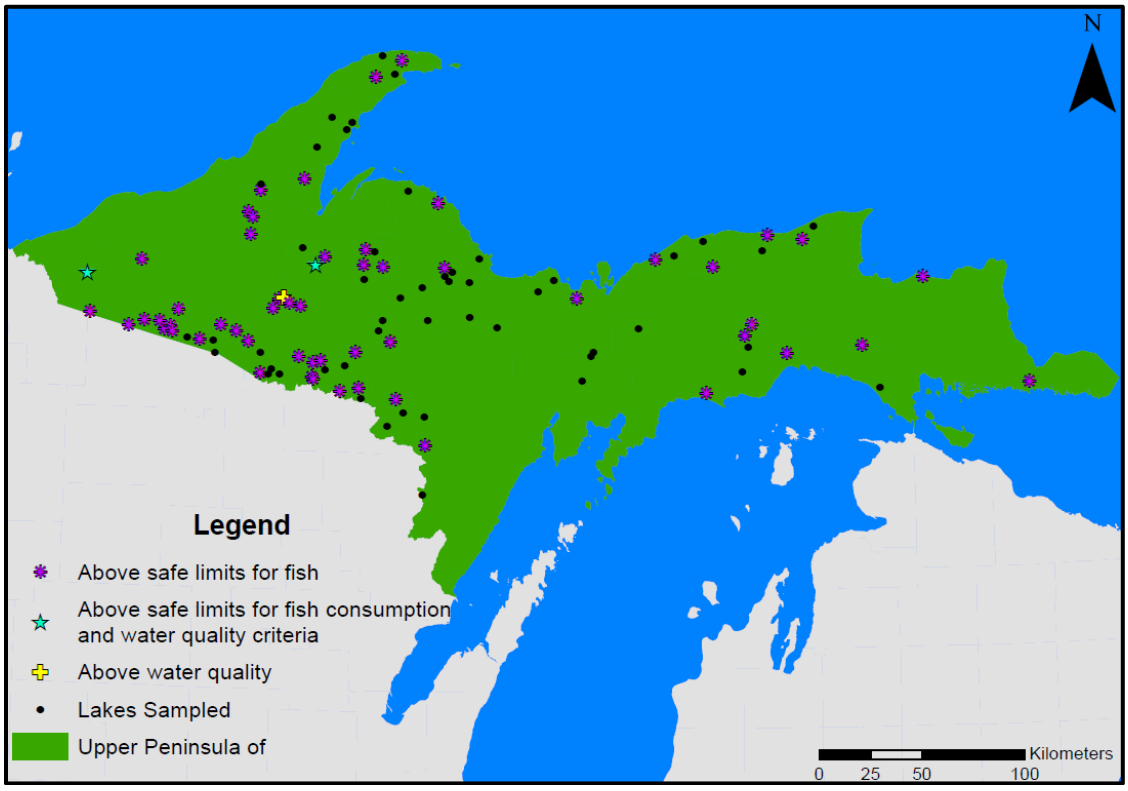

Figure 1.4. Map of the lakes sampled in the Upper Peninsula of Michigan for Mercury (State of Michigan 2005; Wisconsin Department of Natural Resources 2017 Kerfoot et al. 2017; Priyadarshini 2017).

1.2 Introduction to Modeling Mercury

There have been multiple mercury models reported in the literature to predict concentrations in systems ranging from the atmosphere (Petersen et al. 1998), to fish (Knightes et al. 2009; Barber 2008b), seas (Salvagio Manta et al. 2016; Rajar et al. 2004), watersheds (Futter et al. 2012; Ambrose et al. 2005), and lakes (Either et al. 2008; Zhang et al. 2014; Hudson et al. 1994). A mass balance approach is typically used for modeling mercury in these systems (Knightes 2008; Ethier et al. 2008; Zhang et al. 2014; Macleod et al. 2005). Mass balances incorporate in-lake mercury transformations, accumulation of mercury in the lake, loading of mercury to the lake, and loss of mercury from the lake. A mass balance model has several advantages. The model can be used to examine individual processes or factors that could be contributing to elevated levels of mercury (Hudson et al. 1994; Knightes et al. 2009), or to make future predictions for scenarios of future emissions, land use, or climate (e.g., Perlinger et al. 2018). It is not possible to get the same insights by measuring as by modeling. On the other hand, models cannot completely and with full accuracy simulate the natural world. The complexity of the mercury cycle also poses difficulties for modeling. The factors controlling mercury processes in lakes are not entirely known, and often few measurements of process rates exist.

To apply these mathematical models to natural systems, many assumptions need to be made. Lakes are either assumed to be plug flow reactors, completely mixed flow reactors, or sequential series of completely mixed flow reactors (Chapra 2014; Knightes 2008). Reactors are representative of lakes, rivers, or the system for which the mass balance is derived. These mass balance models are either assumed to be steady state (Knightes 2008; Qureshi 2009; Ethier 2008) or non-steady state (Zhang et al. 2014) and are derived from ordinary differential equations (ODEs). Steady state means there is no change in concentrations, inputs or outputs with respect to time; everything is constant over the assumed duration. The non-steady state case predicts concentrations at incremental time steps (day, week, month, year, etc.), and parameters can change over this integration period (e.g., temperature of the water, inflow to the lake, and wind speed over the lake). The non-steady state case is advantageous for incorporating seasonality and predicting the timescale for changes of mercury with changes in emissions or other drivers of the mercury cycle.

Commonly, the three mercury species assumed to be dominant in lacustrine systems are elemental (Hg^0), divalent (Hg^{+2}), and methyl (MeHg, CH_3Hg^+). Total mercury (THg) is the sum of all speciated forms of mercury (Knightes 2008; Qureshi et al. 2009; Ethier et al. 2008; Hudson et al. 1994; Zhang et al. 2014). These species can be modeled either as single components or as the sum of species in which they occur such as hydroxide, chloride, sulfide, or DOC complexes; or categories of solids such as abiotic solids, biotic solids, and sediments (Hudson et al. 1994; Knightes 2008). Furthermore, models must be constructed as either one-, two-, or three-dimensional depending on assumptions regarding mixing intensities and on the spatial and temporal resolution that is desired. Typically, models for lakes include interactions with the surrounding air and watershed, and the lake itself is frequently subdivided into compartments such as epilimnion, hypolimnion, and sediments (Knightes 2008; Either et al. 2008; Qureshi et al. 2009).

Models typically require knowledge or measurements of conditions in a lake, and thus many of the models developed have been for specific lakes or regional areas rather than a generalized model for all lakes (see Lessard et al. 2014; Macleod et al. 2005; Zhang et al. 2014; Håkanson 1996). Factors such as trophic status, lake dimensions, and hydrology are needed for modeling. This means that one must either use measured lake characteristics based on previous sampling or make assumptions about these characteristics if no information is readily available. There is also the potential to combine mass balance models for multiple interacting substances (e.g., DOC and algal mass balance). Multiple lake characteristics can be remotely sensed (e.g., surface area, watershed size based on topography, area of wetlands in catchment, surface temperature, water color, chlorophyll) and are available in state, national or global databases (e.g., National Hydrography Dataset, National Wetland Inventory); other characteristics can be predicted based on latitude (lake temperatures, mixing regime; e.g., Mironov et al. 2010) or regional data sets (e.g., Chapra et al. 2017).

One of the first influential mercury models for lakes was the Mercury Cycling Model (MCM) (Hudson et al., 1994; Knightes, 2008). Hudson et al. (1994) applied this model in the steady-state case for the Mercury Temperate Lakes (MTL) study in northern Wisconsin. There have been several mercury models published since including the Lake Michigan mass balance model (LM2-Hg) (Zhang et al. 2014), the Regional Mercury Cycling Model (R-MCM) (Knightes and Ambrose 2004; Knightes and Ambrose 2006b), the mercury Quantitative Water Air Sediment Interaction (Hg QWASI) model (Either et al. 2008), and EPA's Spreadsheet-based Ecological Risk Assesment for the Fate of Mercury (SERAFM) (Knightes and Amborse 2006a; Knightes 2008). However, SERAFM is the most publicly available mercury lake model and is suggested by the EPA for assessing management and remedial strategies (Knightes and Ambrose, 2006a; Knightes 2008). This is a steady state model for predicting aqueous and fish mercury concentrations for any lake.

1.3 Mercury Cycling in Lakes

A diagram of the mercury cycle occurring in a lake is shown in Figure 1.5. This conceptual understanding was used to parameterize the model presented in this study. Mercury species are defined as follows: elemental (Hg0), methyl (MeHg), and divalent (Hg2).

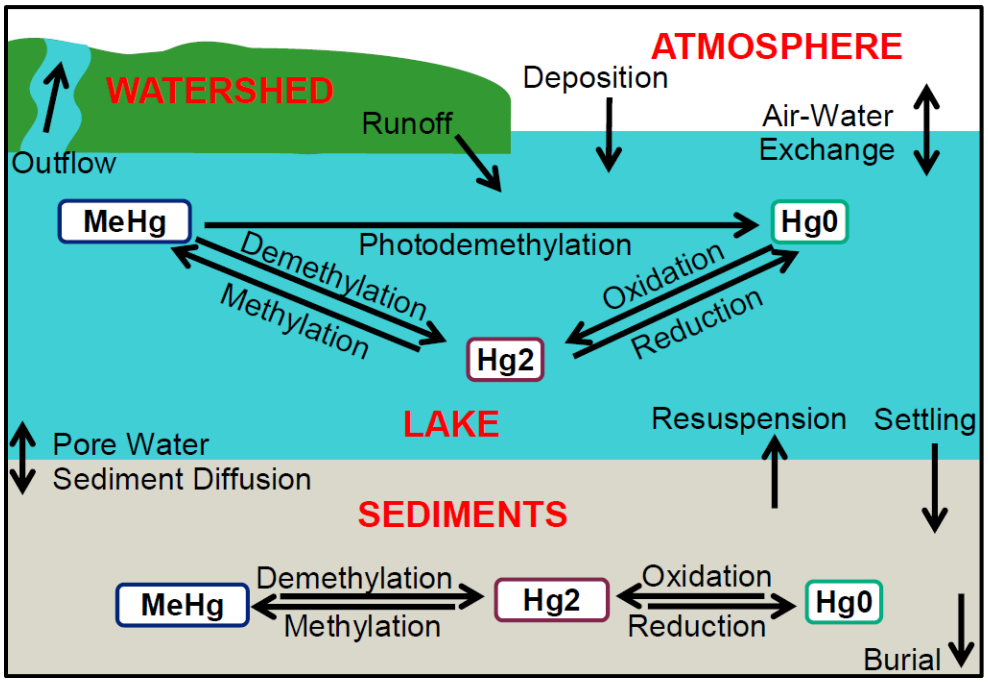

Figure 1.5. Diagram of the lake mercury cycle.

Sources of mercury to lakes include atmospheric deposition (wet and dry), discharge from tributaries, erosion, diffusion from deep sediments, and groundwater. Wet deposition is a source of divalent and methyl mercury; elemental mercury concentrations in precipitation are small (Baker and Bash 2012; Downs et al. 1998). Dry deposition of reactive gaseous mercury (RGM) and particulate bound mercury (PBM) to the lake surface is a source to the lake of divalent mercury (Rea et al., 2000; Zhang et al., 2009). Runoff of mercury from the catchment to the lake is a source primarily of divalent mercury that may have been deposited on vegetation in the catchment as elemental mercury and subsequently oxidized and transported to the lake as divalent mercury (Balogh et al. 1998 and 2005; Hammerschmidt et al. 2006). Dry deposition to the lake surface and runoff from the watershed are also sources of methyl mercury to lakes (Knauer et al. 2011; Chen et al. 2008; Futter et al. 2012). Elemental mercury can be evaded from the lake surface through air-water exchange (Vandal et al., 1991; Fitzgerald et al., 1994).

The main mechanisms for removal of mercury once it is in a lake are outflow, volatilization (evasion) of elemental mercury, and burial or diffusion into deep sediments (Rajar et al. 2004; Zhu et al. 2017, Knightes 2008; Hudson et al. 1994). Physical processes affecting mercury in lakes include settling of mercury partitioned to abiotic and biotic solids, burial and resuspension of mercury in all phases (dissolved and partitioned to solids), dispersion across the thermocline in all phases, and pore water diffusion in the dissolved phase (Zhu et al. 2016; Qureshi et al. 2009; Zhang et al. 2014). Biotic, abiotic, and chemical reactions of mercury include demethylation of dissolved and DOC-partitioned methyl mercury to divalent mercury (Knightes 2008; Hintelmann et al. 2000), methylation of dissolved divalent to methyl mercury (Avramescu et al. 2011; Heyes et al. 2006; Celo et al. 2006), photodemethylation and mer-operon cleavage of dissolved methyl to elemental mercury (Knightes 2008; Black et al. 2012), reduction of dissolved divalent to elemental mercury (Alberts et al. 1974; Allard and Arsenie, 1991; Amyot et al. 1997a,b,c), and oxidation of dissolved elemental to divalent mercury (Amyot et al. 1997b and 2000). Methyl mercury is bioavailable and taken up by microorganisms including phytoplankton; from there it will biomagnify up the food chain (Downs et al. 1998; Knightes 2008; Watras et al. 1998).

1.4 Approach for Model Validation

1.4.1 Motivation for Validation

According to Liu and Gupta (2010), the inherent errors within models are input data, initial and boundary conditions, model structure, and model parameters. The model developed in this study is structured as a complex biogeochemical mass balance model. The mass balance is structured as a system of ordinary differential equations (ODEs). There is no analytical solution and thus an ODE numerical solver is used. Numerical solvers have errors within themselves that can contribute to overall uncertainty in model predictions. The initial conditions (or initial mercury concentrations, in this case) also have uncertainty. This model has a time step of one day and is run for one year (365 days) starting on January 1st and ending on December 31st. The model is structured for January 1st and December 31st to have similar input data and parameters such that predicted mercury concentrations should be nearly equal for both days. If the initial conditions are incorrect, one would expect that there would be a big difference between predicted mercury concentrations on January 1st and December 31st. The uncertainty within measured input data can arise from instrument error, interpretation error, and reporting errors. Furthermore, the model has numerous (85) parameters, some of which are not well constrained nor easily measurable. There is also uncertainty that arises from the concept that there exist multiple combinations of the parameter values that can give the same model.

To quantify and minimize this uncertainty, validation becomes a key component in developing a model. For this study, validation consists of calibration, sensitivity analysis, and uncertainty analysis. This approach for validation is different from the conventional methodology, and rather, is an approach developed in the case of a complex model with lack of measurements and information needed for validation. Calibration consists of tuning and structuring the model such that predicted values are within the range of measured concentrations. Conventionally, calibration is not considered to be part of model validation and is rather done prior to validation. In this study, calibration was still performed prior to validation, but was grouped as part of the procedure in validation. Sensitivity analysis is used to identify the model parameters to which the predicted concentrations are most sensitive; this is accomplished by changing individual parameters one at a time by a fixed amount and comparing the magnitude of change in model predictions. Uncertainty analysis gives the range of confidence in predicted values and for the model parameters (Liu and Gupta, 2007; Arhonditsis 2007). The approach used for the uncertainty analysis is also a method for performing more efficient calibration, which will be discussed later.

1.4.2 Current State of Practice for Model Validation of Mercury Models

Calibration and sensitivity analysis are the most common elements of validation applied to mercury models in the literature. For a fugacity model developed for Swedish lakes, Håkanson, (1996) performed a sensitivity analysis by altering values of parameters within a factor of two of their original model value and also within 95% confidence intervals that were generated using Monte Carlo simulations. SERAFM's sensitivity analysis consisted of choosing several important parameters and then altering parameter values as pairs of opposing processes (Knightes, 2008). Few studies have performed uncertainty analyses due to the complexity of the mercury cycle. The most common uncertainty analysis approach used with mercury models has been Monte Carlo simulations using confidence intervals for the parameters. (Håkanson, 1996; Qureshi et al., 2009; Carroll and Warwick, 2001; MacLeod et al., 2002). The confidence interval for a parameter is typically based on the range of reported literature values and a guess of how uncertain each parameter is. A newer uncertainty analysis uses the Bayesian approach; while this has been applied to other biogeochemical models, it has not yet been applied to mercury models.

1.4.3 Bayesian Approach for Uncertainty Analysis of Models

The validation approach in this study focuses on the application of the Bayesian Markov Chain Monte Carlo (MCMC) method. While Monte Carlo simulations have been used, this method has not been applied to mercury models. However, this method has been applied to other biogeochemical and environmental models and has been found to be advantageous for many reasons (Arhonditsis et al. 2007 & 2008; Liu and Gupta 2007; Ajami et al. 2007; McDonald et al. 2012). For example, results from Liu and Gupta (2007) summarized this Bayesian approach to be more reliable, flexible, and accurate than the classical approach. Arhonditsis et al. (2007) stressed the ability of the Bayesian approach to update the model fit as new data become available, whereas the classical approach is based solely on the original dataset.

The Bayesian approach, when applied to biogeochemical models, consists of applying a probabilistic model to the biogeochemical model (including its input parameters and data) to calculate the uncertainty through a posterior distribution for the biogeochemical model parameters and predictions (Gelman et al. 2004). Mathematically this can be illustrated using Baye's Rule (Gelman et al. 2004; Stan Development Team 2017):

$$P(\theta|y,x) \propto P(y|\theta,x)\, P(\theta,x) \quad (1)$$

which requires the estimation of "prior" distributions: the probability distribution, $P(\theta,x)$, and the likelihood function, $P(y|\theta,x)$ for each of the parameters, θ, obtained from the literature. Variable y represents modeled mercury concentrations and x represent fixed model data. With these priors, the model draws random samples to obtain the posterior probability, $P(\theta|y,x)$, for each θ.

The Bayesian approach coupled with the MCMC method, consists of numerous iterations by continuously using the posterior distribution to update the prior belief; in theory, after numerous sampling the posterior distribution will converge (Gelman et al. 2004; Arhonditsis et al. 2007; Plummer et al. 2016). Markov Chains are based on optimizing algorithms that converge after criteria, such as the objective function, has been met. Validation and diagnostics for convergence have been developed and include assessing to ensure the samples are uncorrelated and making sure there is no "stickiness" in the sampling where the model is getting stuck on certain values of the parameters (Stan Development Team 2017; Gelman et al. 2004). The Bayesian approach is more flexible for applications to complex models, such as biogeochemical models, than the frequentist statistical approach involving hypothesis testing and confidence intervals (Gelman et al. 2004).

With this approach, the outcome includes the uncertainty in parameter values and predicted mercury concentrations. The posterior distributions of the parameters best constrain the parameter values based on all existing information and therefore provide the best basis for predicting concentrations and calibrating the model. This methodology is a more efficient and robust calibration approach then the manual calibration initially performed. The initial calibration is done manually by changing parameter values to obtain measured concentrations. Parameter values are altered to be more representative values for the specific lake from literature or within a specific range in literature. The uncertainty analysis approach is limited by computation power, and all parameters could not be sampled for (or used to calibrate the model to). Coupled with a sensitivity analysis, positive outcomes from this method include understanding processes controlling mercury cycling in lakes, determining the lake specific parameters, and furthering the overall understanding of mercury in general. However, there are obstacles to applying this computation-intensive uncertainty analysis to a complex biogeochemical model, such as for mercury. This will be discussed later.

Available software for this method includes Stan, BUGS, and JAGS. Stan was chosen for several reasons. One of the biggest advantages of Stan is that it is open sourced. Stan was initially set up to closely resemble the structure of BUGS. Stan utilizes the Hamiltonian Monte Carlo (HMC) sampling technique, (a type of MCMC method) which is a more efficient sampling technique compared to the two alternative models which use the Gibbs sampling technique (Stan Development Team, 2017). The advantage of HMC over the Gibbs Sampling technique is that the HMC technique can sample the entire parameter space whereas Gibbs focuses on only one parameter at a time. The HMC generally has better convergence requiring fewer total iterations, but each iteration may have a longer run time than Gibbs.

1.5 Objectives

The objectives of this project were to make a flexible, non-steady state model of mercury cycling in lakes with a level of complexity justified by the literature, and to use validation of the model to understand the sources and magnitude of uncertainty in model parameters and predictions of mercury concentrations. The model was to be flexible to enable application to different classes of lakes. The non-steady state approach was to enable study of seasonal dynamics as well as rates of response to external forcings such as regulation of mercury emissions or of climate change. A thorough review of the literature was used to select a model structure that could be justified based on the availability of measured parameters as well as be applicable to different lake types. Finally, this project sought to define an approach to validate a complex model such as the mercury model presented here.

2 Methods

The model developed in this study is a mass balance model based on the EPA model SERAFM (Knightes and Ambrose, 2006a) and was transformed from an Excel spreadsheet steady-state model to non-steady state with a daily time step. As a non-steady state model, the model presented in this study can incorporate seasonal changes that are important for mercury cycling in northern latitudes. Seasonality integrated into the model includes daily changes in hydrology, thermal stratification, temperature, light attenuation, solar radiation, dissolved organic carbon (DOC) concentrations, and phytoplankton concentrations. Advantages of including seasonality are the ability to look at the magnitude of temporal changes over an annual cycle and the ability to model rates of response to changes in atmospheric deposition or other controlling factors (e.g., climate). The disadvantage is that it makes the model more complex and thereby increases the uncertainty of model predictions.

2.1 Coupling of a mercury model with a water quality model

The seasonal model is independent of mercury and was developed in a separate code in which a system of ordinary differential equations was solved numerically. Daily values of parameters were saved to a text file, and for every mercury model run, the model uses this text file as an input to the model. The definitions of all variables can be found in Table 6.1 of the Appendix. For examination of scenarios of climate change, lake eutrophication, or other external drivers, this model would be used to generate new output files to serve as input to the mercury model.

Seasonal parameters are vector or matrix based. Each row contains the daily values of a parameter for one year. For matrices, columns represent the compartment of the lake. The index for time, t, is based on a non-leap year calendar which ranges from t = 1 to 365 where t = 1 represents January 1st and t = 365 represents December 31st. Measured daily values were averaged over the ten-year span, 2004 to 2013, to give a contemporary, climatological average. The index, n, for the column of the matrices is indicative of the lake compartment; a value of n = 1 represents the epilimnion layer, n = 2 the hypolimnion layer, and n = 3 the surface sediment layer. The mercury mass balances in R were solved with a stiff numerical ordinary differential equation (ODE) solver using “lsoda” in the deSolve package (Soetaert et al., 2017). A stiff solver had to be used because the mercury concentrations between species and lake compartments ranged over many orders of magnitude. All seasonal ODEs were solved simultaneously in MATLAB using the “ode45” solver (MathWorks, 2018) which is a non-stiff solver based on a fourth and fifth order Runge Kutta. The seasonal ODEs had to be solved simultaneously since many of the parameters were affected by each other (e.g., temperature in the water affected algal growth rate, and the algal concentrations in the water affected the amount of solar radiation in the water column).

In-lake processes occur in three compartments: epilimnion, hypolimnion, and surface sediments. The assumption is made that each of these compartments is completely mixed. The volume and areas of these compartments also use the index, n. Table 2.1 defines the representative compartment for each n value of the compartment area, A, and volume, V.

Table 2.1. Indices for the area and the volume of the lake compartments.

Index of Area, A[n] or Volume, V[n]	Dimension Represented
A[1]	Surface area of the lake
A[2]	Area of the thermocline
A[3]	Area of the surface sediments
V[1]	Volume of the epilimnion layer
V[2]	Volume of the hypolimnion layer
V[3]	Volume of the active surface sediment layer

Seasonal changes in the lake are defined by a calendar day of the year. These changes include formation and melting of ice cover on the lake, allowing accumulation of precipitation and deposition to occur on top of the ice, and periods of mixing and stratification. Measured wind speed and solar radiation were obtained from Michigan Technological University Keweenaw Research Center (KRC) historical weather. The KRC is located close to Torch Lake, less than five kilometers due west. Data for the dew point temperature, precipitation, and air temperature were obtained from Weather Underground's historic weather data for Lake Linden, Michigan. Lake Linden is located on the north shore of the lake.

2.2 Study Location

The lake chosen for this analysis is Torch Lake (47.167975 ^{o}N, -88.410621 ^{o}E). This lake is an oligotrophic, dimictic lake that becomes completely ice covered during winter. Torch Lake is located in the Upper Peninsula of Michigan; the lake is connected to Lake Superior through the Portage Canal (see Figure 2.1). Shown on this figure is the 2011 National Land Cover Dataset from the National Map Viewer (U.S. Geological Survey, 2014). The watershed area was delineated using a 1/3-arc second Digital Elevation Map (DEM) and the National Hydrography Dataset (NHD) for Michigan from the National Map Viewer (TNM) (U.S. Geological Survey, 2013a; U.S. Geological Survey, 2013b; U.S. Geological Survey, 2017). The National Wetlands Inventory (NWI) shape file was used to determine the area of wetlands in Torch Lake's watershed (U.S. Fish and Wildlife Services, 2017). The volume of the epilimnion, volume of the hypolimnion, the lake surface area, and area of the thermocline were calculated using a hypsographic curve (Urban, unpub.). Further

characteristics of the lake used as an input to the lake mercury model are provided in Table 6.1 of the Appendix.

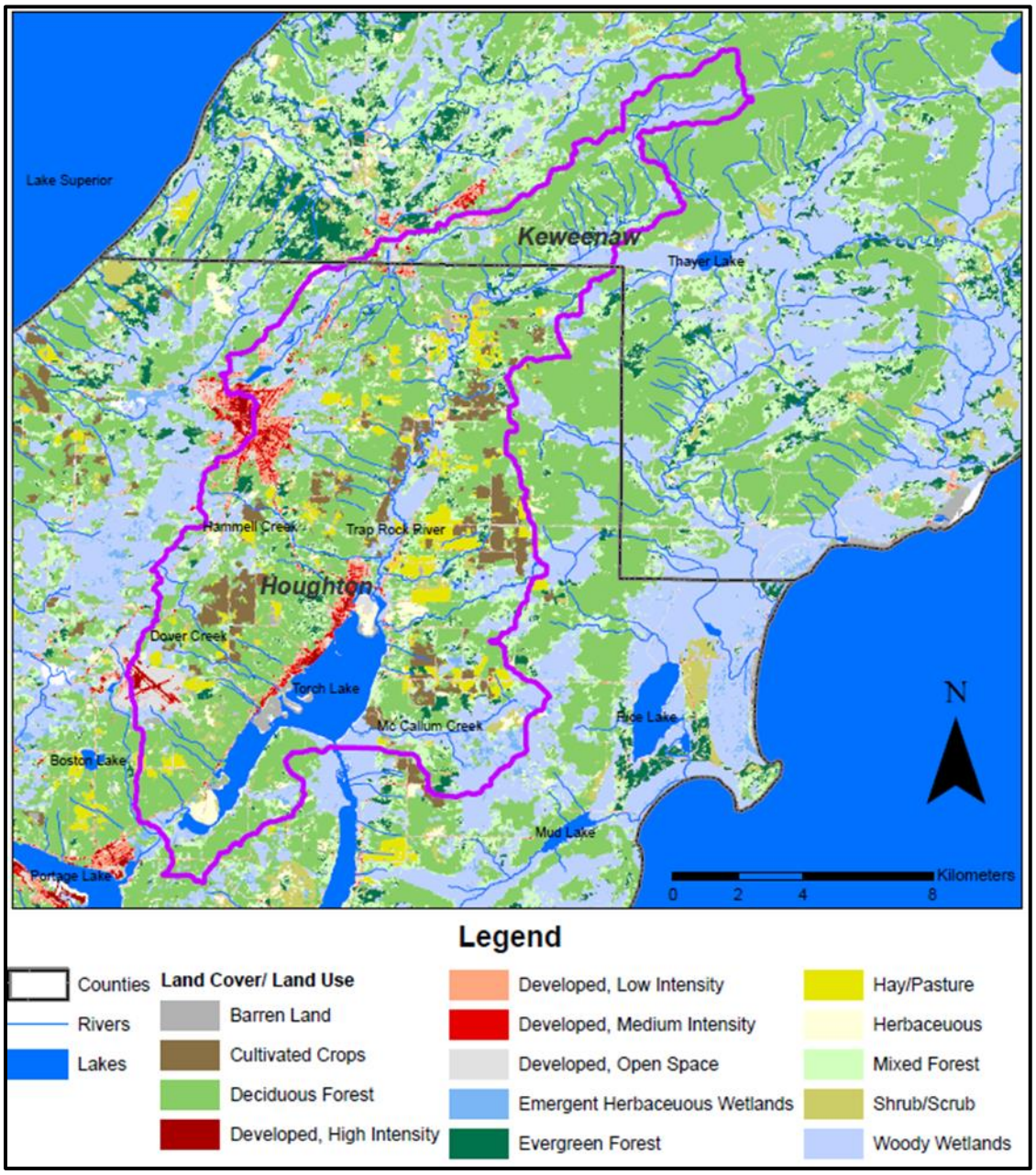

Figure 2.1. Map of the study location.

2.3 Seasonality and Water Quality Model

2.3.1 Water Balance

The hydrologic budget was developed to calculate the outflow rate, $Q_{outflow}$, from Torch Lake using the equation:

$$\frac{dV}{dt} = Q_{inflow}[t] + H_{precipitation}[t]\, A[1] - Q_{evaporation}[t] - Q_{outlfow}[t] \quad (2)$$

Groundwater inflow and outflow were assumed to be negligible. By assuming the volume of the lake did not change over time (setting the righthand side of the equation 1 equal to zero), the equation could be rearranged to solve for the daily outflow rate. Torch Lake is connected to Lake Superior by the Portage Canal, and therefore, Torch Lake's water levels closely follow Lake Superior's. Lake Superior's water levels fluctuated less than 0.7 m from 2004 to 2013 based on monthly average measurements (NOAA 2018a, b). The inflow rate was calculated based on measurements provided by the USGS gauging station for Trap Rock River Discharge, USGS 04043050 (U.S. Geological Survey, 2015). The total inflow to Torch Lake, Q_{inflow}, was calculated as the discharge rate from the Trap Rock River multiplied by the total watershed area of Torch Lake, divided by the watershed area upstream of the Trap Rock River gauging station. The upstream watershed area of the Trap Rock River was 72.5 km^2. The watershed was delineated similarly to the delineation of the Torch Lake Watershed and utilized the same GIS layers (U.S. Geological Survey, 2013a; U.S. Geological Survey, 2013b; U.S. Geological Survey, 2017).

Precipitation measurements ($H_{precipitation}$) were adjusted for accumulation of the precipitation on ice. Using the measured water content of snow pack, precipitation was converted to snow depths. Evaporation was estimated with the equation (Chapra, 2014)

$$Q_{evaporation}[t] = \frac{0.01\,(1-f_{ice}[t])\;\; f(U_{w,7m})[t]\,(e_{sat}[t]-e_{air}[t])\,A[1]}{L_e[t]\rho_w[t]} \quad (3)$$

The term, $f_{ice}[t]$, was used to prevent evaporation from occurring during ice cover. The latent heat of water vaporization, L_e, was calculated according to Chapra (2014):

$$L_e[t] = 597.3 - 0.57\, T_{air}[t] \quad (4)$$

The function to correct evaporation for wind at a height of 7 m above the lake surface, $f(U_{w,7m})$, is defined as (Chapra, 2014):

$$f(U_{w,7m})[t] = 19.0 + 0.95\,(U_{w,7m}[t])^2 \quad (5)$$

The original wind speed measurements were measured at 10 m above the lake surface, $U_{w,10m}$, and had to be corrected to 7 m, $U_{w,7m}$, using the log law (Manwell et al., 2009):

$$U_{w,7m}[t] = U_{w,10m}[t] \frac{\log\left(\frac{7}{z^*}\right)}{\log\left(\frac{10}{z^*}\right)} \tag{6}$$

where z* is the surface roughness length over a lake with open water set equal to 0.001 m (Manwell et al., 2009). The surface roughness length changes depending on if the lake is covered in ice or snow; the model did not account for this since there is no evaporation or surface heat exchange going on when the lake surface is frozen. The saturated vapor pressure, $e_{sat}[t]$, and the vapor pressure of air, $e_{air}[t]$, are functions of the temperature, T, of the surface water and at the dew point, respectively (Chapra, 2014):

$$e[t] = 4.596 \exp\left(\frac{17.27\, T[t]}{237.3 + T[t]}\right) \tag{7}$$

2.3.2 Heat Budget

The heat budget was used to predict temperatures of the epilimnion and hypolimnion. For simplification, the temperature of the lake surface was assumed to be equal to the temperature of the epilimnion and the temperature of the sediment layer was assumed to be the same temperature as the hypolimnion. The heat budget is defined as follows:

$$\frac{dT[t,1]}{dt} = \frac{Q_{inflow}[t]\, T_{inflow}[t]}{V[1]} + \frac{v_{thdp}[t]\, A[2]}{V[1]}(-T[t,1] + T[t,2])$$

$$- \frac{Q_{outflow}[t]\, T[t,1]}{V[1]} + \frac{J[t]\, A[1] \cdot 10^{-6}}{\rho_w\, C_{p,w}\, V[1]} \tag{8}$$

$$\frac{dT[t,2]}{dt} = \frac{v_{thdp}[t]\, A[2]}{V[2]}(T[t,1] - T[t,2]) \tag{9}$$

The heat budget neglects heat input from groundwater. Daily inflow temperatures were estimated throughout the year, and it was assumed that the inflow did not completely freeze during winter. The temperature of the inflow, T_{inflow} was estimated using the following relationship (Mohseni et al., 1998; Mohseni et al., 2003):

$$T_{inflow}[t] = T_{inflow,min} + \frac{T_{inflow,max} - T_{inflow,min}}{1 + \exp\left(\gamma\left(T_{air,inflect} - T_{air}[t]\right)\right)} \tag{10}$$

where T_{air} is the air temperature, $T_{inflow,min}$ is the minimum inflow temperature, and $T_{inflow,max}$ is the maximum inflow temperature. Characteristic parameters of the inflow temperature as a function of the air temperature were $T_{air,inflect}$, the air temperature at the inflection point, and γ, a unitless parameter to describe the steepest slope of the relationship. All temperature values are reported in units of Celsius. The specific heat of

water, $c_{p,w}$, was assumed to be constant (4.184 J $^{o}C^{-1}$) with temperature. The total surface heat flux, J, is defined as (Chapra, 2014):

$$J[t] = J_{SW}[t] + J_{LW\,total}[t] - J_{LW\,reflect}[t] - J_{cond}[t] - J_{evap}[t] \quad (11)$$

The surface heat fluxes were corrected for ice cover. Daily measurements of shortwave radiation were taken from the Michigan Technological University Keweenaw Research Center (Michigan Technological University Keweenaw Research Center, 2017). These radiation measurements were pre-corrected for cloud cover. Radiation was corrected for albedo and light extinction; this is further discussed in the section on Light Attenuation. The surface heat flux from net evaporation and condensation, J_{evap}, were calculated as (Chapra, 2014):

$$J_{evap}[t] = (1 - f_{ice}[t])\, f(U_{w,7m})[t]\, (e_{sat}[t] - e_{air}[t]) \cdot (4.184 \times 10^4) \quad (12)$$

The surface heat flux from net conduction and convection, J_{cond}, were calculated as (Chapra, 2014):

$$J_{cond} = (1 - f_{ice}[t])c_1\ f(U_{w,7m})[t]\, (T[t,1] - T_{air}[t]) \cdot (4.184 \times 10^4) \quad (13)$$

where c_1 is the Bowen coefficient of 0.47 mmHg $^{o}C^{-1}$. The coefficient of 4.184 x 10^4 is used to convert units into J m^{-2} day^{-1}. The longwave radiation reflected by the lake surface, $J_{LW\,reflect}$, is defined as (Chapra, 2014):

$$J_{LW\,reflect}[t] = (1 - f_{ice}[t])\sigma\, \epsilon\, (T[t,1] + 273.15)^4 \quad (14)$$

where σ is the Stefan-Boltzmann constant of 4.9 x 10^{-3} J m^{-2} day^{-1} K^{-4}, and ϵ is the dimensionless emissivity of water of 0.97. The total long wave radiation incoming to the lake surface, $J_{LW\,total}$, was defined as (Chapra, 2014):

$$J_{LW\,total}[t] = (1 - f_{ice}[t])\, \sigma(T_{air}[t] + 273)^4 (A + 0.031\sqrt{e_{air}[t]})(1 - R_L) \quad (15)$$

where A is a coefficient ranging from 0.5 to 0.7 (set at 0.5), and R_L is the reflection coefficient of the lake surface (0.03).

2.3.3 Light Attenuation

The albedo of the ice and of the water itself was calculated to determine the amount of solar radiation penetrating the surface of the water column:

$$\alpha[t] = \alpha_{ice}\, f_{ice}[t] + (1 - f_{ice}[t])\alpha_{water} \quad (16)$$

where the albedo of ice, α_{ice}, is 0.75, and the albedo of water, α_{water}, is 0.08 (Fang and Stefan, 1996). The amount of radiation that then is received through the surface, which is corrected for the albedo and light extinction coefficients according to the Beer-Lambert Law is given by:

$$I_{surface}[t] = (1 - \alpha[t])\, I_0[t] \exp\left(-k_{e,ice}\, f_{ice}[t]\, z_{ice\,max}[t] - f_{ice}[t]\, k_{e,snow}\, z_{snow}[t]\right) \quad (17)$$

where I_0 is the uncorrected radiation at the surface of the lake compartment. The light that has penetrated through the ice and snow layer, then is corrected for the light extinction in the water column as a function of depth:

$$I_a[t,n] = I_{surface}[t] \exp(-k_e[t,n]\ z_{water}[n]) \quad (18)$$

where the light extinction coefficients are calculated differently depending on wave length. Visible light (photosynthetically active radiation or PAR) was assumed to be 50% of total incoming shortwave radiation. Ultraviolet-B (UVB) was assumed to be 4% of the total (Xia et al. 2008). Light attenuation and shortwave radiation were both first calculated as the average to the epilimnion layer (or n = 1). The average light attenuation in the hypolimnion layer (or n = 2) is then calculated from the amount of light that penetrates through the epilimnion. The overall light extinction coefficient for PAR (Chapra, 2014):

$$k_{e,PAR}[t,n] = k'_{e,PAR}[n] + 0.0088\, C_{algae}[t,n] + 0.054\, \left(C_{algae}[t,n]\right)^{2/3} \quad (19)$$

where $k'_{e,PAR}$ is defined as (Chapra, 2014):

$$k'_{e,PAR}[n] = k_{ew} + 0.052N + 0.174D \quad (20)$$

and is the light extinction of PAR due to non-volatile solids, N; detritus solids, D; and the light extinction of particle-free water and color, k_{ew}. At present, the attenuation of PAR by DOC is not explicitly included in the formulation. The overall light extinction coefficient for UVB is (Morris et al., 1995):

$$k_{e,UVB}[t,n] = 0.415\, (C_{DOC}[t,n])^{1.86} \quad (21)$$

The light attenuation for PAR and UVB were all calculated using the equation:

$$\emptyset_{light}[t,n] = \frac{2.718\, f[t]}{k_e[t,n]\, (H_2[n] - H_1[n])} (\exp(-\alpha_1[t,n]) - \exp(-\alpha_0[t,n])) \quad (22)$$

where H_1 is the depth of the water at bottom of the lake compartment and H_2 is the depth of the surface of the compartment; the difference of the two is the thickness of the compartment. The coefficients, α_1 and α_0 are defined as:

$$\alpha_0[t,n] = \frac{I_a[t,n]}{I_s} \exp(-H_1[n]\, k_e[t,n]) \tag{23}$$

and

$$\alpha_1[t,n] = \frac{I_a[t,n]}{I_s} \exp(-H_2[n]\, k_e[t,n]) \tag{24}$$

where $I_a[t]$ is the average daylight intensity and I_s is the light intensity for optimal growth. The parameters for light extinction coefficients, k_e, and I_s are characteristic of the wavelength (PAR, UVB, and UVA). The photoperiod, or the fraction of the day sunlight is present, f[t], is given by:

$$f[t] = \frac{t_s[t] - t_r[t]}{T_p} \tag{25}$$

where t_s and t_r are the time of sunset and sunrise, respectively, and T_p is the daily period. Daily data for time of the sunset and sunrise were from the U.S. Naval Observatory, 2015.

2.3.4 Dissolved Organic Carbon Mass Balance

Daily estimates of dissolved organic carbon (DOC) concentrations were needed for computation of light (UVB) attenuation, mercury photolytic reactions, and partitioning of mercury to DOC. Light extinction of UV radiation has been found to be due to DOC in the water column (Morris et al., 1995). DOC is also an important parameter as some previous literature has shown a correlation between DOC and mercury. A DOC mass balance was derived to predict concentrations in the epilimnion, $C_{DOC}[t,1]$ and in the hypolimnion $C_{DOC}[t,2]$:

$$\frac{dC_{DOC}[t,1]}{dt} = \frac{Q_{inflow}[t]}{V[1]} DOC_{inflow}[t] - \frac{Q_{outlfow}[t]}{V[1]} C_{DOC}[t,1] + \frac{v_{thdp}[t]\, A[2]}{V[1]} (-C_{DOC}[t,1] + C_{DOC}[t,2]) \quad (26)$$

$$\frac{dC_{DOC}[t,2]}{dt} = \frac{v_{thdp}[t]\, A[2]}{V[2]} (C_{DOC}[t,1] - C_{DOC}[t,2]) \quad (27)$$

The mass balance included the inflow, outflow, and thermocline dispersion of DOC in the epilimnion and hypolimnion. The DOC concentration in the sediment was assumed to be constant over the annual duration. The DOC concentration in the inflow to the lake was estimated using a sinusoidal function:

$$DOC_{inflow}[t] = \overline{DOC_{inflow}} + a \sin(b\, t + c) \quad (28)$$

where $\overline{DOC_{inflow}}$ is the annual average concentration of DOC in the inflow of 7 mg L^{-1} (Urban unpub.), a is the amplitude of 2 mg L^{-1}, b is the angular frequency of 0.0172 day^{-1}, and c is the phase shift. The phase shift is calculated by solving for the variable, c in the above equation based on the input of peak DOC concentration of 9 mg L^{-1} as $DOC_{inflow}[t]$ and the day, t of peak DOC concentration occurring around May 11th (peak inflow from snow melt runoff). The average annual DOC concentration in the sediments is 40 mg L^{-1} (Cusack & Mihelcic, 1999).

2.3.5 Chlorophyll Mass Balance

Algal concentrations were important for predicting light attenuation, photolytic reactions of mercury, and mercury partitioning to biotic solids. The algal mass balance for algae in the epilimnion, $C_{algae}[t,1]$, and hypolimnion, $C_{algae}[t,2]$, are calculated as (Chapra, 2014):

$$\frac{dC_{algae}[t,1]}{dt} = \frac{Q_{inflow}[t]}{V[1]} Algae_{inflow} - \frac{Q_{outflow}[t]}{V[1]} C_{algae}[t,1] + \emptyset_{PAR}[t,1]\, \emptyset_{nutrients} k_{growth,ref} \theta_g^{T[t,1]-T_{ref,g}}\, C_{aglae}[t,1]$$

$$+ \frac{v_{thdp}[t]\, A[2]}{V[1]} \left(-C_{algae}[t,1] + C_{algae}[t,2]\right) - \frac{v_{setl,algae}[t]\, A[1]}{V[1]} C_{algae}[t,1]$$

$$- k_{mortality,ref} \theta_m^{T[t,1]-T_{ref,m}} C_{aglae}[t,1] \quad (29)$$

$$\frac{dC_{algae}[t,2]}{dt} = \emptyset_{PAR}[t,2]\, \emptyset_{nutrients} k_{growth,ref} \theta_g^{T[t,2]-T_{ref,g}}\, C_{aglae}[t,2] + \frac{v_{thdp}[t]\, A[2]}{V[2]} \left(C_{algae}[t,1] - C_{algae}[t,2]\right) + \frac{v_{setl,algae}\, A[1]}{V[2]} C_{algae}[t,1]$$

$$- \frac{v_{setl}[t]\, A[2]}{V[2]} C_{algae}[t,2] - k_{mortality,ref} \theta_m^{T[t,1]-T_{ref,m}} C_{aglae}[t,1] \quad (30)$$

The mass balance considers inflow, outflow, thermocline dispersion, settling, mortality rate, and growth. Algal concentrations in the sediments were assumed to be zero. The growth rate of algae is assumed to be limited by available PAR, nutrients, and temperature. The growth rate due to temperature, $k_{growth,ref}$, was set to a value of 0.52 day^{-1}, the mortality rate, $k_{mortality,ref}$, was 0.052 day^{-1}, the settling velocity, $v_{setl,algae}$, was set to 0.5 m day^{-1} (Chapra 2014; McDonald and Urban 2009). The nutrient growth factor is estimated based on the half-saturation constant for phosphorus:

$$\emptyset_{nutrients} = \frac{C_{phosphorus}}{C_{phosphorus} + K_{SP,phosphorus}} \quad (31)$$

where $C_{phosphorus}$ is the concentration of phosphorus of 5 µg P L^{-1} and $K_{SP,phosphorus}$ is the half-saturation concentration of phosphorus of 1 µg P L^{-1} (McDonald & Urban, 2009; Massey, 1970), both assumed to be annually constant due to limitation of available measured data. Algal growth limitation due to temperature in each of the compartments was parameterized using the theta expression where the reference growth rate, $k_{growth,ref}$, at reference temperature, $T_{ref,g}$, is multiplied by θ_g, the temperature correction coefficient (Chapra, 2014). The theta expression was also used to correct the reference mortality rate of the algae, $k_{mortality}$, for temperature. The mortality rate is the net loss of algae due to respiration, excretion, and grazing by zooplankton. For mercury partitioning, algal concentrations were converted to biotic solids concentrations using the ratio of carbon to chlorophyll-a of 40 mg C (mg chla)$^{-1}$ for Torch Lake (Urban unpub.).

2.3.6 Corrections for Ice Cover

There are three atmospheric sources of mercury that are influenced by ice cover and need to be corrected; the three inputs include air-water exchange, wet deposition, and dry deposition. The correction for ice cover is based on four different seasons: no ice cover, ice cover is forming, complete ice cover, and ice cover is melting. Maximum ice thickness was assumed to reach about one meter. Calendar dates for the changing of these seasons were initially chosen based on historical measurements of air temperature and water temperature and then were calibrated to fit the modeled water temperatures and thermocline dispersion rates.

Both wet and dry deposition were corrected for ice cover, such that the loading of deposition during ice cover is zero, or, rather, it accumulates on the ice. During spring melt, the accumulated deposition then becomes a loading to the lake. Daily wet deposition values were corrected prior to running the model. Since dry deposition is not based on daily measurements, the term, $f_{ddp}[t]$, was used to correct for ice cover. During complete ice cover, both wet and dry deposition are equal to zero ($f_{ddp}[t] = 0$). During no ice cover, wet deposition is equal to the daily measured wet deposition value and for dry deposition, $f_{ddp}[t] = 1$. During ice formation, dry deposition was corrected using a linear decrease of $f_{ddp}[t]$ from 1 to 0, and the amount of dry deposition accumulated is equal to $1 - f_{ddp}[t]$. Wet deposition was corrected similarly to precipitation.

2.3.7 Thermocline Dispersion

The thermocline dispersion velocity was calibrated to the heat budget and solids (phytoplankton and DOC) balances. Parameterization was based on four different seasons: stratification during ice cover and no ice cover, and mixing during ice formation and melting. The magnitude of the velocity was orders of magnitude larger during mixing than during stratification. A linear change of the velocity between seasons was too sudden for the numerical solvers to handle, and, to compensate, a quadratic function was used. The maximum velocity during mixing periods was used as the critical point, and the values at which the equation started and ended were the velocities for the beginning and ending of stratification. During stratification periods, the velocities remained constant. A smaller velocity was used for summer than for winter.

2.4 Mercury Model

2.4.1 Lake Mass Balance

The lake mercury model predicts concentrations for elemental, divalent, and methyl mercury in the lake compartments epilimnion, hypolimnion, and sediments. The model was initially derived from the U.S. Environmental Protection Agency's mercury model SERAFM (Knightes and Ambrose, 2006a; Knightes 2008). The model was altered for the non-steady state case to predict daily concentrations throughout a year. Further differences between this model and SERAFM are described below (Knightes and Ambrose, 2006a; Knightes, 2008). SERAFM categorized watershed runoff to include riparian and urban land types; this area is small in the region of the study and therefore is neglected by the model in this study. In SERAFM, burial and resuspension only occur in the particulate phase of mercury; this model considers all phases. This model also excludes mer-operon cleavage of methyl to elemental mercury; there was inadequate documentation in the literature on rates of this process, and thus only photodemethylation is considered to occur between the two mercury species. Methyl mercury can also be demethylated to divalent mercury. Methylation and demethylation in the sediments occurs in all phases in SERAFM, rather than just in the dissolved phase as considered by this model. Oxidation and reduction in SERAFM are broken into photo-catalyzed, dark, and biological components. For this model there is a single oxidation and reduction rate that is the sum of all these components. To compensate partially for the influence of photolysis, different rates are given to the water and sediments. Reduction in SERAFM additionally includes mercury hydroxide complexes as well as freely dissolved Hg(II); this model does not consider the inorganic speciation of dissolved Hg(II) apart from complexation with DOM. SERAFM includes speciation of mercury with hydroxide, chloride, and sulfide ligands. This model includes temperature corrections of reaction rates to simulate seasonality. SERAFM uses the parameterization of air-water exchange for atmospheric dry deposition of methyl and divalent mercury. Here, this loading is parameterized with dry deposition velocities multiplied by the air concentrations.

The overall mercury mass balance is represented as a system of ordinary differential equations (ODEs) below.

$$\frac{\partial}{\partial \mathrm{t}}\mathrm{HG} = \mathrm{K} \cdot \mathrm{HG} + \mathrm{W} \tag{32}$$

Each element in the matrix HG represents the mercury concentration in units of mg L^{-1}, indexed 1 through 9 for time "t", the day of the year.

$$\mathrm{HG} = \begin{pmatrix} \mathrm{HG}[\,\mathrm{t}, 1\,] \\ \vdots \\ \mathrm{HG}[\,\mathrm{t}, 9\,] \end{pmatrix} \tag{33}$$

The corresponding matrix index for each mercury species in each of the lake compartments is specified in Table 2.2.

Table 2.2. Defined indices for matrices in mercury mass balance equation

Index	Mercury Species	Compartment
1	Elemental	Epilimnion
2	Elemental	Hypolimnion
3	Elemental	Sediments
4	Divalent	Epilimnion
5	Divalent	Hypolimnion
6	Divalent	Sediments
7	Methyl	Epilimnion
8	Methyl	Hypolimnion
9	Methyl	Sediment

The matrix K is the net process rate between each of the mercury species, indexed 1 through 9, for time "t" occurring in the three lake compartments epilimnion, hypolimnion, and sediments. All process rates are in units of day^{-1}. The diagonal of this matrix is the loss term of each of the mercury species; each value is expressed as a negative number.

$$K = \begin{pmatrix} K[\,t,1,1] & \cdots & K[\,t,1,9\,] \\ \vdots & \ddots & \vdots \\ K[\,t,9,1] & \cdots & K[\,t,9,9] \end{pmatrix} \tag{34}$$

The net loading to each of the mercury species at time t is expressed in matrix W. These loadings consist of inputs to the epilimnion from the atmosphere, inflow from rivers, watershed runoff; and the input to the sediments from the deep sediments. Each element in this matrix has units of mg L^{-1} day^{-1}.

$$W = \begin{pmatrix} W[\,t,1\,] \\ \vdots \\ W[\,t,9\,] \end{pmatrix} \tag{35}$$

Matrices K and W are expressed as the sum of the following individual process matrices shown below.

$$K = K_{awxc} + K_{burl} + K_{dmth} + K_{dpdf} + K_{meth} + K_{outf} + K_{oxid} + K_{phdm} + K_{redn} + K_{resp} + K_{setl} + K_{ssdf} + K_{thdp} \tag{36}$$

$$W = W_{awxc} + W_{ddpT} + W_{dpdf} + W_{infl} + W_{wdpT} \tag{37}$$

Parameterization for each of these processes for matrix K is illustrated in Table 2.3 and for matrix W in Table 2.4. The definitions, values, and units for all the variables used in this table can be found in Table 6.1. Illustration of these processes occurring in the lake is shown as a diagram in Figure 2.2. Mercury species are defined as follows: elemental (Hg0), methyl (MeHg), divalent (Hg2), reactive gaseous (RGM), and particulate bound (PBM) mercury. Mercury species followed by a dash and the letter "D" or "P" denote dissolved and particulate, respectively.

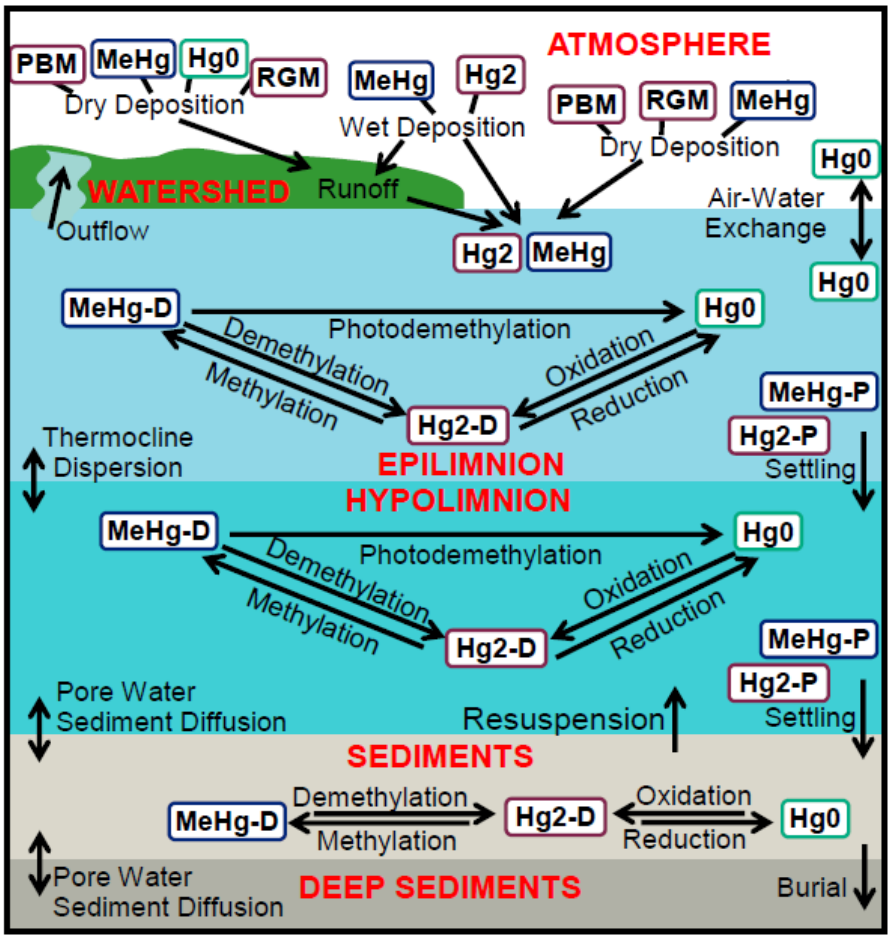

Figure 2.2. Diagram of in-lake mercury cycling used to parameterize the model.

Table 2.3. Parameterization and description of process matrices, K

Process and Description	Parameterization
Air-water exchange of elemental mercury (volatilization)	$K_{awx}[t,1,1] = -f_{dissolved}[t,1]\frac{v_{awxc}[t]\,A[1]}{V[1]}$
Burial of mercury from surface sediments to deep sediments	$K_{burial}[t,i,i] = -\frac{v_{burl}A[3]}{V[3]}$
Demethylation (MeHg -> Hg2)	$K_{dmth}[t,i,j] = \pm(f_{dissolved}[t,j] + f_{DOC}[t,j])\,k_{dmth,ref}[n_i]\theta^{T[t,n_i]-T_{ref}}$
Diffusion from surface sediments to deep sediments	$K_{dpdf}[t,i,i] = -f_{dissolved}[t,i]\frac{D_w[t,Hg_i]\,A[3]\emptyset_{dpsed}}{z_{dpsed}\,V[3]}$
Methylation (Hg2 -> MeHg)	$K_{meth}[t,i,j] = \pm f_{dissolved}[t,j]\,k_{meth,ref}[n_i]\theta^{T[t,n_i]-T_{ref}}$
Outflow	$K_{outf}[t,i,i] = -\frac{Q_{ouflow}[t]}{V[1]}$
Oxidation (Hg0 -> Hg2)	$K_{oxid}[t,i,j] = \pm f_{dissolved}[t,j]\,k_{oxid,ref}[n_i]\theta^{T[t,n_i]-T_{ref}}$
Photodemethylation (MeHg -> Hg0)	$K_{phdm}[t,i,j] = \pm f_{dissolved}[t,j]\,k_{phdm,ref}\emptyset_{PAR}[t,n_i]$
Reduction (Hg2 -> Hg0)	$K_{redn}[t,i,j] = \pm f_{dissolved}[t,j]\,k_{redn,ref}[n_i]\,\theta^{T[t,n_i]-T_{ref}}$
Resuspension of mercury from the surface sediments to hypolimnion	$K_{resp}[t,i,j] = \pm\frac{v_{resp}A[3]}{V[n_i]}$
Settling of mercury from epilimnion to hypolimnion and from hypolimnion to surface sediments	$K_{setl}[t,i,j] = \pm f_{particulate}[t,j]\frac{v_{setl}\,A[n_j]}{V[n_i]}$
Diffusion between surface sediments and hypolimnion	$K_{ssdf}[t,i,j] = \pm f_{dissolved}[t,j]\frac{D_w[t,Hg_i]\,A[3]\emptyset_{ssed}}{z_{ssed}\,V[n_i]}$
Thermocline Dispersion between epilimnion and hypolimnion	$K_{thdp}[t,i,j] = \pm\frac{v_{thdp}[t]\,A[2]}{V[n_i]}$

Table 2.4. Parameterization and description of loading matrices, W

Process and Description	Parameterization
Air-water exchange of elemental mercury, loading	$W_{awx}[t,i] = \frac{v_{awxc}[t]\ Hg_{atm}[1]\ A[1]}{K_{Henry}[t]\ V[1]}$
Diffusion loading from deep to surface sediments*	$W_{dpdf}[t,i] = -f_{dissolved,dpsed}[t,Hg_i]\frac{D_w[t,Hg_i]\ A[3]\emptyset_{dpsed}}{z_{dpsed}\ V[3]} Hg_{dpsed}[Hg_i]$
Watershed runoff of dry deposition***	$W_{ddpc}[t,i] = \frac{f_{ddp}[t]\ v_{ddpc}[Hg_i]\ Hg_{atm}[Hg_i]\ A[1]}{V[1]}$
Dry deposition to the lake surface**	$W_{ddps}[t,i] = \frac{f_{ddp}[t]\ v_{ddps}[Hg_i]\ RC[Hg_i]Hg_{atm}[Hg_i]\ A_{watershed}}{V[1]}$
Total dry deposition for runoff and to the lake surface**	$W_{ddpT}[t,i] = W_{ddpc}[t,i] + W_{ddps}[t,i]$
Total wet and dry deposition to lake surface	$W_{dpls}[t,i] = W_{ddps}[t,i] + W_{wdps}[t,i]$
Inflow of mercury from rivers	$W_{infl}[t,4] = \frac{Hg_{inflow}Q_{inflow}[t]}{V[1]}$
Total watershed runoff from dry and wet deposition	$W_{rnff}[t,i] = W_{ddpc}[t,i] + W_{wdpc}[t,i]$
Watershed runoff of wet deposition***	$W_{wdpc}[t,i] = \frac{f_{THg,wdp}[Hg_i]\ RC[Hg_i]\ THg_{wdp}\ A_{watershed}}{V[1]}$
Wet Deposition to the lake surface***	$W_{wdps}[t,i] = \frac{f_{THg,wdp}[Hg_i]\ THg_{wdp}\ A[1]}{V[1]}$
Total wet deposition from runoff and to the lake surface***	$W_{wdpT}[t,i] = W_{wdpc}[t,i] + W_{wdps}[t,i]$

*The index i only represents loadings to mercury species in the surface sediment layer of the lake, where i = 3, 6, or 9.

**The index i only represents loadings to mercury species in the epilimnion layer of the lake, where i = 1, 4 or 7.

***The index i only represents loadings to divalent and methyl mercury in the epilimnion layer of the lake, where i = 4 or 7. For elemental mercury, the parameterization for air-water exchange is used instead. For divalent mercury (index i = 4), dry deposition is expressed as the sum of dry deposition from particulate and reactive gaseous mercury, both having different dry deposition velocities. For dry deposition of divalent mercury to the catchment that runs off to the lake, the dry deposition of elemental mercury is included as it is assumed that elemental mercury is immediately oxidized to divalent and runs off as divalent.

For temperature-dependent reaction rates, the empirical theta formulation was used to correct the reaction rate at the reference temperature to the daily estimated temperature for the lake compartment. In the case when the indices i and j are equal, K is negative; when indices i and j are not equal, K is positive. The indices n_i and n_j can be 1, 2, or 3 depending on the layer which is associated with index i or j; these indices do not depend on any of the mercury species. For an index of i = 1, 4, and 7 the index $n_i = 1$ and denotes the epilimnion layer; for an index of i = 2, 5, and 8 the index n_i (value of 2) indicates the hypolimnion layer; and for an index of i = 3, 6, and 9 the index n_i (value of 3) indicates the surface sediment layer. For example, if i = 1 then $V[n_i]$ would be the volume of the epilimnion layer. Similarly, $A[n_i]$ or $A[n_j]$ when $n_i = 1$ would be the area of the lake surface; when $n_i = 2$, $A[n_i]$ is the area of the thermocline; and the surface area of the surface sediments is for $A[n_i]$ when $n_i = 3$. The indices for Hg_i and Hg_j can be 1, 2, or 3. The index corresponds to the species of mercury and does not depend on any of the compartments. E.g., Hg_i or $Hg_j = 1$ represents elemental mercury corresponding with indices i or j = 1, 2, or 3; Hg_i or $Hg_j = 2$ denotes divalent mercury corresponding with the indices i or j = 4, 5, or 6; and Hg_i or $Hg_j = 3$ represents methyl mercury corresponding with the indices i or j = 7, 8, or 9. For example, when index i = 1 and $D_w[Hg_i] = [1]$ this would be the aqueous diffusivity of elemental mercury.

2.4.2 Air-Water Exchange

Air-water exchange was parameterized for only the dry deposition of elemental mercury to the lake surface. Dry deposition to the lake catchment and dry deposition of methyl and divalent mercury to the lake surface were parameterized using a dry deposition velocity. This differed from SERAFM which applied air-water exchange for divalent and methyl mercury to the lake surface. This was altered due to the poor support in the literature for the required parameters. Furthermore, the parameterization of the air-water exchange was altered for elemental mercury to reflect freshwater and calculations that had more thorough support by literature. The overall air-water exchange mass transfer coefficient, v_{awxc}, has units of m day^{-1} and is derived by the two-film theory (Whitman 1923):

$$v_{awxc}[t] = (1 - f_{ice}) \left(\frac{1}{v_w[t]} + \frac{1}{v_a[t]\, K'_{Henry}[t]} \right)^{-1} \quad (38)$$

For elemental mercury, air-water exchange is water-phase controlled (Brezonik 2004; Poissant 2000) such that the term $v_w << v_a K_{Henry}$. The term $(1 - f_{ice})$ is used as a correction for ice cover on the lake surface and ranges from 0 to 1. When there is complete ice cover, f_{ice} is equal to a value of 1 and prevents air-water exchange from occurring. During summer when there is no ice cover, f_{ice} is equal to 0, and air-water exchange is allowed to happen. During freezing and thawing of the ice, f_{ice} increases linearly to 1 and decreases linearly to 0, respectively. The dimensionless Henry's Law Constant for elemental mercury is defined as (Gradfeldt 2003):

$$K'_{Henry}[t] = \frac{MW_{H_2O} K_{Henry}[t]\, 10^{-6}}{\rho_{H_2O}[t]\, R\, (T[t,1]+273.15)} \quad (39)$$

For simplification, the assumption is made that the temperature of the water surface is equal to the temperature of the epilimnion. A unit conversion of 10^{-6} is used as a conversion from cm^3 to m^3. The Henry's Law Constant in units of atmospheres is defined with the following equation (Sanemasa 1975):

$$K_{Henry}[t] = 10^{-\frac{1078}{T[t,1]+273.15}+6.250} \quad (40)$$

The water-side mass transfer coefficient for elemental mercury is expressed as a relationship with the mass transfer coefficient for carbon dioxide (CO_2) using a ratio between the Schmidt numbers of elemental mercury and CO_2 (Hornbuckle 1994; Wanninkhoff 1992):

$$v_w[t] = v_{w,CO_2}[t] \left(\frac{SC_{Hg0}[t]}{SC_{CO_2}[t]} \right)^{-0.5} \quad (41)$$

The mass-transfer coefficient for CO_2 is defined as a function of the wind velocity in units of m s^{-1} measured at a height of 10 m above the lake surface (Hornbuckle 1994; Wanninkhoff 1992; Poissant 2000):

$$v_{w,CO_2}[t] = 0.24 \cdot (\ 0.45\ (U_{w10m}[t])^{1.64}\ ) \quad (42)$$

The coefficient is converted from units of cm hr^{-1} to units of m day^{-1} by multiplying the expression by 0.24. For freshwater, the Schmidt number for CO_2 is determined from an empirical relationship with temperature (Wanninkhof 2014):

$$SC_{CO_2}[t] = 1923.6 - 125.06\ T[t,1] + 4.3773\ T[t,1]^2 - 0.085681\ T[t,1]^3 + 0.00070284\ T[t,1]^4 \quad (43)$$

The Schmidt Number for elemental mercury is also given for freshwater and is calculated as the ratio of the kinematic viscosity of water to the molecular diffusion coefficient of elemental mercury (Wanninkhof 1992). The molecular diffusion coefficient D'_w (units of $cm^2\ s^{-1}$) of elemental mercury in freshwater as a function of water temperature is defined using the activation energy of mercury (Kuss 2009):

$$D'_w[t,1] = 0.01768 \exp\left(-\frac{16.98}{R\ (T[t,1]+273.15)\ (101.325)}\right) \quad (44)$$

The coefficient 101.325 is used for unit conversion. Because divalent mercury has the same molecular weight as elemental mercury, the molecular diffusivity coefficients are equal. The term D_w is D'_w converted to units of $m^2\ day^{-1}$. The kinematic viscosity of freshwater, v_w is the ratio of the dynamic viscosity, μ_{H_2O} (g $cm^{-1}\ s^{-1}$) to the density of water, ρ_{H_2O} (g cm^{-3}). Both terms are related to the temperature of water using the equations below (Crittenden et al. 2012):

$$\rho_{H_2O}[t] = \frac{\left(\begin{array}{c}999.83952+16.945176\ T[t,1]-7.9870401\times10^{-3}(T[t,1])^2-46.170461\times10^{-6}(T[t,1])^3\\ +105.56302\times10^{-9}(T[t,1])^4-280.54253\times10^{-12}(T[t,1])^5\end{array}\right)}{(1+16.879850\times10^{-3}\ T[t,1])\cdot10^3} \quad (45)$$

$$\mu_{H_2O}[t] = 10^{-2}\ 10^{\left(\frac{1301}{998.333+8.1855(T[t,1]-20)+0.00585\ (T[t,1]-20)^2}-1.30223\right)} \quad (46)$$

The air-side mass transfer coefficient is related to the mass transfer coefficient for water vapor and the ratio of the molecular diffusivity coefficient of water and mercury in air (Hornbuckle 1994; Smith 1980):

$$v_a[t] = v_{a,H_2O}[t]\left(\frac{MW_{H_2O}}{MW_{Hg0}}\right)^{0.5} \quad (47)$$

The air side mass transfer coefficient for water vapor is defined below (Hornbuckle 1994; Schwarzenbach 1993). The coefficient of 864 is used to convert from units of cm s^{-1} to m day^{-1}.

$$v_{a,H_2O}[t] = 864 \cdot \left(0.2\ U_{w,10m}[t] + 0.3\right) \quad (48)$$

2.4.3 Deposition

Total mercury wet deposition flux values, THg_{wdp}, were taken from the National Atmospheric Deposition Program's Mercury Deposition Network. The data were collected as weekly total deposition for a ten-year span (2004-2013), and for the purpose of this model, were converted to daily values. Since there were no monitoring sites near the study location, an average of the nearest sites was used. These sites were Trout Lake (WI36), Seney National Wildlife Refuge-Headquarters (MI48), and Popple River (WI09). There was no input of wet deposition to the lake during ice cover; rather, deposition was accumulated on the ice. This accumulation was calculated the same way as the precipitation. During spring melt, the accumulated wet deposition slowly became an input to the lake as the ice melted. This phenomenon was calculated in the same way as precipitation volume was accumulated in ice.

2.4.4 Runoff Coefficients

Only a portion of the deposition falling to the watershed runs off, and the remainder is stored; the runoff coefficient is used to account for this. The overall runoff coefficient for mercury is adjusted for the amount of wetland to upland land cover in the watershed. This was an adjustment made from SERFAM; SERAFM considered runoff from impervious, wetland, riparian, and upland areas. For Torch Lake, the area of impervious surfaces and riparian zones in the total watershed was negligible. For elemental and divalent mercury, the runoff coefficients for upland and wetland are equal. For methyl mercury, the runoff coefficient for wetlands is a much larger value than the runoff coefficient for upland. The upland runoff coefficient was set to the same value of 0.05 for all mercury species. The wetland runoff coefficient is 0.2 for divalent mercury and 4.9 for methyl mercury.

$$RC[Hg_i] = f_{watershed,wetland} RC_{wetland}[Hg_i] + f_{watershed,upland}\, RC_{upland}[Hg_i] \quad (49)$$

2.4.5 Partitioning

Mercury exists in multiple phases in each compartment of the lake. These phases include the truly dissolved phase, the dissolved organic carbon-bound phase, and the particle bound phase. Following the convention in SERAFM, particles in the water column are further divided into biotic and abiotic solids. For each lake compartment, the total concentration of each form of Hg can be expressed as the sum of the concentrations associated with each phase. A common formulation is to take the ratio of concentration in a phase to the total concentration in a lake compartment and denote it as the fraction of that form of Hg in that phase. Concentrations of all non-aqueous phases, C_{solid}, are expressed in units of mg phase L^{-1}. Each fraction, f, is calculated from the partition coefficient, $K_{d,solid}$, and the concentration of the respective phase as shown below:

$$f_{dissolved}[t,i] = \frac{1}{1+\sum K_{d,solid}[Hg_i]C_{solid}[t,n_i]} \quad (50)$$

$$f_{solid}[t,i] = f_{dissolved}[t,i]\ K_{d,solid}[Hg_i]\ C_{solid}[t,n_i] \quad (51)$$

The particulate fraction is the sum of the biotic and abiotic solids fractions and is the fraction of mercury that will settle out of the water column. The solids ratio in the sediments is calculated as the ratio of the bulk density to the porosity of the sediments. In the deep sediments, it is assumed that the only two phases of mercury are the dissolved and the particle-bound (sediment) phase. Partition coefficients were taken from Knightes (2008) and Allison (2005).

2.5 Predictions for mercury concentrations in fish

Mercury concentrations in fish tissue are estimated in units of ppm using the equation presented in SERAFM as a function of the bioaccumulation factor (BAF) and the annual average methyl mercury concentration in the water column (Knightes, 2008):

$$\mathrm{Hg_{fish}} = \mathrm{BAF_{fish}MeHg_{lake}} \tag{52}$$

Bioaccumulation factors are the ratios of mercury concentrations in fish tissue to mercury concentrations in water. Two trophic levels of fish were considered; piscivorous and mixed-feeding fish. A distribution of the estimated mercury concentrations in fish were estimated from the 5th, 25th, 50th, 75th and 95th percentiles for the BAF values as shown in Table 2.5 (Knightes, 2008):

Table 2.5. Mercury Bioaccumulation Factors (BAF) in fish

Percentile	Mixed feeders $10^6 \frac{(\mu g\ Hg_{fish})(L\ water)}{(kg\ fish\ tissue)(\mu g\ Hg_{water})}$	Piscivorous Fish $10^6 \frac{(\mu g\ Hg_{fish})(L\ water)}{(kg\ fish\ tissue)(\mu g\ Hg_{water})}$
5th	0.46	3.3
25th	0.95	5.0
50th	1.6	6.8
75th	2.6	9.2
95th	5.4	14

This calculation using BAFs is a steady-state, linear relationship. Non-steady state mass balance models have been developed for predicting mercury concentrations in fish that consider factors such as the uptake of mercury in fish gills, half-life of mercury in the fish, fish growth rate, and excretion of mercury from the fish (Håkanson 2000; Barber 2008a, 2008b). This steady state calculation also ignores the time lag required for fish uptake and elimination of mercury to reach steady state (Paterson, 2017); for walleye populations the lag time can be 3 to 7 years (Barber 2008a, 2008b; Perlinger et al. 2018). However, the steady state assumption was found to provide comparable and as accurate predictions as the non-steady state case for chemicals with a log $K_{ow} < 5$ according to the study by Barber 2008a. K_{ow} is defined as the octanol-water partition coefficient. This condition is valid for methyl mercury, the bioavailable form of mercury; methyl mercury has a log K_{ow} ranging from 1.7 to 2.54 (Environment Canada 2002).

2.6 Validation Methods

2.6.1 Calibration

Historical measurements for Torch Lake included total mercury in the epilimnion and hypolimnion (Great Lakes Environmental Center, 2003); total mercury, methyl mercury, and ratio of methyl mercury to total mercury in the in the upper one-centimeter layer of the sediments (Kerfoot et al., 2016); and total mercury in fish. Since there are no available measurements for methyl mercury in the water column, an alternative for calibration of these concentrations was to use the methyl mercury concentrations in the fish to calculate the mercury concentrations in the water column and compare these values to measurements. Measurements of mercury concentrations in walleye, northern pike, white sucker, and smallmouth bass were available from the Michigan Department of Environmental Quality's Fish Contaminant Program. Calibration consisted of reparametrizing the model and altering parameter values and rate constants within the range of values supported by literature to achieve model estimates comparable with measured concentrations. Once the model predictions were within the range of measured values, the sensitivity and uncertainty analyses were performed to obtain a better understanding of the ranges for parameters that could be tuned for further calibration.

Calibration of the seasonal models also was performed using measurements (GLEC 2003; MDEQ 2018; Urban, unpub.). The DOC inflow was calibrated to reflect measured concentrations and seasonality in the river inflow to Torch Lake. The chlorophyll-a concentrations were calibrated by altering values of the growth and death rates. FLake Global is an open source, online modeling system for lakes that takes as input the lake's longitude, latitude, mean depth, and transparency (Mironov, 2008; Kirillin, 2011). The model provides estimates for ice thickness, water temperature (surface and bottom), depth of the mixed layer, and surface energy fluxes that were used for validating parameters for which there were no measurements. Calibration of the seasonal models focused on thermocline dispersion rates, the dates for ice formation and melting, and the dates for changes in thermal mixing. For the seasonal model, validation consisted only of calibration.

2.6.2 Sensitivity Analysis

Sensitivity analysis consisted of changing each model parameter separately by 10% of its original value. Parameter sensitivity was quantified as the magnitude (percent) of change in resultant mercury concentrations from their original values. For each parameter the model was run multiple times until the initial mercury concentrations converged, such that the mercury concentrations on January 1st and December 31st were about 0% different.

2.6.3 Uncertainty Analysis

Parameters chosen for the uncertainty analysis were based on parameters that were least well supported by literature and to which the model predictions were found to be most sensitive. To apply the Bayesian MCMC method to the mercury aqueous model, RStan version 2.17.3 was used (Stan Development Team, 2017; Guo et al., 2018). RStan is a free source package available for R. The 3.3.1 version of R was used. RStan was installed according to instructions (https://github.com/stan-dev/rstan/wiki/Installing-RStan-on-Windows) and also required that the package RTools version 3.4.0.1964 (Ripley and Murdoch, 2017) was installed. The model was run using Michigan Technological University's remote cluster Portage. The remote cluster also had the advantage of running parallel cores, where each chain ran on its own core.

The model was organized similarly to other ODE models (Carpenter, 2014; Margossian and Gillespie, 2017). The code was organized such that there was an external R code that would extract values from input text files (variable constants and initial values) and would structure this input for RStan. The R code called the "stan" function which would call the uncertainty analysis to be performed. Once the uncertainty analysis had finished, the R code would then save the results to a text file and the environments to an ".Rdata" file. The output from RStan included the posterior mean, standard deviation, percentiles (2.5, 25, 50, 75, and 97.5%), Rhat, and the effective sample size for each parameter.

The stan function required several inputs. These inputs included the path of the ".stan" code, the input data, the number of iterations, the number of warm-up iterations, the number of chains, and the number of cores. The number of iterations were chosen such that the model had converged, the samples were random, and the samples did not depend on the initial values. Due to the complexity of the model and the numerous MCMC iterations, the number of parameters that could be sampled was limited, and only the mercury concentrations during a period of five days (rather than the annual 365 days) were sampled. Seasonal, daily values that would normally change over the five-day duration, were set to constant values averaged over this five-day period. These parameters were outflow, wind speed, temperature, thermocline dispersion, light attenuation, DOC, chlorophyll a, and wet deposition. To ensure that the samples were not dependent on their initial values, a burn-in period was used such that half of the iterations were discarded and considered to be "warm-up" iterations. For the initial values for the parameter samples, Stan was able to take either user defined values or Stan could randomly choose values; random initial values with different initial values for each chain were chosen to avoid bias. Model variables not included in the uncertainty analysis and assumed to be well constrained or effectively constant were set to their normal model values.

In the ".stan" file, the calculations for the mercury model were translated into the Stan language. The Stan code contained several sections as follows: functions, data, transformed data, parameters, model, and generated quantities. Input data were defined in the "data" section. In the "parameter" section, the parameters were defined by data type (real numbers) and their ranges were defined. For the parameter (variable theta), the lower

limit was defined as zero and the upper limit was set at a value of 100. The parameter sampled for the standard deviation of the mercury concentrations (variable sigma) was also defined in the parameter section and had a lower limit of zero. The prior distributions and likelihood functions were specified in the "model" section of the Stan code.

Priors for the mercury model input parameters were assumed to have an uninformative distribution and were not explicitly specified in the Stan model. Uninformative distribution was assumed because there is little known about these parameters; the values of the parameters range over several orders of magnitude. The predicted mercury concentrations were assumed to have a normal distribution with a mean concentration set to a value measured in Torch Lake. There was only one measurement in the epilimnion and hypolimnion for total mercury that was used for the prior mean of divalent mercury in the epilimnion and hypolimnion (GLEC 2003). There were three measurements each for methyl and total mercury that were used for the prior means of methyl and divalent mercury in the sediments (Kerfoot et al. 2016). There were no measurements for methyl mercury in the epilimnion and hypolimnion, but the theoretical methyl mercury concentration in the water column could be back calculated using the measurements of mercury in fish from the Michigan Department of Environmental Quality's Fish Contaminant Program and the bioaccumulation factors (Knightes 2008; Knightes and Ambrose 2006a). The initial manually calibrated methyl mercury concentrations were used to calculate the magnitude of difference in the epilimnion and hypolimnion based on the water column concentrations. Prior means for elemental mercury concentrations in the epilimnion, hypolimnion, and sediments were based on what mean concentrations of lakes in a similar region, Northern Wisconsin by Watras et al. (1995). The standard deviation of the mercury concentrations was assumed to follow a Cauchy distribution. Three chains (each with the same number of iterations) were chosen for the purpose of checking for convergence; if convergence has occurred the chains all end on nearly the posterior mean for all parameters and predicted mercury concentrations. The posterior means of the predicted mercury concentrations, ideally, would converge to the measured (or prior) mercury concentrations. By doing this, Stan is calibrating the model parameters with the objective of the predicted mercury concentrations converging to be equivalent to the measured concentrations. The objective function used by Stan is variational, called evidence lower bound (ELBO) and is calculated using Monte Carlo integration via the Automatic Differential Variational Inference (ADVI) (Stan Development Team, 2017).

The function in the Stan file consisted of all the calculations needed for the mass balance and the actual ODE mass balance itself. The stiff ODE solver "bdf integrator" developed for the RStan language was used (Stan Development Team, 2017). Inputs for the ODE solver included the function containing the calculations for the ODE, the initial values, the initial time, the observation times (as an array), input data (as an array; both real and integer values), the relative tolerance, the absolute tolerance, and the maximum step size. The relative tolerance, absolute tolerance, and maximum number of samples were changed from their default values to 1×10^{-11}, 1×10^{-14}, and 1×10^{8} respectively. These were changed to increase the accuracy of the model. The initial values, or initial mercury concentrations for the mass balance, were taken from the model runs after calibration had

been performed on the model. The ODE solver was called in both the model and generated quantity sections.

To check for convergence several tests were used which included diagnostics built into RStan and in another R package, coda (Plummer et al., 2016). Stan's built in convergence tests consist of R-hat, the effective sample size, and a trace plot. A value of R-hat less than 1.1 indicates the chains have converged (Margossian and Gillespie, 2017). The effective sample size is an estimate of effective samples from the total iterations for all chains combined. If there is no correlation between samples and chains, the value of the effective sample size should equal the number of iterations (Plummer et al., 2016). The trace plot is a graphical illustration for the value of the parameter as a function of the number of iterations. It was used as a visualization to check if the samples were getting stuck at any certain values and if there was thorough mixing of the samples.

The coda package included further diagnostics such as the Geweke Diagnostic, Gelman and Rubin's Diagnostic, autocorrelations of the samples, trace plots, and the effective sample size. The function for calculating the effective sample size was advantageous in coda because it gave the ability to look at the effective size for the chains combined and individually. The Geweke Diagnostic is a test of whether the mean of the first 10% and last 50% of samples after the burn-in period are equal. If the output value is less than two, this suggests that the samples are well mixed (Wang, 2016).

3 Results

3.1 Water Quality Model Results

3.1.1 Water Balance

Inflow and outflow followed similar trends and peaked during spring melt runoff (see Figure 3.1). Precipitation and evaporation did not occur during ice cover months of December to about April.

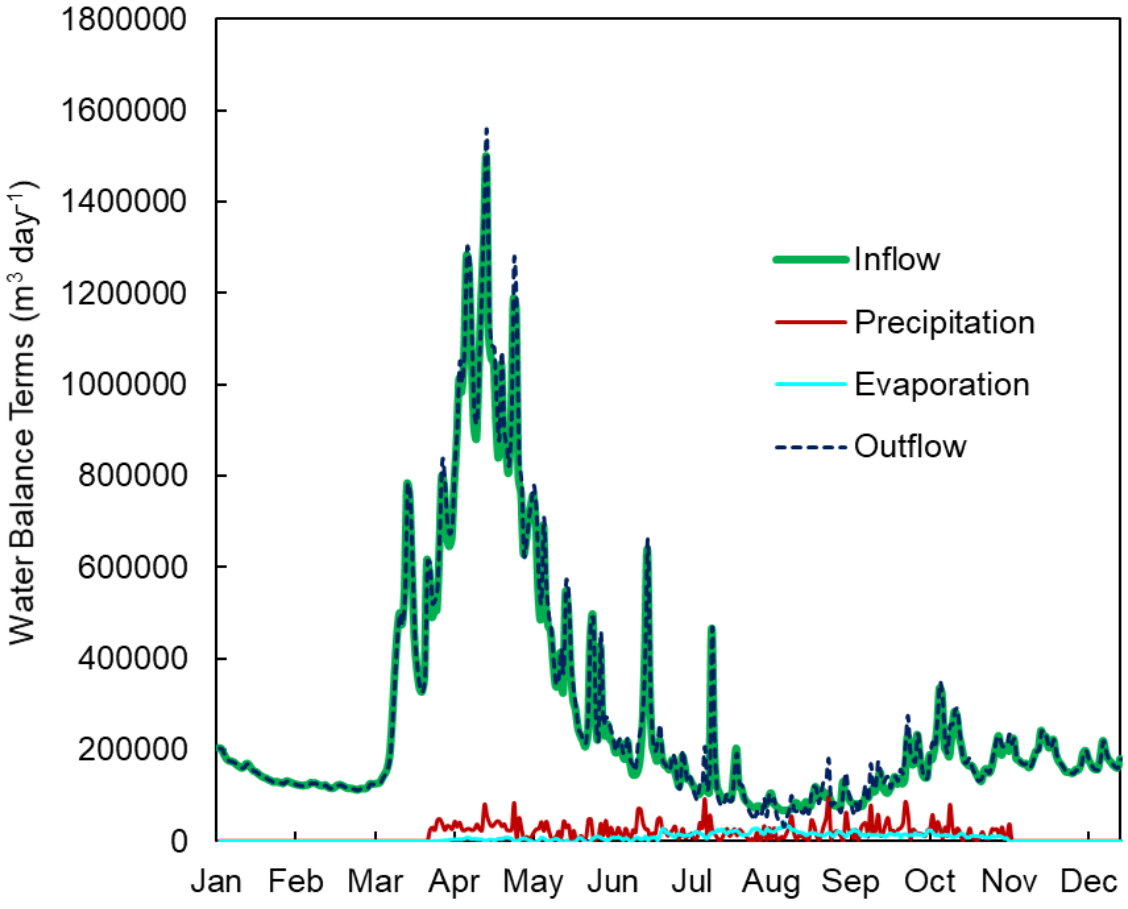

Figure 3.1. Water balance over one year. Values represent ten-year averages.

3.1.2 Heat Budget

Modeled epilimnion temperatures underestimated measured values (see Figure 3.2 below). However, because these measured epilimnion temperatures are warmer than the average decadal air temperatures, no further calibration was performed. During spring mixing the modeled lake temperatures appeared to have a slight decrease; this is likely a result of the exclusion of the latent heat required to melt the ice. Inflow temperatures were calculated to be proportional to air temperatures (Mohseni et al., 1998; Mohseni et al., 2003). One measured inflow temperature of 22°C was available for June 28, 2002 (GLEC, 2003); modeled inflow temperatures underestimated this value.

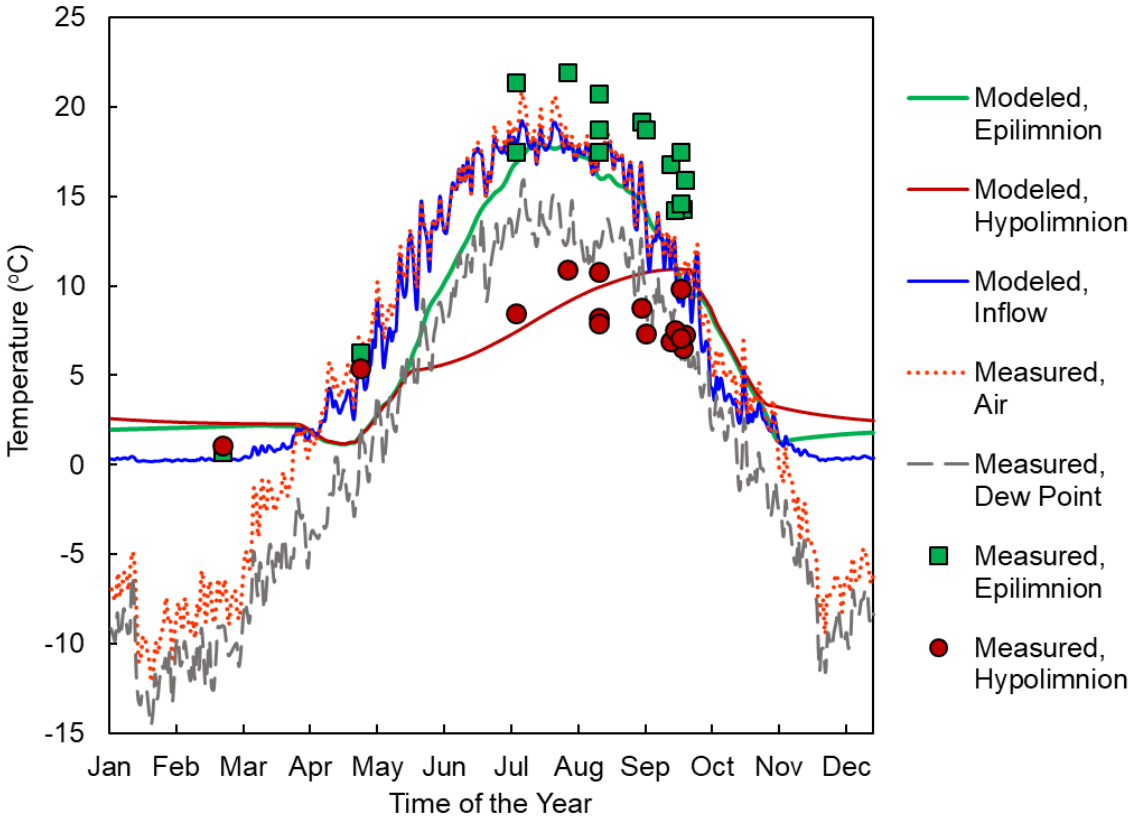

Figure 3.2. Measured and modeled temperatures in water and air for Torch Lake. Measured values were taken from GLEC 2003, Weather Underground historical data for Lake Linden, MI and MDEQ 2018.

USGS does not measure temperature at the Trap Rock River gauging site. The USGS does measure temperature at the Sturgeon River gauging station which is in a similar region as Torch Lake, in the southern part of the Keweenaw Peninsula (USGS, 2018). These temperatures over the ten-year time frame (2004 to 2013) are compared with the modeled inflow temperatures shown in Figure 3.3. The modeled inflow temperatures are at the low range of the temperatures from the Sturgeon River. There are no measurements in the Sturgeon River to compare during October to March. The air temperatures measured near the Trap Rock River are also lower than the measured temperatures in the Sturgeon River. Since the modeled inflow temperatures are estimates from the air temperature, the modeled inflow temperature cannot be increased to be warmer then the air temperatures.

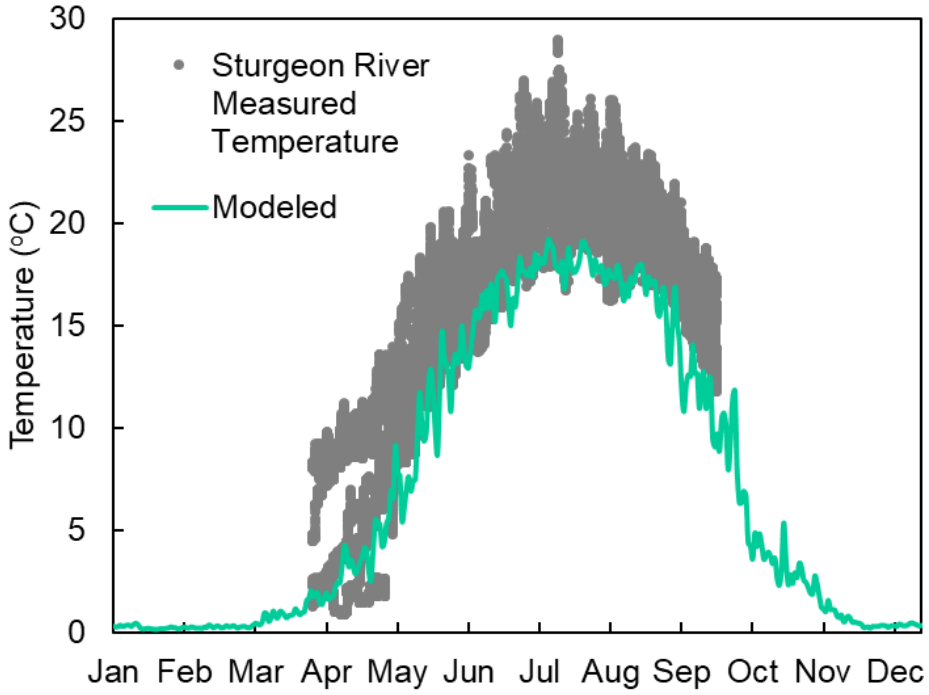

Figure 3.3. Modeled inflow temperatures for the Trap Rock River compared to temperatures in the Sturgeon River.

3.1.3 DOC Mass Balance

Modeled inflow DOC concentrations peaked in spring melt runoff and had minimum values in winter (see Figure 3.4). These concentrations fell within the range of the measured inflow DOC concentrations (Urban, unpub.; GLEC, 2003), although the measured concentrations were highly variable. Modeled concentrations in the epilimnion and hypolimnion were nearly constant throughout the year. Concentrations peaked after spring snowmelt, and the lake layers diverged slightly during summer and fall. Modeled and measured concentrations in the epilimnion and hypolimnion (Urban, unpub.; GLEC, 2003) also were within range of each other.

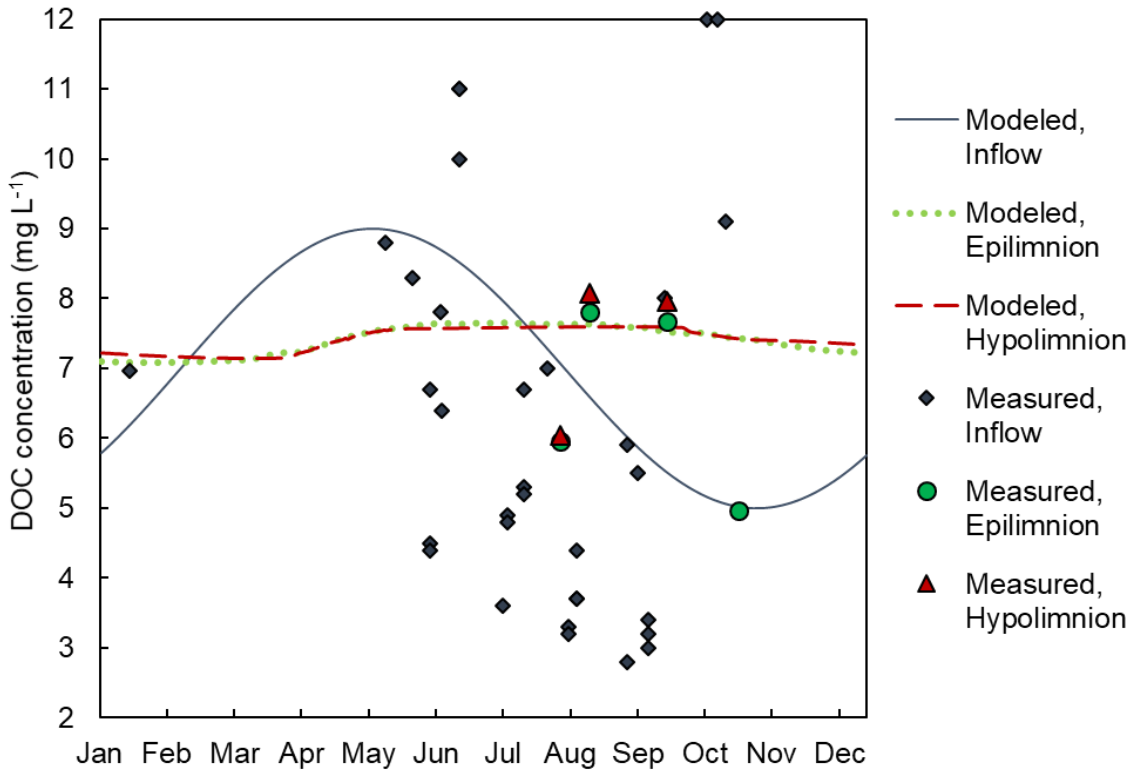

Figure 3.4. Annual DOC measured and modeled concentrations in Torch Lake.

3.1.4 Chlorophyll-a Mass Balance

Chlorophyll-a predicted concentrations peaked during late August; concentrations in the epilimnion reached 2.6 µg L^{-1} (Figure 3.5). In general, predicted concentrations are within the range of reported measurements from MDEQ, 2018 and Urban, unpub. Modeled and measured concentrations show a similar time of onset of mixing in late September.

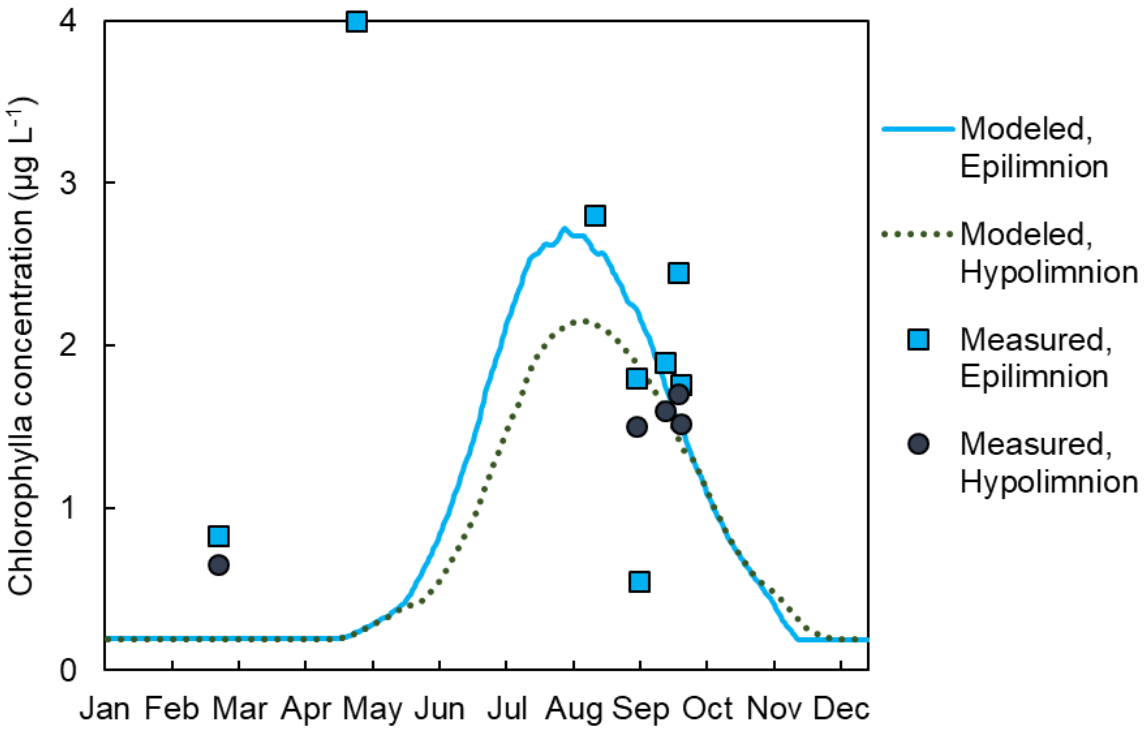

Figure 3.5. Chlorophyll A Concentrations for Torch Lake over a year duration.

3.2 Mercury Model Results

3.2.1 Lake Mercury Model Results

The mercury model was run with the posterior means of the model input parameters from the uncertainty analysis, which is further discussed later. As shown in Figure 3.6 below, there is seasonality in predicted mercury concentrations. During spring and fall mixing, mercury concentrations in the epilimnion and hypolimnion are equal. The hypolimnion concentrations are about 1.3 times larger than the epilimnion during stratification. Seasonal changes are driven by two effects of ice cover. First, mercury accumulated on top of the ice from wet and dry deposition slowly becomes an input during spring melt and causes concentrations to increase. Concentrations then decline as gas exchange and settling remove the mercury from the water column. In winter, reduced inputs combined with ongoing losses through settling and outflow lead to mercury depletion. For all mercury species, the hypolimnion has higher mercury concentrations than the epilimnion during stratification periods as a result of release from sediments in the hypolimnion and release from the epilimnion into the atmosphere.

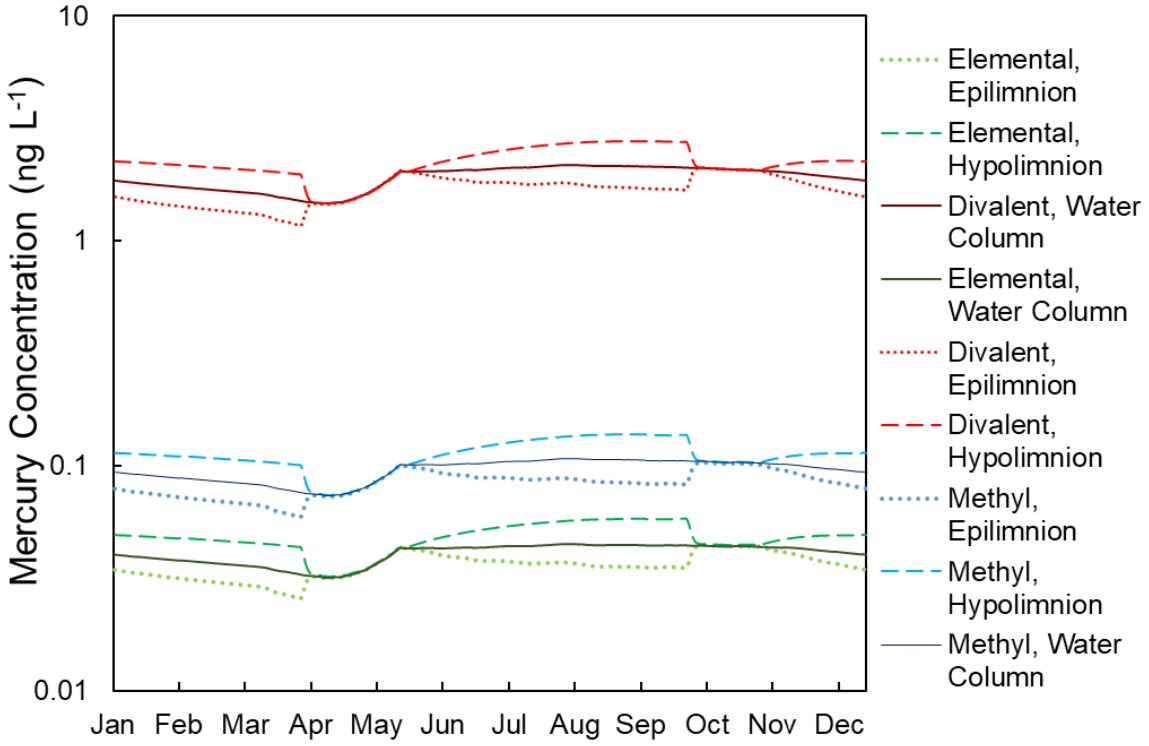

Figure 3.6. Annual divalent, methyl, and elemental mercury concentrations predicted for Torch Lake.

The Great Lakes Environmental Center (2003) sampled Torch Lake in August of 2002 and measured total mercury to be 0.8 ng L^{-1} in the epilimnion and 1.6 ng L^{-1} in the hypolimnion. These measurements are within the range of modeled total mercury concentrations as shown in Figure 3.7. The modeled epilimnion overestimates the measured slightly; since there is only one measurement available there was no further calibration performed. The box and whiskers show the 5th and 95th percentiles about the annual median modeled total mercury concentrations in the epilimnion (on the left in green) and hypolimnion (on the right in blue). The blue line parallel with the x-axis is the measured hypolimnion concentration, and in green is the measured epilimnion concentration. Both measured and model concentrations agree that the hypolimnion has higher concentrations than the epilimnion.

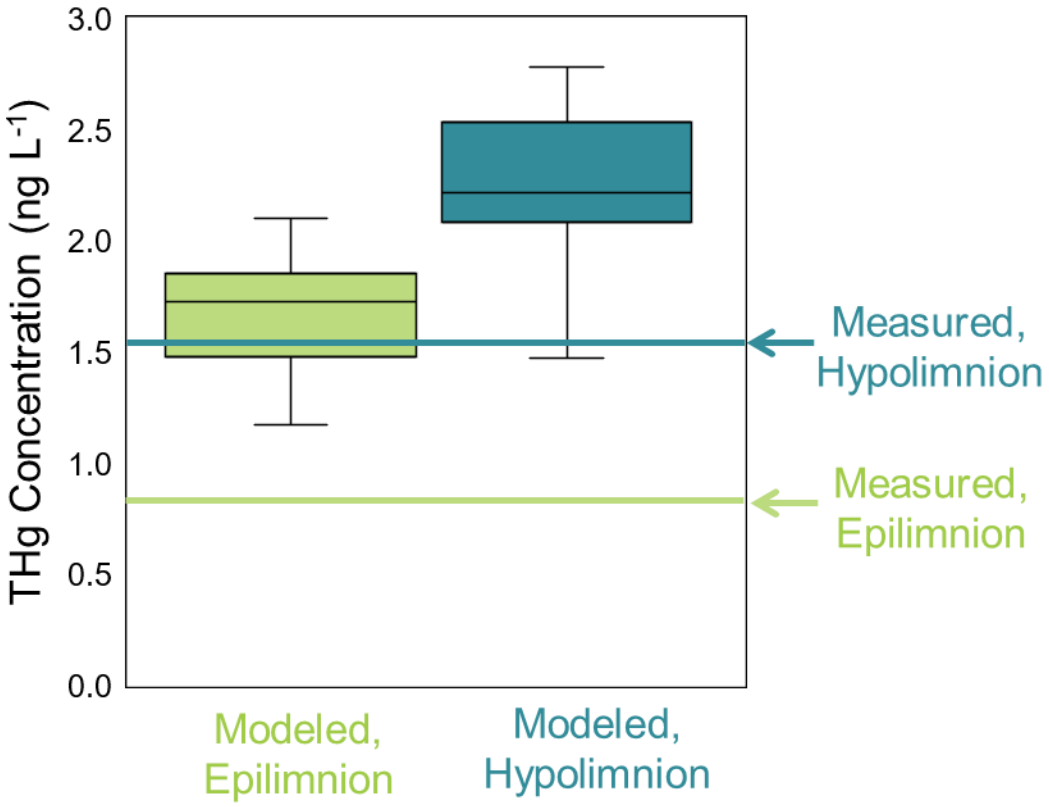

Figure 3.7. Comparison of total mercury concentrations modeled and measured in Torch Lake.

The ratio of methyl to total mercury in the upper one-centimeter layer of the sediments was predicted by the model to be about 0.11% while measured values averaged 0.12%. Average elemental mercury concentrations in sediments were predicted to be about 3.3 ng kg^{-1}. Predicted methyl mercury concentrations are shown in the right graph and total mercury on the left graph of Figure 3.8 with the 5^{th} and 95^{th} percentiles about the annual median modeled concentrations. The points show the three measurements available from two core samples taken in Torch Lake for the upper, first centimeter (Kerfoot et al., 2016).

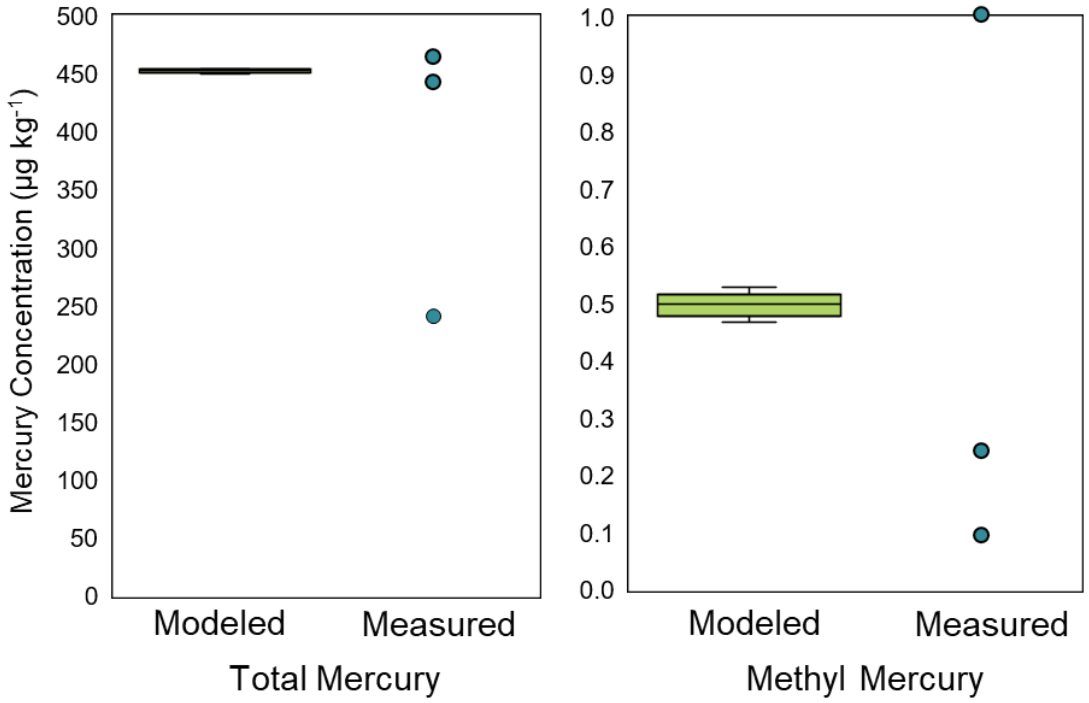

Figure 3.8. Comparison of modeled and measured total and methyl concentrations in sediment as dry weight.

Measurements for elemental and methyl mercury are not available for Torch Lake. However, in 1993 measurements were made in 23 northern lakes in Vilas County, Wisconsin (Watras et al., 1995). These results are used as a comparison for annual averaged mercury concentrations in similar regional lakes (see Table 3.1). These were not used for calibration, but rather for comparison with measured ranges for lakes in a similar region. The Watras et al. (1995) study did not measure mercury partitioned to DOC, and this is assumed to be part of dissolved concentrations. The modeled DOC-partitioned mercury was added to the dissolved phase for comparison.

Table 3.1. Modeled lake mercury concentrations compared with measurements in northern Wisconsin lakes.

Mercury	Fraction	Epilimnion - Surface Concentrations (ng L^{-1})	
		Modeled	Reported by Watras et al., 1995
Total	Total	1.8 (1.3 - 2.3)	1.48 (0.15 - 4.79)
	Dissolved	1.7 (1.2 - 2.1)	1.2 (0.23 - 4.5)
	Particulate	0.12 (0.074 - 0.16)	0.37 (0.02 - 1.22)
Methyl	Total	0.084 (0.059 - 0.10)	0.27 (0.04 - 2.2)
	Dissolved	0.079 (0.056 - 0.10)	0.16 (0.012 - 0.83)
	Particulate	0.0051 (0.0031 - 0.0070)	0.06 (0.005 - 0.24)
Elemental	Total	0.036 (0.026 - 0.044)	0.04 (0.002 - 0.14)

Daily process rates were totaled annually and are shown in Table 3.2. Transformation processes (reduction, oxidation, methylation, and demethylation) dominated the mass balance by a couple of orders of magnitude. Divalent mercury dry deposition to the catchment was 215 g yr^{-1} with 22 g yr^{-1} reactive gaseous mercury, 12 g yr^{-1} particulate bound mercury, and 181 g yr^{-1} elemental mercury. For divalent mercury, dry deposition to the lake totaled 2.5 g yr^{-1}comprising 1.6 g yr^{-1} reactive gaseous mercury and 0.89 g yr^{-1} particulate bound mercury.

Table 3.2. Model process rates (g yr^{-1}) summed annually for Torch Lake.

Process	Epilimnion			Hypolimnion			Sediments		
	Hg0	Hg2	MeHg	Hg0	Hg2	MeHg	Hg0	Hg2	MeHg
Air-Water Exchange	-112								
Air-Water Exchange	20.6								
Burial							-0.000950	-131	-0.144
Demethylation		46236	-46236		36147	-36147		48.0	-48.0
Dry Deposition to Catchment		215	0.977						
Dry Deposition to Lake Surface		2.50	0.0071						
Methylation		-46234	46234		-36161	36161		-30.0	30.0
Outflow	-3.55	-166	-8.29						
Oxidation	-19656	19656		-15452	15452		-278	278	
Photode-methylation	1.44		-1.44	1.64E-07		-1.64 E-07	0		0
Pore-Water Surface Sediment Diffusion				-2.83	-49.8	-1.75	2.83	49.8	1.75
Pore-Water Surface Sediment Diffusion				19.0	295	1.61	-19.0	-295	-1.61
Pore-Water Deep Sediment Diffusion							-0.528	-8.18	-0.0448
Pore-Water Deep Sediment Diffusion							0	3.87	0.0361
Reduction	19744	-19744		15442	-15442		295	-295	
Resuspension				0.000240	33.1	0.0364	-0.000240	-33.1	-0.0364
Settling	0	-370	-16.2	0	370	16.2			
Settling				0	-414	-18.1	0	414	18.1
Thermocline Dispersion	-158	-7412	-369	158	7412	369			
Thermocline Dispersion	164	7664	381	-164	-7664	-381			
Wet Deposition to Catchment	0	99.4	15.3						
Wet Deposition to Lake Surface	0	73.0	1.11						

3.2.2 Predictions of Mercury in Fish

Predicted mercury concentrations in mixed-feeding and piscivorous fish overlap with measurements for northern pike, smallmouth bass, white sucker, and walleye in Torch Lake from the Michigan Department of Environmental Quality's Fish Contaminant Program. A box and whiskers plot with the 5th and 95th percentiles about the median is shown in Figure 3.9. Measured fish concentrations were normalized to the median length for each of the species (northern pike - 65 cm, smallmouth bass - 39 cm, white sucker - 41 cm, and Walleye - 52 cm); this reduces some of the variability caused by different sized fish being caught in each of the four years of collection (1988, 2000, 2007, and 2013).

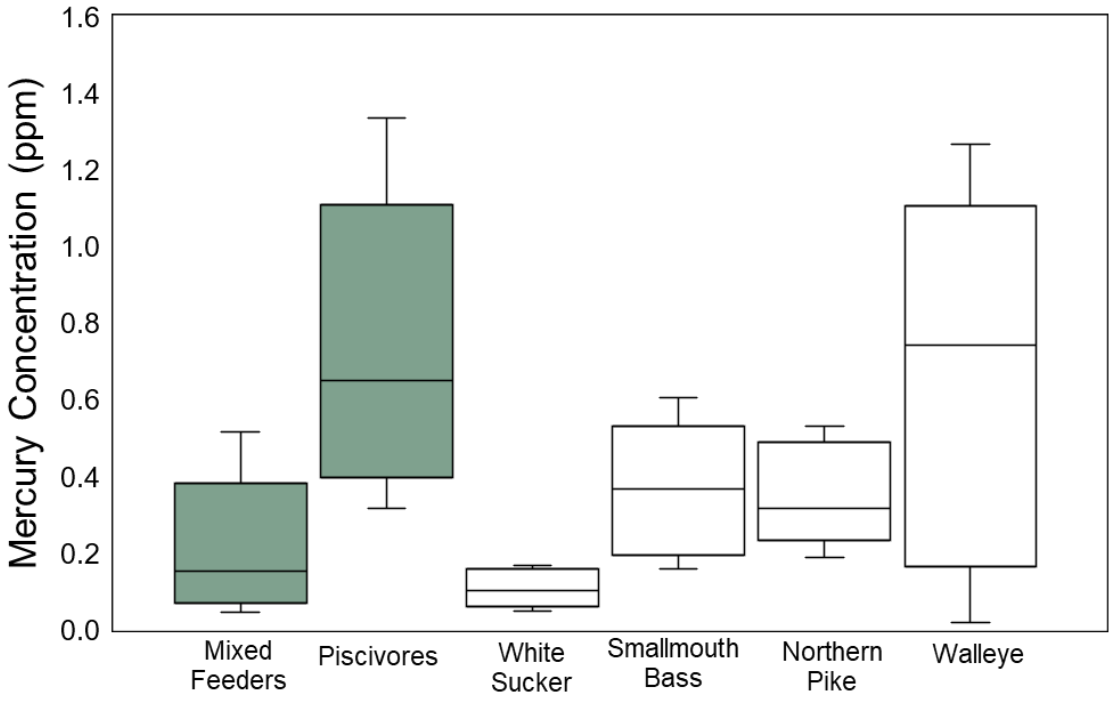

Figure 3.9. Modeled (on the left in green) and measured (on the right in white) concentrations in Torch Lake.

3.3 Sensitivity Analysis Results

It is clear that the model was sensitive to some mercury parameters, but not to others. Results are shown in Figure 3.10 for 28 of the parameters; a total of 70 model parameters were tested for model sensitivity. The change of mercury concentrations, expressed as a percentage, on the x-axis of the graph is the overall maximum change (an absolute value of positive and negative changes) of all mercury species concentrations in all compartments. The results for all parameters are summarized in Table 6.2 of the Appendix. Overall the most influential parameters, when altered by an increase of 10%, caused changes in mercury concentrations of less than 10%. The most sensitive parameters, i.e., those causing > 8% change in mercury concentration, include oxidation in the sediments, reduction in the sediments, methylation in the water, demethylation in the water and sediments, the methyl mercury DOC partitioning coefficient, and the methyl mercury sediment partitioning coefficient. The next tier of influential parameters (those causing changes of 5-8% in Hg concentrations) included oxidation in the water, reduction in the water, methylation in the sediments, area of the watershed, area of the sediments, settling velocity, DOC concentration in the sediments, divalent mercury sediment partitioning coefficient, and the solids ratio in the surface sediments.

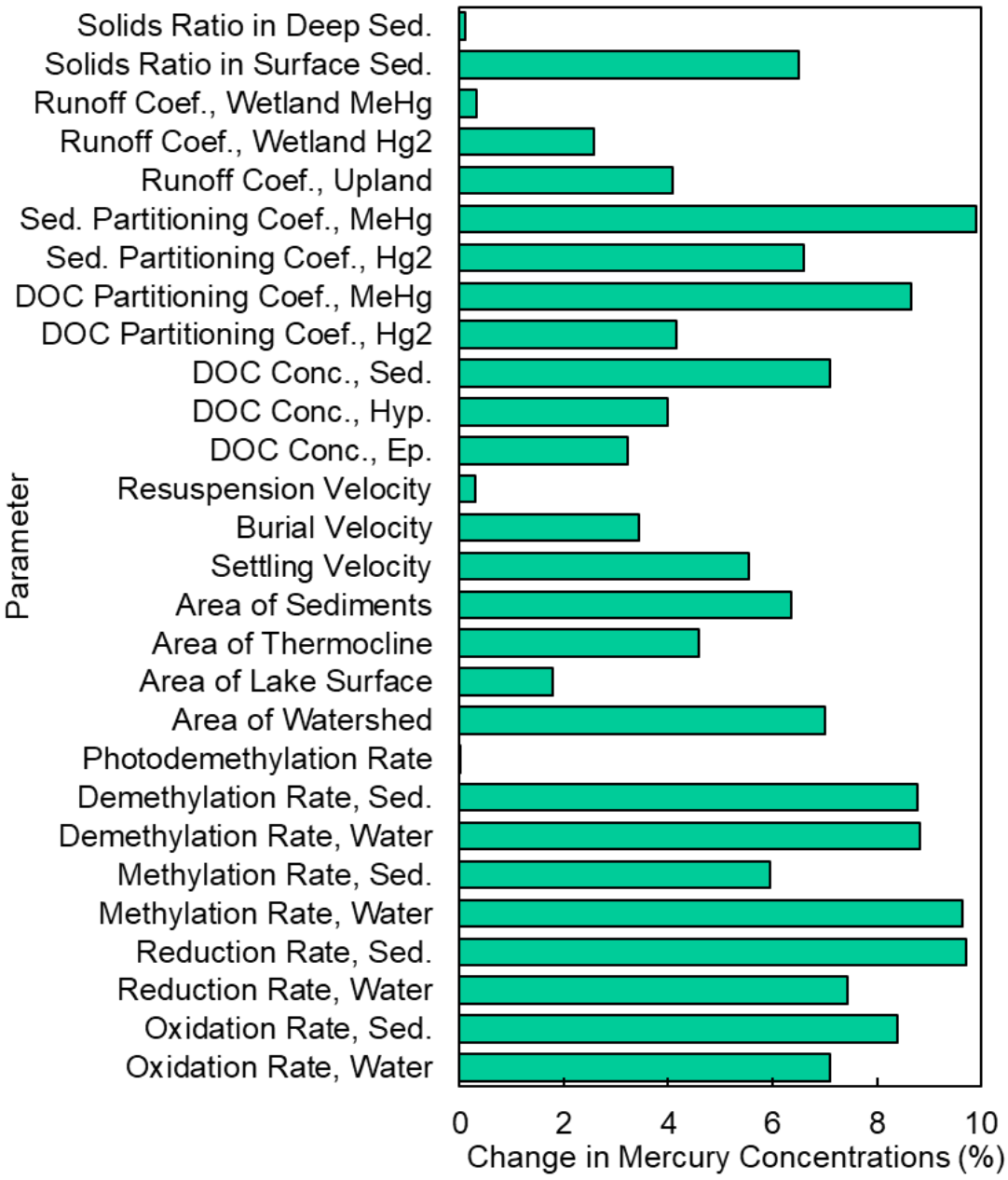

Figure 3.10. Sensitivity analysis results for the resultant change in mercury concentrations from changing the values of the model parameters.

3.4 Uncertainty Analysis Results

The uncertainty analysis was run for 5000 iterations (2500 iterations were warm-ups). The diagnostics (effective sample size, Rhat, and the Geweke Diagnostic) for convergence are shown in Table 3.3. The Geweke Diagnostic is less than the absolute value of two for all parameters and the Rhat values are also within an absolute value of 1.1. Two parameters, the methylation and demethylation rate in the water column, only had an effective sample size of three; whereas the other two water reaction rates (oxidation and reduction) had effective sample sizes of 343. The sediment reaction rates all had effective sample sizes over 500. All parameters had an Rhat value of less than 1.1 except for methylation and demethylation in the water column.

Table 3.3. Posterior means of the model parameters (day^{-1}) and convergence diagnostics.

Parameter	Posterior Mean	Standard Deviation	Effective Sample Size	Rhat	Geweke Diagnostic
Oxidation, Water	65.0	24.6	343	1.00	-0.0091
Oxidation, Sediments	65.2	25.3	568	1.00	-0.79
Reduction, Water	1.99	0.757	343	1.00	-0.014
Reduction, Sediments	4.46	1.70	554	1.00	-0.76
Methylation, Water	4.66	4.90	3	1.91	0.016
Methylation, Sediments	0.634	0.453	543	1.01	-0.13
Demethylation, Water	35.7	37.4	3	1.92	0.013
Demethylation, Sediments	9.05	13.2	552	1.01	0.0077

Similar to the mercury model input parameters, the convergence of the mercury species concentrations in the water column has worse convergence than in the sediments (Table 3.4). Notably, the epilimnion concentrations had a small effective sample size of less than four and the value for Rhat was greater than a value of one for all three mercury species. Divalent and methyl mercury had smaller effective sample sizes for the hypolimnion, but the Rhat value for both was about one indicating convergence.

Table 3.4. Convergence diagnostics of the predicted mercury concentrations.

Mercury Species Concentration	Effective Sample Size	Rhat
Elemental, Epilimnion	4	1.6
Elemental, Hypolimnion	7043	1.0
Elemental, Sediments	2010	1.0
Divalent, Epilimnion	3	2.8
Divalent, Hypolimnion	96	1.0
Divalent, Sediments	1942	1.0
Methyl, Epilimnion	3	2.8
Methyl, Hypolimnion	93	1.0
Methyl, Sediments	2614	1.0

Trace plots were also used for a visual diagnostic of convergence. The model parameter with the best and worst, in terms of reaching convergence, trace plots are shown in Figure 3.11. The trace plots for all eight parameters sampled are in Figure 6.1 and Figure 6.2 of Appendix A. Trace plots show the parameter value sampled as a function of the iteration number. Iterations before 2500 are warm-up iterations; they are discarded and are not used for calculating the posterior distribution. The methylation and demethylation rates in the water column showed the worst convergence in terms of the trace plot and the best convergence could be observed with the parameters: reduction, oxidation, methylation, and demethylation rates in the sediments. "Stickiness" can be observed in the trace plot of the methylation rate in the water for the second chain as it is stuck on a very small value. Results indicate that the water column parameters are more uncertain than the sediments; this could be due to the fact that there are fewer processes occurring in the sediments.

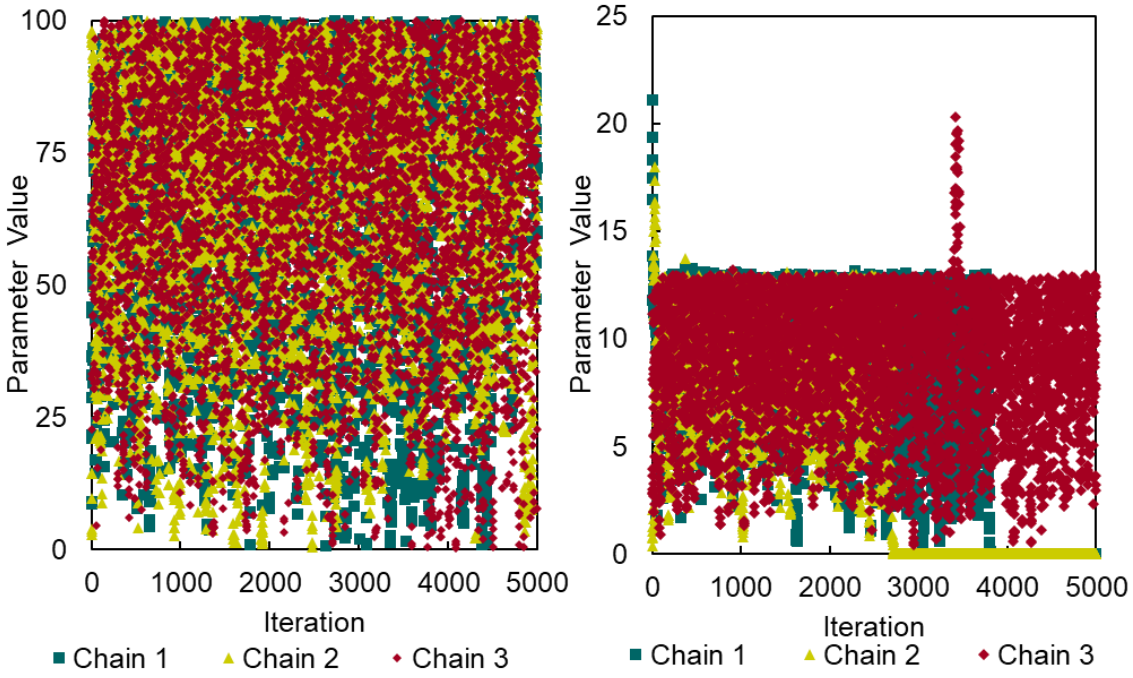

Figure 3.11. Trace plots of the parameter value as a function of the iterations after the warm-up period for oxidation in the sediments (a) and methylation in the water column (b).

The ranges in the model parameters defined by the Bayesian MCMC sampling compared to the ranges of values reported in literature are shown in Figure 3.12 below. The model values are the initial calibration values used for the model to obtain predicted mercury concentrations within the range of measured. It should be noted that during calibration, a model value for demethylation in the sediments of 100 (which was larger than what was found in literature) was needed for calibration. At the high range of values reported in literature was a demethylation rate of about 40 day^{-1} from Heyes et al. (2006) for the Bay of Fundy between New Brunswick and Nova Scotia, Canada. Comparing model values and posterior means for the model parameters, the posterior mean values do not get as low as what is reported in literature and are generally at the upper range or above of what has been reported in literature. This could mean that there are numerical accuracy errors with the model that prevent estimates from getting this low.

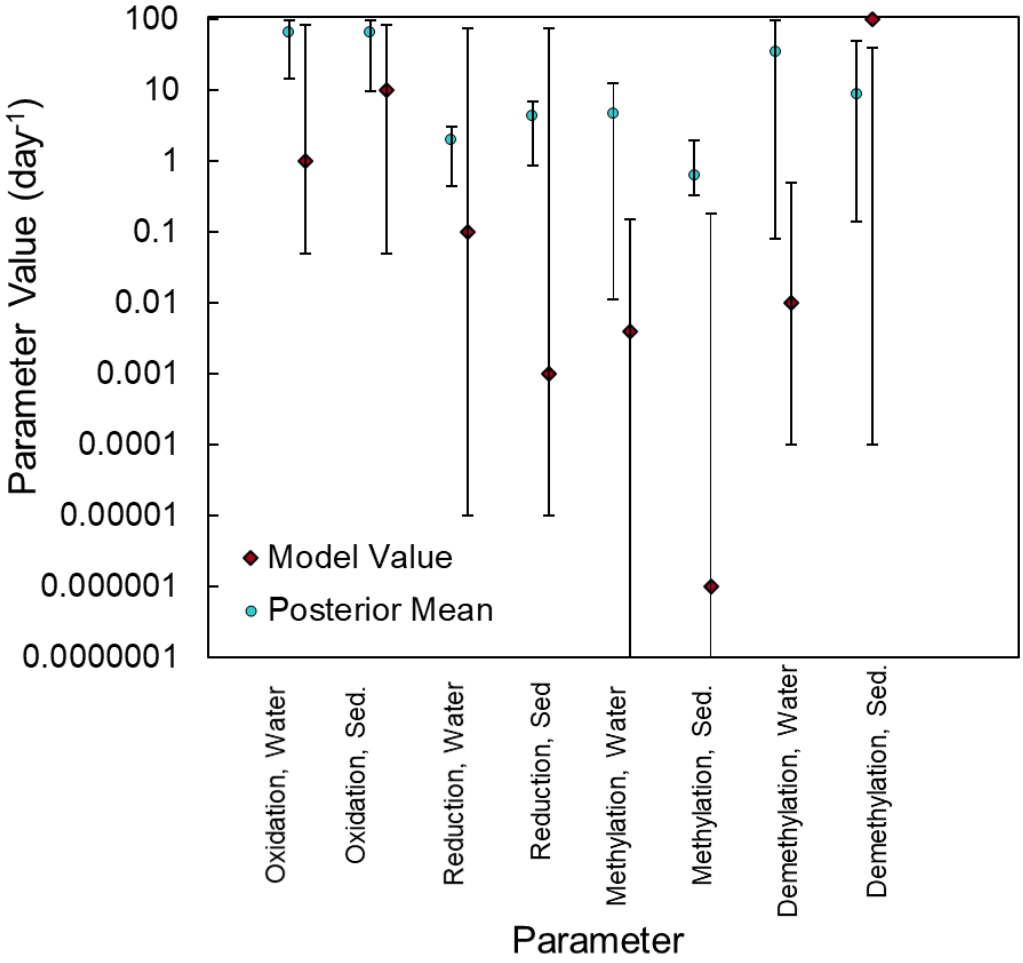

Figure 3.12. Posterior mean and model values compared. Error bars around the model value indicate the range of values reported in literature. Error bars around the posterior mean indicate the 2.5th and 97.5th percentiles about the posterior mean.

4 Discussion and Conclusions

4.1 Mercury Cycling in Torch Lake

4.1.1 In-Lake Cycling of Mercury in Torch Lake

The sources of mercury to Torch Lake's water column were dry deposition (to the lake surface and runoff from the catchment), wet deposition (to the lake surface and runoff from the catchment), air-water exchange to and from the lake surface for elemental mercury, resuspension, and pore-water diffusion from the sediments. Illustrations of the magnitudes of the process rates in the mercury mass balance are shown for total mercury in Figure 4.1, methyl mercury in Figure 4.2, elemental mercury in Figure 4.3, and transformations of the three mercury species in Figure 4.4.

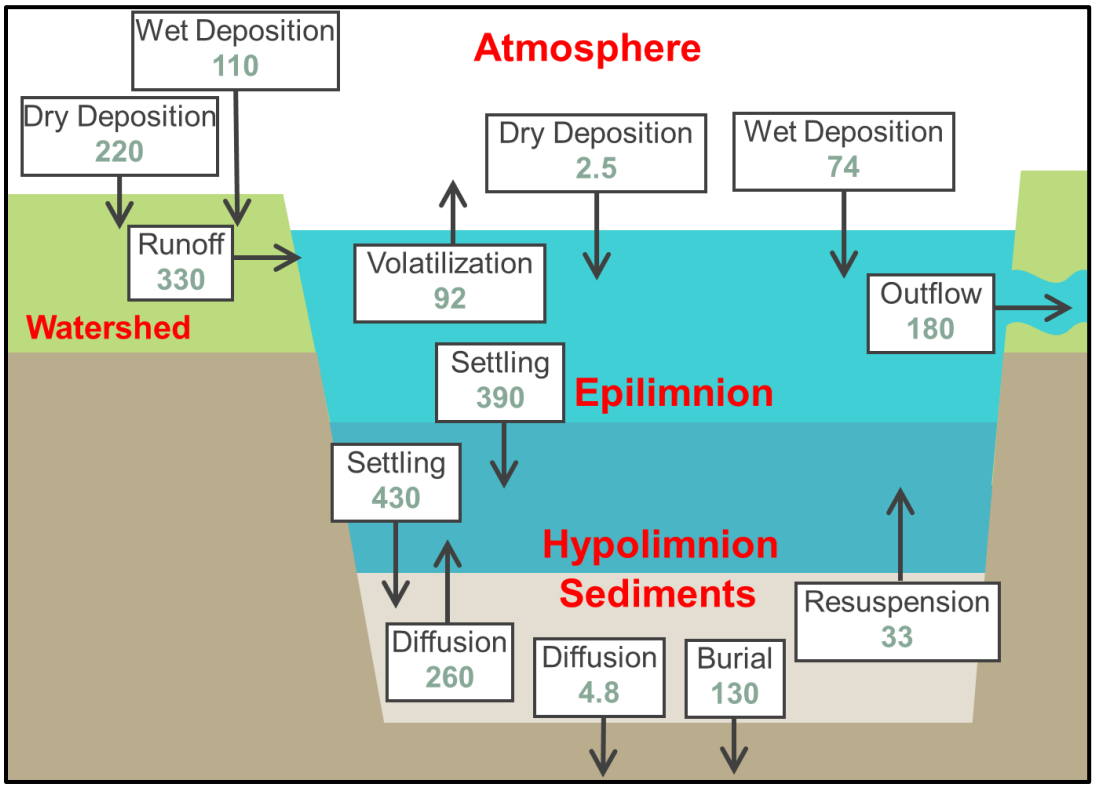

Figure 4.1. Magnitude of the process rates (g yr^{-1}) for the mass balance of total mercury.

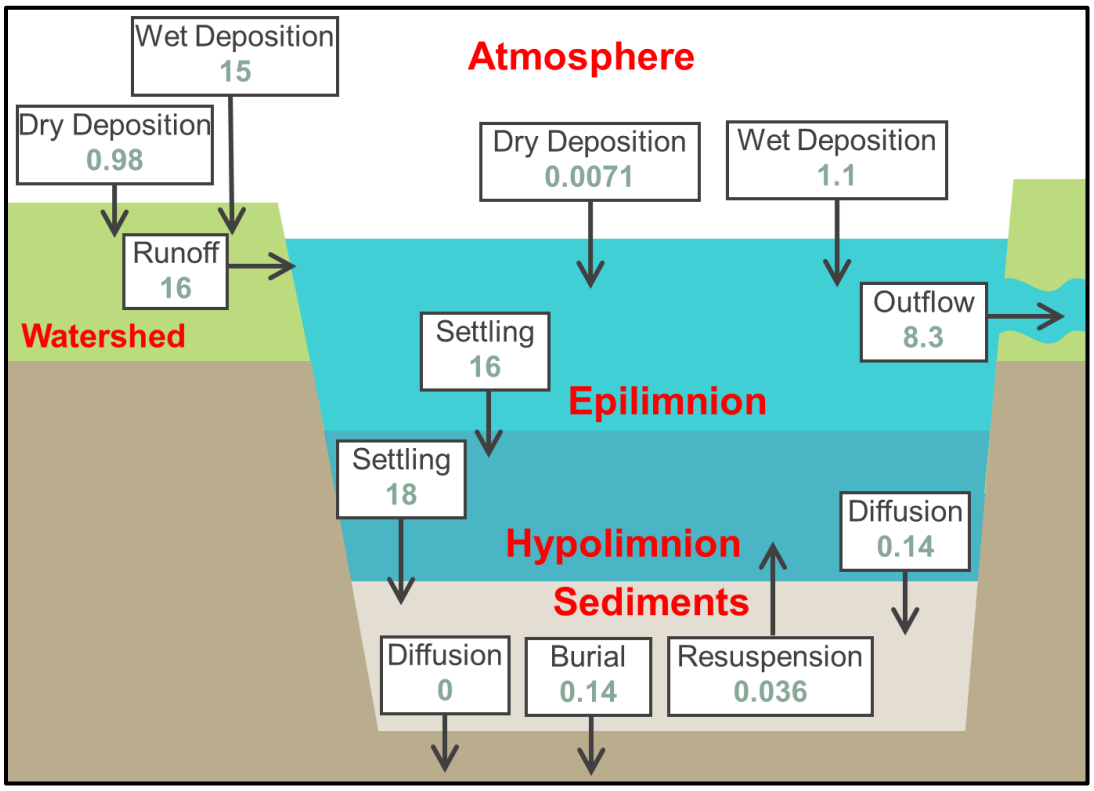

Figure 4.2. Magnitude of the process rates (g yr^{-1}) for the mass balance of methyl mercury.

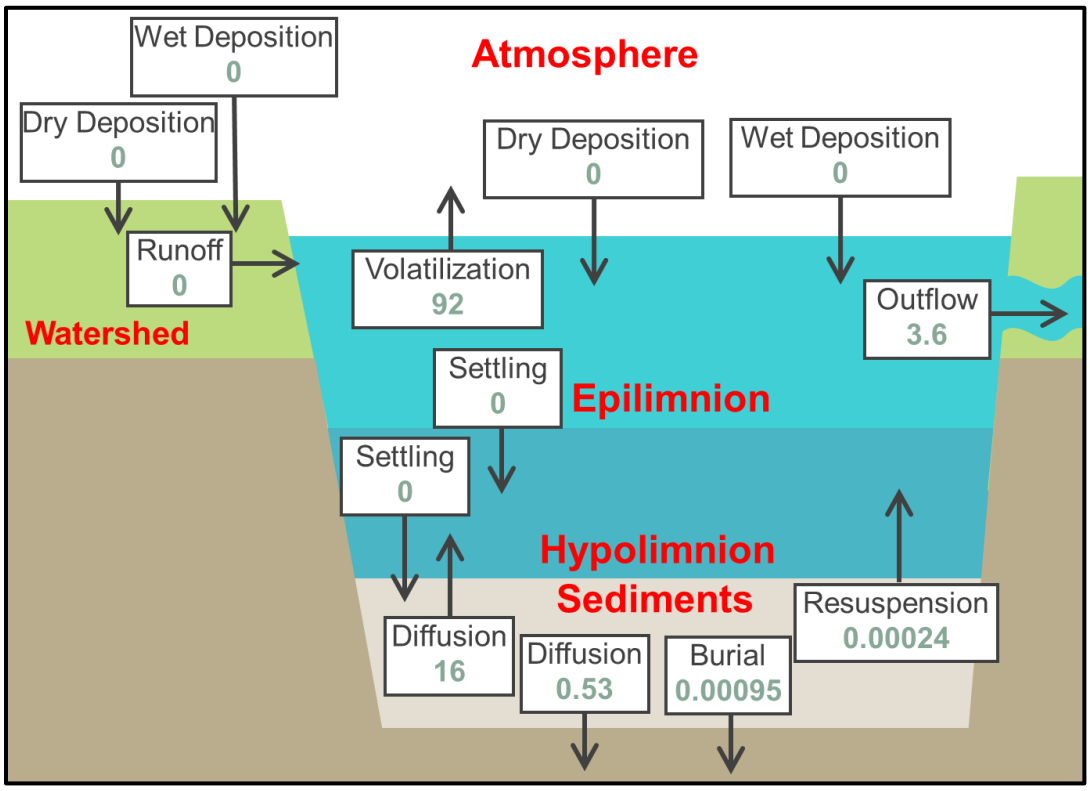

Figure 4.3. Magnitude of the process rates (g yr^{-1}) for the mass balance of elemental mercury.

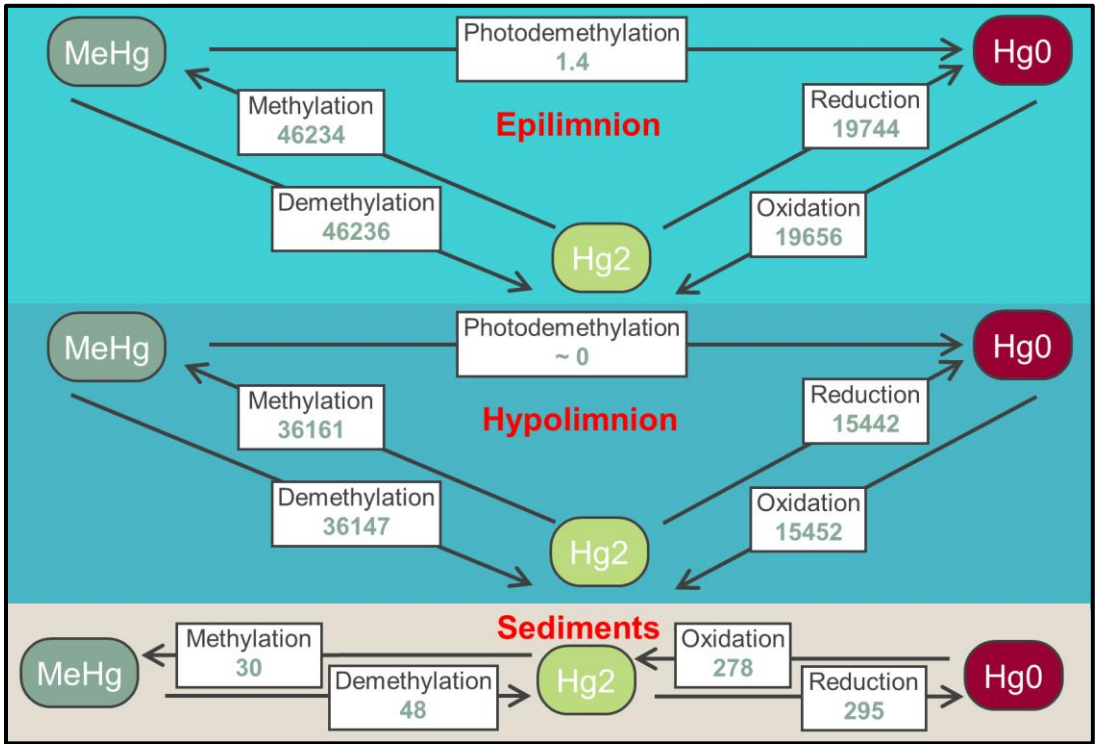

Figure 4.4. Magnitude of the process rates (g yr^{-1}) for the transformation processes of the three mercury species in the overall mass balance of mercury in the lake and sediments.

Net pore-water diffusion between the hypolimnion and surface sediments exhibited a net loss of methyl mercury to the surface sediments, whereas for elemental and divalent mercury this was a net loading to the hypolimnion. Within Torch Lake, mercury cycling is dominated by the processes of oxidation, reduction, settling, and thermocline dispersion. The air-water exchange of elemental mercury results in a net evasion of mercury from the lake, rather than absorption which would be a net loading of mercury to the lake.

Photodemethylation has been found to be a significant process in some lakes (Hammerschmidt et al. 2006; Black et al. 2012; Lehnherr et al. 2011; Zhang et al., 2017; Poste et al., 2015), and thus was added as a parameter to the model. This was found to be the smallest transformation process rate for elemental mercury with a production of 1.4 g yr^{-1} in the epilimnion. For methyl mercury, this loss is about equal to the sum of dry deposition to the lake surface/catchment and wet deposition to the lake surface. This process might be smaller for Torch Lake than for lakes lacking the seasonal ice cover that curtails light-dependent reactions for five months of the year.

In the hypolimnion there is a net methylation, whereas in the epilimnion and sediments there is a net demethylation of methyl mercury. Methylation in Torch Lake was 46.2 kg yr^{-1} in the epilimnion and 36.1 kg yr^{-1} in the hypolimnion, which is small compared to the lakes modeled in Qureshi et al. 2009. Compared with a lake of similar surface area, methylation was 15.6 kg yr^{-1} in the water column for Lake Onondaga. Little Rock Lake is smaller than Torch Lake and it was estimated that methylation in the water column was 0.28 g yr^{-1}. However, Little Rock Lake has an anoxic hypolimnion, which would mean that it would have more methylation than an oxic lake like Torch Lake (Watras et al. 1994).

4.1.2 Atmospheric and Watershed Loading to Torch Lake

The overall air-water exchange mass transfer rate was 1.4 ± 0.28 m day^{-1} (wind speed was 4.7 ± 0.57 m s^{-1} and lake surface temperature was 12 ± 4.8 ^{o}C) when the lake was free of ice cover. This mass transfer rate is higher than was reported for northern Wisconsin (0.36 m day^{-1}) (Vandal et al., 1991; Fitzgerald et al., 1994). However, the average wind speed was about 2 m s^{-1} in the Wisconsin studies. For this wind speed and similar temperatures as in the Wisconsin study, the model predicts a mass transfer rate of about 0.33 m day^{-1}. Volatilization of mercury was about 119 g yr^{-1} (12 µg m^{-2} yr^{-1}).

Ambrose et al. (2005) reported that the ratio of methyl mercury to total mercury deposition is small, ranging from 0.2 to 0.5 %. This study predicted methyl mercury to have a larger contribution, with a ratio of 0.51% for deposition to the watershed and 1.5% to the lake surface (see Table 4.1). This difference results from the fact that the dry deposition velocity to the watershed is larger than to the lake; thus significantly less dry deposition to the lake combined with the same (lake and watershed) amount of wet deposition increases the fraction of methyl mercury to 1.5% of total deposition. Methyl mercury wet deposition is calculated based on the assumption that 1.5% of total mercury wet deposition is methyl mercury in the Upper Peninsula of Michigan (Hall et al. 2005). Total mercury wet deposition rates to the lake surface are about 97% of total deposition (wet plus dry) whereas to the watershed it is only 32% of total deposition. Of the total dry deposition rate to the watershed, about 84% is from elemental, 10% is from reactive gaseous mercury (RGM), 6% is from particulate bound mercury (PBM), and < 1% is methyl mercury (see Table 4.2). Elemental mercury dominates dry deposition to the catchment; this agrees with findings by Zheng et al. (2016). For dry deposition rates to the lake surface, about 65% is from reactive gaseous mercury (RGM), 35% is from particulate bound mercury (PBM), and < 1% is methyl mercury.

Table 4.1. Comparison of deposition rates (μg m^{-2} yr^{-1}) to the watershed and lake surface for methyl and total mercury.

Surface	Watershed			Lake		
Deposition	Wet	Dry	Total	Wet	Dry	Total
MeHg	0.11	0.0073	0.12	0.11	0.00073	0.11
THg	7.6	16	24	7.6	0.26	7.9
% MeHg	1.5	0.045	0.51	1.5	0.28	1.46

Table 4.2. Comparison of dry deposition rates (μg m^{-2} yr^{-1}) to the watershed and lake surface for inorganic mercury.

Surface	Watershed	Lake
Hg0	13.7	
RGM	1.66	0.166
PBM	0.913	0.0913
Hg2 – Total	16.2	0.258

The mercury runoff from the watershed to the lake has a higher percentage of methyl mercury to total mercury of 4.8% than the deposition rates to the watershed. This is because wetlands are sites of active methylation and result in a net production of methyl mercury within the watershed.

4.1.3 Mining impacts on mercury cycling in Torch Lake

It is important to note that Torch Lake has been highly impacted by historical copper mining. The model does not account for mining, and thus the model may be underestimating mercury loading to the lake. Specifically, the model does not incorporate known mine discharges to Torch Lake tributaries; tributaries such as Hammell Creek, Slaughterhouse Creek, and Fulton Creek have elevated mercury concentrations (GLEC 2003) due to mine discharges and ultimately flow into Torch Lake. However, it is not known if all of the Hg discharged from the mines is carried to the lake or retained in wetlands along the rivers. Because this potential input was ignored, it is possible that during calibration runoff parameters may have been over-tuned to compensate for the mining loads.

The model-predicted, flow-weighted, average total and methyl mercury concentrations in the inflow were 3.4 and 0.16 ng L^{-1}, respectively. There is one measurement of total mercury in the Trap Rock River inflow to Torch Lake reported as 4.7 ng L^{-1} (GLEC, 2003). Known mine discharges in the catchment release about 600 g yr^{-1} (3.36 µg m^{-2} yr^{-1} expressed per watershed area), but it is unknown what fraction of the total makes it to the lake (Kerfoot et al., 2018). Model-predicted fluxes of total and methyl mercury to the lake from the watershed were about 1.8 and 0.087 µg m^{-2} yr^{-1}, expressed per watershed area. These are within the ranges of what has been reported for oher watersheds in the Upper Peninsula. For the Peshekee River, total and methyl mercury runoff were 2.8 and 0.15 µg m^{-2} yr^{-1}, whereas, for the Little Black River, total and methyl mercury were 2.2 and 0.09 µg m^{-2} yr^{-1} (Knauer et al., 2011). In Minnesota, total mercury runoff was found to be around 0.70 to 2.82 µg m^{-2} yr^{-1} (Kolka et al., 1999); another study found total mercury runoff to be 0.35 to 6.4 µg m^{-2} yr^{-1} and methyl mercury to be 0.033 to 0.090 µg m^{-2} yr^{-1} (Balogh et al., 2005).

4.2 Seasonality of Mercury Cycling

4.2.1 Motives for Inclusion of Seasonality in the Model

The model developed in this study focuses on seasonal changes in chemical and biological factors that affect mercury cycling. One of the main reasons for choosing to include seasonality in the model was the location of the lake. Torch Lake is a northern latitude lake that experiences the extremes from all seasons (freezing during winter and completely thawing during spring) compared to lakes in the artic that are frozen for most of the year and southern lakes that never freeze. Another objective was to quantify the relative importance of the seasonal factors that alter mercury cycling in lakes, furthering scientific understanding of mercury cycling. The non-steady state model structure with seasonal resolution also provides the flexibility to evaluate scenarios and to quantify the effects of climate change, ice cover, and latitude on the mercury cycle.

4.2.2 Seasonal Parameterization in the Model

To incorporate seasonality into the model, information about or a means of predicting the magnitude of seasonal changes in important lake characteristics (e.g., temperature, light attenuation) is needed as well as information on the response of component processes of the mercury cycle to those changes in lake characteristics. For this study, seasonality was included only for components whose effect on Hg cycling was well documented in the literature. These variables include wind speed, temperatures, solids concentrations, runoff, outflow, light attenuation, ice cover, and thermocline dispersion rates.

Wind speed was needed for calculating the air-water exchange velocities (Hornbuckle 1994; Schwarzenbach 1993; Wanninkhoff 1992; Poissant 2000). For the water quality model, wind speed was also needed for calculating the surface heat exchange and the water balance (Chapra 2014). Wind speed had a significant impact on air-water exchange for Torch Lake. The air-water exchange velocity for Torch Lake was four times larger than the estimate for a lake in Wisconsin, largely as a result of differences in wind speed (Vandal et al. 1991; Fitzgerald et al. 1994).

Hydrology of a lake includes all inflows to and outflows from the lake. Mercury can enter a lake in the inflow or runoff to the lake and it can also be removed from a lake in the outflow (Balogh et al. 2005; Hammerschmidt et al. 2006).

Thermocline Dispersion causes the epilimnion and hypolimnion to mix; temperatures, solids, and mercury concentrations are assumed to be constant throughout the water column during times of high dispersion rates (spring, fall) (Chapra 2014). Stratification will cause the epilimnion and hypolimnion to have different characteristics.

Temperature was important for calculating the air-water exchange of mercury which include the equations for Henry's Law Constant (Gardfeldt 2003; Sanemasa 1975) and the Schmidt Number (Wanninkhof 1992 & 2014). The aqueous diffusion coefficients for mercury are also dependent on temperature (Kuss 2009); thus temperature affects the air-water exchange and sediment pore-water diffusion processes. However, the aqueous diffusion coefficient of methyl mercury was given a constant value (Knightes 2008; Knightes and Ambrose 2006a) because its relationship with temperature was not found in the literature. Temperature was also important for correcting the process rates for methylation, demethylation, oxidation, and reduction. These rates have been reported in the literature to be affected by temperature (Ahn et al. 2010; Celo et al., 2006; Zhang et al. 2014). Temperature was also used for correcting growth and death rates in the chlorophyll-a mass balance and evaporation rates in the hydrologic budget for the lake (Chapra 2014; McDonald and Urban 2009).

Deposition also has been found to be seasonally variable. Seasonal changes in wet deposition were observed in measurements from the National Atmospheric Deposition Network (NADN). For lakes that freeze in winter, this deposition accumulates on top of the ice and snow and during spring melt becomes an input to the lake (Chételat et al. 2015). The model incorporated this seasonality for both wet and dry deposition of mercury. Atmospheric concentrations of mercury have been found to change seasonally, which would in turn cause seasonality in dry deposition and air-water exchange. This is supported by a study in Vilas County, Wisconsin, which found atmospheric mercury concentrations to be much larger in summer than winter, excluding particulate methyl mercury (Lamborg et al., 1995). Due to the lack of available atmospheric concentrations in the region during the period chosen for the model input, it was decided that an average annual mercury concentration would be used. Air-water exchange was assumed not to occur during ice cover as ice serves as a barrier preventing this process. Air-snow exchange during winter has been observed in arctic regions (Poulain et al. 2004 and 2007) but is not included in the model currently.

Precipitation of water also changed seasonally and accumulated on the ice similarly as for mercury deposition. Seasonal changes in precipitation drove seasonal changes in lake hydrology. The accumulated precipitation on the ice was also used for calculating the amount of light that penetrated into the water column by using snow and ice light extinction coefficients (Chapra 2014; Fang and Stefan 1996).

DOC influences a variety of mercury processes in lakes. DOC affects reduction, oxidation, methylation, and demethylation rates in lakes (Amyot et al. 1997a,b,c; Ahn et al. 2010; Knightes and Ambrose 2006a; Zhu et al. 2017). Mercury also can partition to DOC (Knightes 2008; Zhu et al. 2017). DOC also decreases the amount of radiation received in the water column (Morris et al. 1995).

Chlorophyll-a also reduces the amount of radiation received in the water column (Morris et al. 1995; Chapra 2014). In the mercury cycle, increasing concentrations of some algal species have been found to increase reduction of divalent mercury to elemental mercury

(Deng et al. 2008, 2009, 2010, and 2015). Chlorophyll-a is also related to the total biotic solids concentrations in lakes; mercury can partition to biotic solids and settle out of the water column (Knightes 2008). Labile carbon from phytoplankton also is an important determinant of methylation rates (e.g., Driscoll et al. 2012) although that relationship was not included in this model.

Radiation plays a key role in the water quality model in terms of the lake water temperature and chlorophyll-a concentrations (Chapra 2014). In the mercury cycle, light affects reduction, oxidation, and photodemethylation (Amyot et al. 1994; Costa and Liss 1999; Hammerschmidt et al. 2006; Black et al. 2012; Lehnherr et al. 2011; Poste et al. 2015; Zhang et al. 2017; Zhu et al. 2017).

4.2.3 Seasonality Observed in Torch Lake's Mercury Cycle

By including seasonality, several phenomena were observable that would not have been under a steady-state assumption (refer to Figure 3.6 results section for seasonal changes in mercury concentrations). Seasonal changes were observed with the mixing and stratification of mercury in lakes; hypolimnetic concentrations were noticeably larger than epilimnetic. Watras et al. (1994) reported the magnitude of difference of northern Wisconsin lakes for methyl and total mercury to be up to 100 and 10 times, respectively, larger in the hypolimnion than in the epilimnion. In this study, hypolimnion concentrations were only 1.3 times larger than epilimnion.

It was observed that spring melt caused an increase in mercury concentrations leading to increasing mercury concentrations throughout summer. In winter, concentrations decreased slowly until spring. Seasonality was also observed in methyl and total mercury concentrations for Little Rock Lake in Wisconsin (Watras et al. 1994): mercury concentrations were observed to mix and stratify, concentrations were also higher in the bottom layer of the lake than the top, and concentrations decreased in the winter and increased in summer. In summer, concentrations in Torch Lake's water column were 1.2 times larger than concentrations in winter for methyl and total mercury.

The observable change in the magnitude of process rates were also valuable for further understanding of mercury cycling (see Figure 4.5). Reduction and oxidation peaked in the summer as temperatures increased. Thermocline dispersion only dominated during spring and fall mixing. Oxidation and reduction followed a peculiar trend during mixing. During the onset of spring and fall mixing, reduction and oxidation showed a sudden increase. It is unclear why this occurs. There is no point during the year when photodemethylation becomes dominant in the elemental mercury mass balance in the epilimnion. Lastly, it can be observed that air-water exchange is slightly and consistently larger during fall than during the rest of the year. Late-May and mid-August also experience a sudden increase in air-water exchange fluxes.

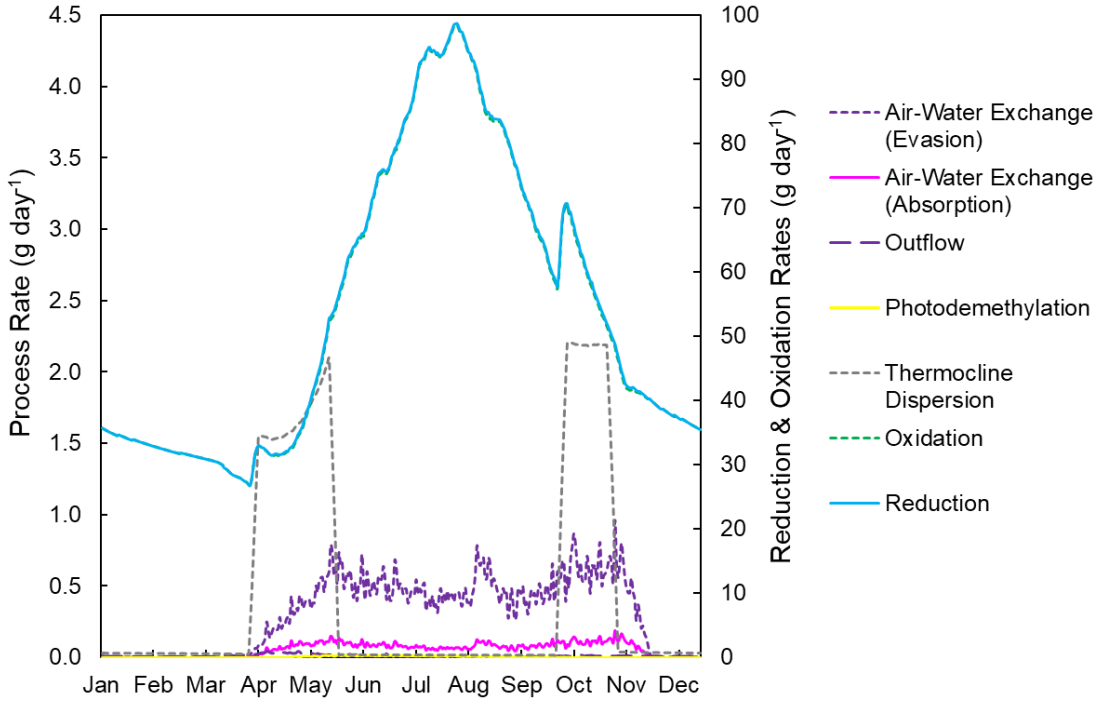

Figure 4.5. Seasonality in the process rates for elemental mercury in the epilimnion. Production of methyl mercury is represented by solid lines and losses by dashed lines.

In contrast to the elemental mercury process rates in the epilimnion, the methyl mercury process rates in the epilimnion are shown in Figure 4.6. Photodemethylation in the elemental mercury balance was not significant, but looking at the methyl mercury balance, this process is significant in the summer and is more dominant than dry deposition. This could not be observed by looking at the annual totals of the process rates. Furthermore, this also would not be observed if seasonality was not included in the model. Outflow was one of the most dominant processes during spring melt in the methyl mercury mass balance and even was larger than methylation-demethylation; this process appeared to be negligible in the elemental mercury mass balance. The methylation, demethylation, and settling processes for methyl mercury all seemed to follow the same general trend as temperature in the lake; this agrees with the oxidation and reduction processes for elemental mercury. Methylation and demethylation were also observed to have seasonality and peak during summer in Lake Clara, Wisconsin (Korthals and Winfrey 1987). As discussed in Qureshi et al. (2009), the seasonal cycle of stratification can affect methylation rates in the epilimnion and hypolimnion; this is evident in the results from this model. The epilimnion shows a net demethylation whereas the hypolimnion show a net methylation.

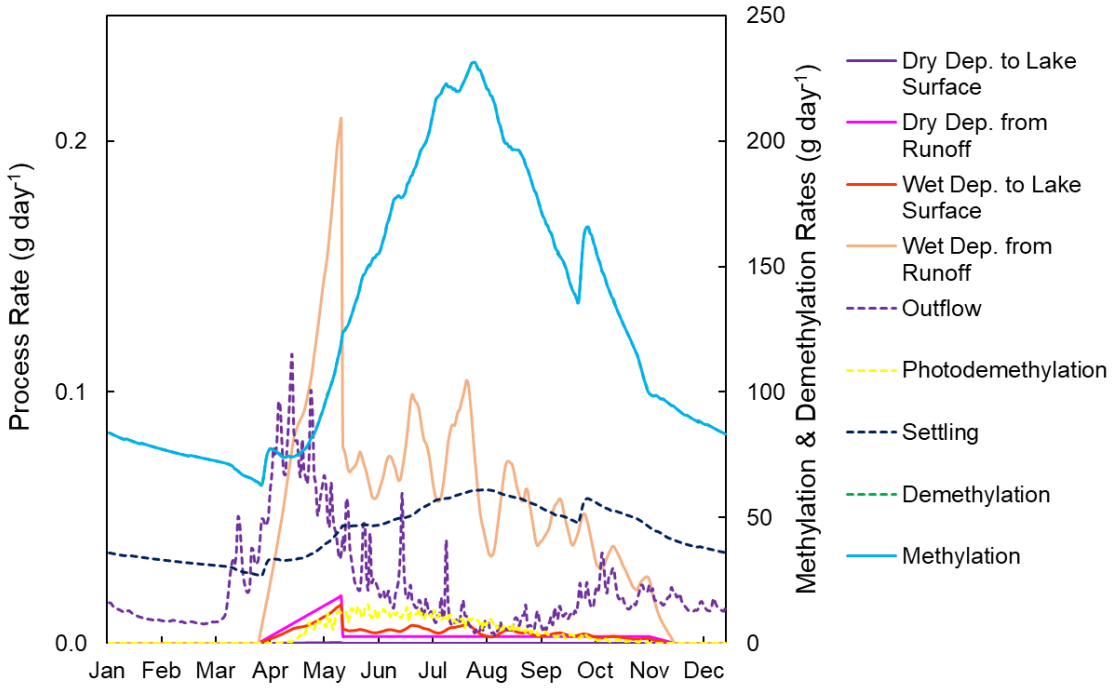

Figure 4.6. Seasonality in the process rates for methyl mercury in the epilimnion. Production of methyl mercury is represented by solid lines and losses by dashed lines.

By including seasonality, changes in watershed runoff could be observed throughout the year. Mercury concentrations peak in runoff to Torch Lake during mid-May when the discharge begins to decline. These results are consistent with a study by Hurley et al. (1995) which found mercury concentrations in Wisconsin rivers to be larger in spring than in fall. Measured concentrations of methyl and total mercury in the Mackenzie River (Chételat et al. 2015) appeared to follow the trend of discharge with no delay in runoff. The Mackenzie River study also indicated that 80% of the mercury loading to the river occurred during spring runoff with snow being a reservoir for mercury; this caused mercury concentrations in the lake to be highest in spring. The model in this study indicated that during spring melt, Torch Lake receives only 40% of its total annual input to the lake. The mercury concentration in runoff to Torch Lake is compared to discharge to Torch Lake in Figure 4.7 below.

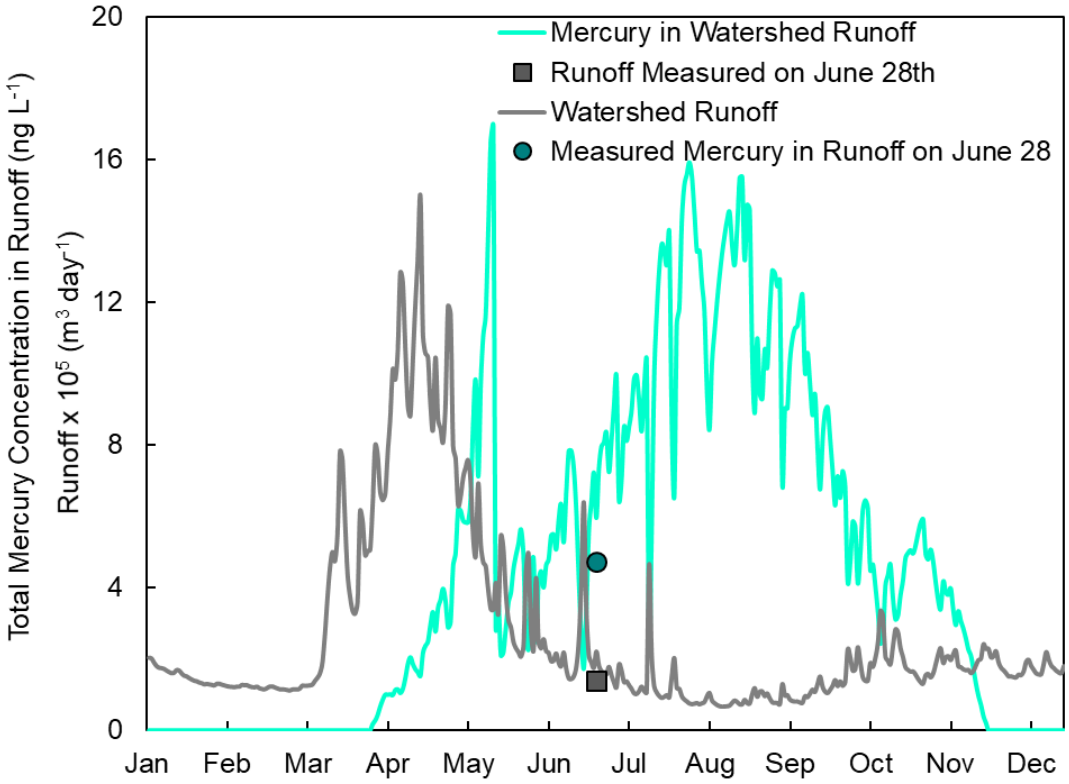

Figure 4.7. Runoff averaged over a ten-year span and modeled mercury concentrations in watershed runoff compared with measurements (GLEC, 2003; U.S. Geological Survey, 2015).

Concentrations in the runoff to Torch Lake are consistently higher during summer when the ratio of mercury deposition to discharge is higher. The total mercury concentration of 4.7 ng L^{-1} measured in Trap Rock River was taken in late June (GLEC, 2003). The discharge from the Trap Rock River to Torch Lake was also measured at the same day and was scaled to the runoff from Torch Lake's watershed; this measurement is close to the ten-year average which suggests that the Hg concentration also should be close to the climatological average predicted by the model. The model may be overestimating mercury in runoff, with a predicted concentration of about 6 ng L^{-1} in runoff around late June as compared to the measured concentration of 4 ng L^{-1}. Looking at the flux of mercury runoff from the watershed to the lake compared to the runoff throughout the year (see Figure 4.8), the flux of mercury peaks right as the runoff also peaks. Hurley et al. (1998) found similar results for tributaries to Lake Michigan; mercury fluxes in the tributaries peaked during spring melt and intense precipitation events.

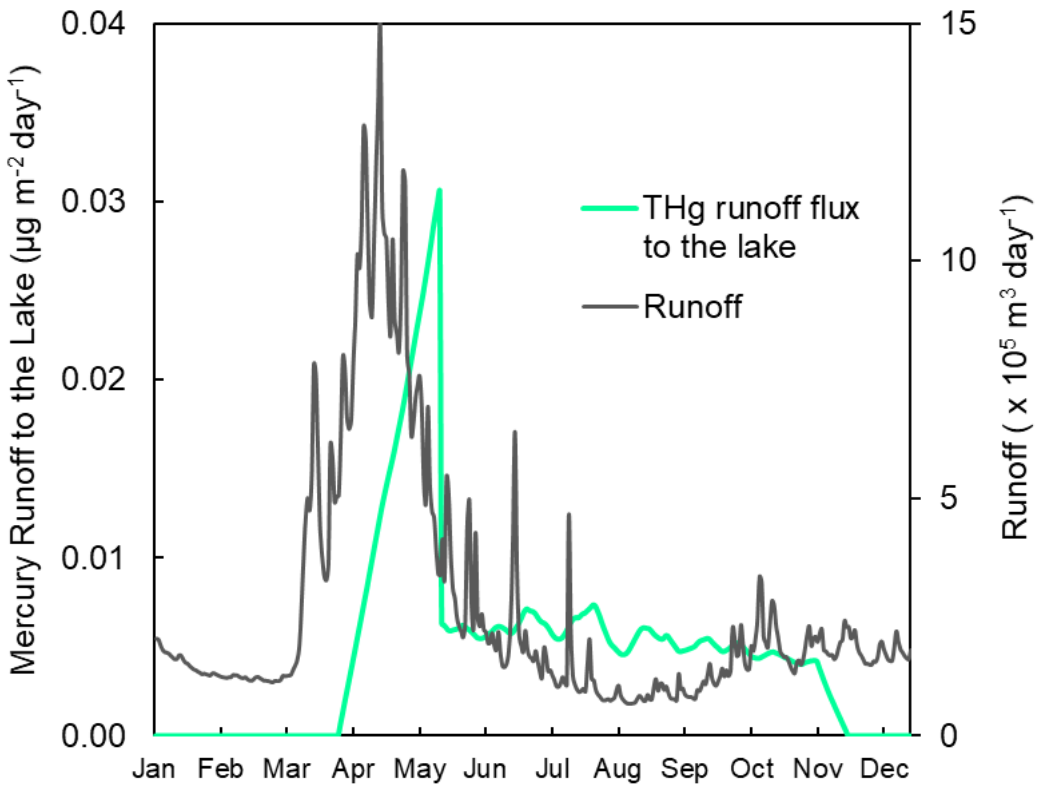

Figure 4.8. Annual total mercury runoff from the watershed to the lake (per watershed area) compared with runoff.

4.2.4 Disadvantages of Including Seasonality

One of the disadvantages of including seasonality in the model is that it can cause the model to be overparameterized and can add uncertainty to model predictions. It also can add redundancy; for example, this model included seasonality in DOC concentrations in both the epilimnion and hypolimnion. However, results show little fluctuation of concentrations throughout the year and between the lake compartments, epilimnion and hypolimnion (see Figure 3.4 in the results section). Seasonal changes and the non-steady state case can also add run time to the model; this was a challenge when the uncertainty analysis was performed. Nonetheless, the magnitude difference between the mercury species concentrations called for a stiff ODE, adding additional run time (Stan Development Team 2017). Furthermore, another challenge with adding seasonality to the model arises when applying the model to a different lake. Seasonality differs between lakes, even in similar regions and latitudes. An example of this would be the inclusion of vertical mixing in the model. Portage lake is connected to Torch Lake and undergoes similar seasonality except for the fact that Portage lake is polymictic and Torch Lake is dimictic (Kerfoot et al. 2016).

The seasonal model would need to be reparametrized to accurately be applied to Portage Lake.

4.2.5 Recommendations for Improving Seasonality in the Model

One of the assumptions made for this model was that all mercury deposition to the lake catchment immediately runs off. This assumption is clearly an over-simplification of reality, but lack of data rendered inclusion of seasonal change in runoff to be unwarranted. The lag time of catchment runoff to the lake is specific to the lake's watershed; it depends on factors such as the soil type, vegetation, and topography of watershed (Wurbs and James, 2014). Methylation in wetlands also likely follows strong seasonal cycles (Jeremiason et al. 2006), but here it was assumed to occur at a constant rate throughout the year.

As indicated above, seasonality of DOC could be removed. There is little fluctuation within the year and even between the epilimnion and hypolimnion. Sensitivity analysis results indicated that a change of 10% in the epilimnion and hypolimnion would cause a minimal change in the average annual mercury concentrations of about 3%. This finding could differ between lakes; it is suggested that this seasonal process for other lakes be examined before removing it.

4.3 Approaches for Model Validation

The general approach to validate a model presented here is to perform calibration, sensitivity analysis, and uncertainty analysis. The uncertainty/calibration analysis method used in this study, the Bayesian Monte Carlo Markov Chain (MCMC) method using the model Stan is useful for understanding the probable range in model parameters and the uncertainty in model predictions. However, this method is limited by computational power. Depending on the number of iterations and parameters sampled, the uncertainty analysis might take upwards of multiple days or weeks to run. The ability to run chains on parallel processor cores on a remote cluster was a necessity for speeding up the analysis.

The important methodology here is to optimize the model in a simpler form and then to apply the results to the complex model. The simpler case includes running the uncertainty analysis for only the parameters least supported by multiple literature studies and to which the model was found to be sensitive. Rather than assessing the uncertainty for daily concentrations throughout a year for all mercury species in all compartments (three species, three compartments, and 365 days for a total of 3285 values to be predicted), the uncertainty assessment was restricted to a short period of the year during summer stratification when all mercury cycling processes occur (i.e. winter was avoided due to air-water exchange being cut off by ice and deposition being accumulated on the ice). To

decrease the computer run time the model was simplified such that seasonally variant parameters were held constant using average values applicable to that season. These parameters were outflow, wind speed, temperature, thermocline dispersion, light attenuation, DOC, chlorophyll a, and wet deposition. To implement this strategy, a five-day period was chosen during mid-July.

Even more than confirming that the chains and iterations have converged, it is important to compare the posterior means and distributions to what has been reported in literature as shown in Figure 3.12 of the Results section. This provides some means of validation, even if few parameter values are available in the literature. However, the parameters chosen for the uncertainty analysis in this study span a wide range of values over multiple orders of magnitude, and the model output could not be confirmed by comparison with literature. The fraction of methyl to total mercury in wet deposition would be an example of a useful parameter to use for validating the uncertainty analysis because its value is tightly constrained by the literature. The fraction cannot be greater than 100%, and the highest values found in the literature are about 18% (Hall et al., 2005). This parameter was not used in the uncertainty analysis because regional measurements were available that were consistent with other literature.

A major limitation of this study was the lack of measured mercury concentrations in all compartments of Torch Lake. The measurements available in the lake included one measurement of total mercury in the epilimnion and hypolimnion. There were also sediment concentrations available for total and methyl mercury. Thus, data from Watras et al. (1995) were used as comparison for ranges of mercury measured in lakes in a similar region as Torch Lake. More data would restrict the prior distributions and lead to much shorter run times for the MCMC model. Field measurement of process rates would be even more valuable than measurement of mercury concentrations.

4.4 Future Work

Research is needed to assess the model's performance for lakes with different characteristics than Torch Lake. Specifically, Little Rock Lake in Vilas County, Wisconsin is recommended as the next lake for application of the model because of the availability of measurements (mercury concentrations, in-lake process rates, and deposition to the lake), as mentioned earlier. This lake differs from Torch Lake in several ways that would affect in-lake mercury cycling. Little Rock Lake, compared to Torch Lake, is smaller, shallower, has less DOC, has an anoxic hypolimnion, and is fed primarily by rainfall to the lake surface rather than catchment runoff (Watras et al., 1998). To analyze the dependency of the reaction rates on lake specific characteristics, these values would be left as calibrated for Torch Lake, and site-specific variables (runoff, DOC concentrations, size, etc.) would be changed. Ideally, the model is formulated in terms of the factors regulating process rates such that process rates do not have to be tuned for application to each lake.

Ultimately it is desirable to apply this or a similar model to multiple individual lakes or categories of lakes. This requires an understanding of the ranges of each parameter that are appropriate for a set of lake characteristics. This may lead to generalization of the model's structure and establishment of categories for parameter values based on different lake characteristics (i.e. oxic and anoxic lakes, different trophic states). Lakes might be categorized based on model input parameters (e.g., DOC, lake size, watershed size, surrounding wetland area), and an iterative process used to develop corresponding process rates for each lake category as was described above for Little Rock Lake. This may include further calibration of the model's parameters such as methylation, demethylation, reduction, and oxidation. As mentioned earlier, an alternative to arbitrarily calibrating (tuning) these parameters for each lake would be to develop relationships between parameter values and lake characteristics.

Ideally, an expression to calculate reaction rates for mercury based on lake specific characteristics could replace calibration of these parameters to fit measured concentrations. However, this could increase the uncertainty in the model predictions. SERAFM has incorporated some lake characteristics and allows the user to select whether the lake has an oxic or anoxic hypolimnion; the value of methylation rate is then changed accordingly (Knightes & Ambrose, 2006a). SERAFM also allows the abiotic particulate fraction, in addition to the dissolved fraction of mercury, to be methylated in the case of anoxic conditions.

It would be interesting to apply an uncertainty and sensitivity analysis to other lakes. One motive for doing so relates back to the concept that models can be lake-specific. Recall that Little Rock Lake has little to no runoff, whereas Torch Lake receives most of its mercury loading from runoff. Changing a dominant process to zero in a mass balance, allows other processes to become more important. In this situation the sensitivity analysis would, without doubt, change. In Torch Lake, runoff coefficients had a sensitivity of about 2 to 4%. Since in Little Rock Lake there would be no runoff, the sensitivity of these variables would change to 0%. The uncertainty analysis could also change because of differences in lake characteristics such as DOC (affecting demethylation) and oxygen in the hypolimnion (affecting methylation).

Furthermore, the seasonality and flexibility of the model could be applied to scenarios that would increase understanding of the mercury cycling. These scenarios could include altering lake trophic status, latitude of the lake, changes in deposition, climate change, and ice cover on the lake. The model could be run under its current structure and output compared with concentrations from other scenarios (such as decreased deposition). This model has been applied by Perlinger et al. (2018) to observe the changes in mercury concentrations in fish under different management strategies for reducing mercury emissions into the atmosphere (in the goal of decreasing deposition).

5 Reference List

Ahn, M., Kim, B.; Holsen, T.M.; Yi, S.; & Han, Y. (2010). "Factors influencing concentrations of dissolved gaseous mercury (DGM) and total mercury (TM) in an artificial reservoir." Environmental Pollution 158: 347-355.

Ajami, N. K.; Duan, Q.; & Sorooshian, S. (2007). "An integrated hydrologic Bayesian multimodel combination framework: Confronting input, parameter, and model structural uncertainty in hydrologic prediction." Water Resources Research 43.

Alanoca, L.; Amouroux, D.; Monperrus, M.; Tessier, E.; Goni, M.; Guoyoneaud, R.; Acha, D.; Gassie, G.; Audry, S.; Garcia, M.E.; Quintanilla, J.; & Point, D. (2016). "Diurnal variability and biogeochemical reactivity of mercury species in an extreme high-altitude lake ecosystem of the Bolivian Altiplano." Environmental Science Pollution Research 23: 6919-6933.

Alberts, J.J.; Schindler, J. E.; Miller, R. W.; & Nutter Jr., D. E. (1974). "Elemental mercury evolution mediated by humic acid." Science 184: 895-897.

Allard, B. & Arsenie, I. (1991). "Abiotic reduction of mercury by humic substances in aquatic system - an important process for the mercury cycle." Water, Air, and Soil Pollution 56: 457-464.

Allison, J. D.; & Allison, T.L. (2005). "Partition Coefficients for metals in surface water, soil, and waste." U.S. Environmental Protection Agency. Washington, DC.

Ambrose Jr., R.B.; Tsiros, I. X.; Wool, T.A. (2005). "Modeling mercury fluxes and concentrations in a Georgia watershed receiving atmospheric deposition load from direct and indirect sources." Journal of the Air and Waste Management Association 55 (5): 547-558.

Amyot, M.; Mierle, G.; Leans, D.R.S.; & McQueen, D.J. (1994). "Sunlight-induced formation of dissolved gaseous mercury in lake waters." Environmental Science and Technology 28 (13): 2366-2371.

Amyot, M.; Gill, G.A.; & Morel, F.M.M. (1997). "Production and loss of dissolved gaseous mercury in coastal seawater." Environmental Science and Technology 31 (12): 3606-3611.

Amyot, M.; Lean, D.; & Mierle, G. (1997). "Photochemical formation of volatile mercury in high arctic lakes." Environmental Toxicology and Chemistry 16 (10): 2054-2063.

Amyot, M.; Mierle, G.; Lean, D.; & McQueen, D.J. (1997) "Effect of solar radiation on the formation of dissolved gaseous mercury in temperate lakes." Geochimica et Cosmochimica Acta 61 (5): 975-987.

Amyot, M.; Lean, D.R.S.; Poissant, L.; & Doyon, M.R. (2000) "Distribution and transformation of elemental mercury in the St. Lawrence River and Lake Ontario." Canadian Journal of Fisheries and Aquatic Sciences 57: 155-163.

Arhonditsis, G. B.; Qian, S. S.; Stow, C. A.; Lamon, E. C.; & Reckhow, K. H. (2007) "Eutrophication risk assessment using Bayesian calibration of process-based models: Application to a mesotrophic lake." Ecological Modeling 208 (2-4): 215-229.

Arhonditsis, G. B.; Perhar, G.; Zhang, W.; Massos, E.; Shi, M.; & Das, A. (2008). "Addressing equifinality and uncertainty in eutrophication models." Water Resources Research 44 (1).

Austin, D.; Scharf, R.; Carroll, J.; & Enochs, M. (2016). "Suppression of hypolimnetic methylmercury accumulation by liquid calcium nitrate amendment: redox dynamics and fate of nitrate." Lake and Reservoir Management 32 (1): 61-73.

Avramescu, M.; Yumvihoze, E; Hintelmann, H.; Ridal, J.; Fortin, D.; & Lean, D.R.S. (2011). "Biogeochemical factors influencing net mercury methylation in contaminated freshwater sediments from St. Lawrence River in Cornwall, Ontario, Canada." Science of the Total Environment 409: 968-978.

Balough, S.J.; Meyer, M.L.; & Johnson, D.K. (1998). "Transport of mercury in three contrasting basins." Environmental Science Technology 32 (4): 456-462.

Balough, S.J.; Nollet, Y. H.; & Offerman, H. J. (2005). "A comparison of total mercury and methylmercury export from various Minnesota watersheds." Science of the Total Environment 340 (1-3): 261-270.

Barber, M.C. (2008a). "Dietary uptake models used for modeling the bioaccumulation of organic contaminants in fish." Environmental Toxicology and Chemistry 27 (4): 755-777.

Barber, M.C. (2008b). "Bioaccumulation and aquatic system simulation (BASS) User Manual." Version 2.2. U.S. Environmental Protection Agency. Ecosystems Research Division. (EPA 600/R-01/035).

Barkach, J.; & McCauley, D. (2006). "Torch Lake sediment flux and metals analysis study in Houghton CO., MI." Great Lakes Environmental Center. Traverse City, MI.

Bretherton, C. (2016). "Lecture 6. Monin-Obukhov Similarity Theory (Garratt 3.3)." Boundary Layer Meteorology. University of Washington. Seattle, WA.

Brumbaugh, W.G.; Krabbenhoft, D.P.; Helsel, D.R.; Wiener, J.G.; & Echols, K.R. (2001). "A national pilot study of mercury contamination of aquatic ecosystems along multiple gradients: bioaccumulation in fish." Biological Science Report. (USGS/BRD/BSR-2001-0009). 25 pp.

Bowie, G. L.; Mills, W. B.; Porcella, D. B.; Campbell, C. L.; Pagenkopf, J. R.; Rupp, G. L.; Johnson, K. M.; Chan, P. W. H.; Gherini, S. A.; & Chamberlin, C. E. (1985). "Rates, Constants, and Kinetics Formulations in Surface Water Quality Modeling." U.S. Environmental Protection Agency. Athens, GA. (EPA/600/3-85/040). (2nd Ed.)

Byrne, G.D.; & Thompson, S. (2013). "Error Control Matters." Radford University. Radford, VA.

Carpenter, B. (2014). "Soil carbon modeling with RStan." <http://mc-stan.org/users/documentation/case-studies/soil-knit.html>

Carroll, R.W.H.; & Warwick, J.J. (2001) "Uncertainty analysis of the Carson River mercury transport model." Ecological Modeling 137 (2-3): 211-224.

Celo, V.; Lean, D.R.S.; & Scott, S. L. (2006). "Abiotic methylation of mercury in the aquatic environment." Science of the Total Environment 368: 126-137.

Chakraborty, P.; Vudamala, K.; Coulibaly, M.; Ramteke, D.; Chennuri, K.; & Lean, D. (2015). "Reduction of mercury (II) by humic substances." Environmental Science Pollution Research 22 (14): 10529-10538.

Chapra, S. C. (2014). "Surface water-quality modeling." Waveland Press, Inc. Long Grove, IL.

Chapra, S.C.; Boehlert, B.; Fant, C.; Bierman Jr., V.J.; Henderson, J.; Mills, D.; Mas, D.M.L.; Rennels, L.; Jantarasami, L.; Martinich, J.; Strzepek, K.M.; & Paerl, H.W. (2017). "Climate change impacts on harmful algal blooms in U.S. freshwaters: a screening level-assessment." Environmental Science and Technology 51 (16): 8933-8943.

Chen, C.W.; Herr, J.W.; & Goldstein, R.A. (2008). "Model calculations of total maximum daily loads of mercury for drainage lakes." Journal of the American Water Resources Association 44 (5): 1295-1307.

Chételat, J.; Amyot, M.; Arp, P.; Blais, J. M.; Depew, D.; Emmerton, C. A.; Evans, M.; Gamberg, M.; Gantner, N.; Girard, C.; Graydon, J.; Kirk, J.; Lean, D.; Lehnherr, I.; Muir, D.; Nasr, M.; Poulain, A. J.; Power, M.; Roach, P.; Stern, G.; Swanson, H.; & van der Velden, S. (2015). "Mercury in freshwater ecosystems of the Canadian Arctic: recent advances on its cycling and fate." Science of the Total Environment 509-510: 41-66.

Ci, Z.J.; Zhang, X.S.; Yin, Y.G.; Chen, J.S.; & Wang, S.W. (2016). "Mercury Redox Chemistry in Waters of the Eastern Asian Seas: From Polluted Coast to Clean Open Ocean." Environmental Science and Technology 50 (5): 2371-2380.

Costa, M; & Liss, P.S. (1999). "Photoreduction of mercury in seawater and its possible implications for Hg0 air-sea fluxes." Marine Chemistry 68: 87-95.

Crittenden, J.C.; Trussell, R.R.; Hand, D.W.; Howe, K.J.; & Tchobanoglous, G. (2012). "MWH's Water treatment principles and designs." John Wiley & Sons, Inc. Hoboken, NJ. 3rd ed.

Cusack, C.C.; & Mihelcic, J. R. (1999). "Sediment toxicity from copper in the Torch Lake (MI) Great Lakes Area of Concern." Journal of Great Lakes Research 25 (4): 735 - 743.

Deng, L.; Wu, F.; Deng, N.; & Zuo, Y. (2008). "Photoreduction of mercury (II) in the presence of algae, *Anabaena cylindrical*." Journal of Photochemistry and Photobiology B: Biology 91: 117-124.

Deng, L.; Fu, D.; & Deng, N. (2009). "Photo-induced transformations of mercury (II) species in the presence of algae, *Chlorella vulgaris*." Journal of Hazardous Materials 164: (798-805).

Deng, L.; Deng, N.; Mou, L.; & Zhu, F. (2010). "Photo-induced transformations of Hg (II) in the presence of *Nitzschia hantzschiana*, ferric ion, and humic acid." Journal of Environmental Sciences 22 (1): 76-83.

Deng, L.; Shi, J.; Yang, C.; & Deng, N. (2015). "Photoreduction of mercury (II) in aqueous suspensions of different algae." Fresenius Environmental Bulletin 24 (1): 324-334.

Denkenberger, J.S.; Driscoll, C. T.; Branfireun, B.A.; Eckley, C.S.; Cohen, M.; & Selvendiran, P. (2012). "A synthesis of rates and controls on elemental mercury evasion in the Great Lakes Basin." Environmental Pollution 161: 291-298.

Downs, S.G.; Macleod, C.L.; & Lester, J.N. (1998). "Mercury in precipitation and its relation to bioaccumulation in fish: a literature review." Water, Air, and Soil Pollution 108: 149-187.

Driscoll, C.T.; Han, Y.; Chen, C.Y.; Evers, D.C.; Lambert, K.F.; Holsen, T.M.; Kamman, N.C.; & Munson, R.K. (2007). "Mercury Contamination in forest and freshwater ecosystems in the northeastern United States." BioScience 57 (1): 17-28.

Driscoll, C.T.; Chen, C.Y.; Hammerschmidt, C.R.; Mason, R.P.; Gilmour, C.C.; Sunderland, M. E.; Greenfield, B.K.; Buckman, K.L.; & Lamborg, C. H. (2012). "Nutrient supply and mercury dynamics in marine ecosystems: A conceptual model." Environmental Research 119: 118-131.

Drott, A.; Lambertsson, L.; Björn, E.; & Skyllberg, U. (2007). "Importance of dissolved neutral mercury sulfides for methyl mercury production in contaminated sediments." Environmental Science Technology 41 (7): 2270-2276.

Drott, A.; Lambertsson, L.; Björn, E.; & Skyllberg, U. (2008). "Potential demethylation rate determinations in relation to concentrations of MeHg, Hg and pore water speciation of MeHg in contaminated sediments." Marine Chemistry 112 (1-2): 93-101.

Eagles-Smith, C.A.; Silbergeld, E. K.; Basu, N.; Bustamante, P.; Diaz-Barriga, F.; Hopkins, W.A.; Kidd, K.A.; & Nyland, J.F. (2018). "Modulators of mercury risk to wildlife and humans in the context of rapid global change." Ambio 47 (2): 170-197.

Eckley, C.S.; & Hintelmann, H. (2006). "Determination of mercury methylation potentials in the water column of lakes across Canada." Science of the Total Environment 368: 111-125.

Either, A.L.M.; Mackay, D.; Toose-Reid, L.M.; O'Driscoll, N.J.; Scheuhammer, A.M.; & Lean, D.R.S. (2008). "The development and application of a mass balance model for mercury (total, elemental, and methyl) using data from a remote lake (Big Dam West, Nova Scotia, Canada) and the multi-species multiplier method." Applied Geochemistry 23: 467-481.

Environment Canada. (2002). "Canadian tissue residue guidelines for the protection of consumers of aquatic life: methylmercury." Scientific Supporting Document. Ecosystem Health: Science-based Solutions Report No. 1-4. National Guidelines and Standards Office, Environmental Quality Branch, Environment Canada. Ottawa.

Esri, TomTom North America, Inc., U.S. Census Bureau, U.S. Department of Agriculture, & National Agricultural Statistics Service. (2012). "USA States." <http://www.arcgis.com/home/item.html?id=1a6cae723af14f9cae228b133aebc620>.

Evers, D.C.; Wiener, J.G.; Driscoll, C.T.; Gay, D.A.; Basu, N.; Monson, B.A.; Lambert, K.F.; Morrison, H.A.; Morgan, J.T.; Williams, K.A.; Soehl, A.G. (2011). "Great Lakes mercury connections: the extent and effects of mercury pollution in the Great Lakes region." Biodiversity Research Institute. Gorham, Maine. Report BRI 2011-18. 44 pp.

Fang, X. & Stefan, H. G. (1996). "Long-term lake water temperature and ice cover simulations/measurements." Cold Regions Science and Technology 24 (3): 289-304.

Fitzgerald, W.F.; Mason, R.P; & Vandal, G.M. (1991). "Atmospheric cycling and air-water exchange of mercury over mid-continental lacustrine regions." Water, Air, and Soil Pollution 56: 745-767.

Fitzgerald, W.F.; Mason, R.P.; Vandal, G.M.; & Dulac, F. (1994). "Air-Water Cycling of Mercury in Lakes." Mercury Pollution: Integration and Synthesis. Lewis Publishers. Chelsea, MI. Section II, Chp. 3.

Futter, M.N.; Poste, A.E.; Butterfield, D.; Dillon, P.J.; Whitehead, P.G.; Dastoor, A.P.; & Lean, D.R.S. (2012). "Using the INCA-Hg model of mercury cycling to simulate total and methyl mercury concentrations in forest streams and catchments." Science of the Total Environment 424: 219-231.

Gabry, J.; & Goodrich, B. (2018). "Installing RStan on Windows." <https://github.com/stan-dev/rstan/wiki/Installing-RStan-on-Windows>

Gårdfeldt, K.; Sommar, J.; Ferrara, R.; Ceccarini, C.; Lanzillotta, E.; Munthe, J.; Wängberg, I.; Lindqvist, O.; Pirrone, N.; Sprovieri, F.; Pesenti, E.; & Strömberg, D. (2003). "Evasion of mercury from coastal and open waters of the Atlantic Ocean and the Mediterranean Seas." Atmospheric Environment 37 (1): 73-84.

Gelman, A.; Carlin, J. B.; Stern, H. S.; & Rubin, D. B. (2004). "Bayesian data analysis." 2nd Ed. Chapman & Hall/CRC. Boca Raton, FL.

Ghosh, J. K.; Delampady, M.; & Samanta, T. (2006). "An introduction to Bayesian analysis: Theory and methods." Springer Science & Business Media, LLC. New York, NY.

Gilmour, C.C.; Riedel, G.S.; Ederington, M.C.; Bell, J.T.; Benoit, J.M.; Gill, G.A.; & Stordal, M.C. (1998). "Methylmercury concentrations and production rates across a trophic gradient in the northern Everglades." Biogeochemistry 40 (2-3): 327-345.

Granholm, J. M.; Chester, S. E.; Morgan, J. T.; & Kratzer, S. (2008). "MDEQ's current status and recommended future activities toward the goal of eliminating anthropogenic mercury use and releases in Michigan." Michigan Department of Environmental Quality Mercury Strategy Staff Report.

Great Lakes Environmental Center (2003). "Low level mercury concentrations in selected Michigan surface waters, summer/fall 2002." Michigan Department of Environmental Quality. MI/DEQ/WD-03/082.

Grieb, T.M.; Driscoll, C.T.; Gloss, S.P.; Schofield, C.L.; Bowie, G.L.; & Porcella, D.B. (1990). "Factors affecting mercury accumulation in fish in the Upper Michigan Peninsula." Environmental Toxicology and Chemistry 9: 919-930.

Guo, J.; Gabry, J.; Goodrich, B.; Lee, D.; Sakrejda, K.; Trustees of Columbia University; Skyler, O.; The R Core Team; Oehlschlaeger-Akiyoshi, J.; Wickham, H.; Guzman, J.; Fletcher, J.; Heller, T.; & Niebler, E. (2018). "R Interface to Stan." R Package Version 2.17.3.

Håkanson, L. (1996). "A simple model to predict the duration of the mercury problem in Sweden." Ecological Modelling 93: 251-262.

Håkanson, L. (2000). "The derivation and use of a dynamic model for mercury in lake fish based on a static (regression) model." Water, Air, and Soil Pollution (124): 301-317.

Hall, B. D.; Manolopoulos, H.; Hurley, J. P.; Schauer, J. J.; St. Louis, V. L.; Kenski, D.; Graydon, J.; Babiarz, C. L.; Cleckner, L. B.; & Keeler, G. J. (2005). "Methyl and total mercury in precipitation in the Great Lakes region." Atmospheric Environment 39: 7557-7569.

Hammerschmidt, C.R.; & Fitzgerald, W.F. (2004). "Geochemical controls on the production and distribution of methylmercury in near-shore marine sediments." Environmental Science and Technology 38 (5): 1487-1495.

Hammerschmidt, C.R.; Fitzgerald, W.F.; Lamborg, C.H.; Balcom, P.H.; & -Mao Tseng, C. (2006). "Biogeochemical cycling of methylmercury in lakes and tundra watersheds of arctic Alaska." Environmental Science Technology 40 (4): 1204-1211.

Heyes, A.; Mason, R.P.; Kim, E.H.; & Sunderland, E. (2006). "Mercury methylation in estuaries: Insights from using measuring rates using stable mercury isotopes." Marine Chemistry 102 (1-2): 134-147.

Hines, N.A.; Brezonik, P.L.; & Engstrom, D.R. (2004). "Sediment and porewater profiles and fluxes of mercury and methylmercury in a small seepage lake in northern Minnesota." Environmental Science & Technology 38 (24): 6610-6617.

Hines, N.A.; & Brezonik, P.L. (2004) "Mercury dynamics in a small Northern Minnesota lake: water to air exchange and photoreactions of mercury." Marine Chemistry 90 (1-4): 137-149.

Hines, M.E.; Faganeli, J.; Adatto, I.; & Horvat, M. (2006). "Microbial mercury transformations in marine, estuarine and freshwater sediment downstream of the Idrija Mercury Mine, Slovenia." Applied Geochemistry 21 (11): 1924-1939.

Hornbuckle, K. C.; Jeremiason, J. D.; Sweet, C. W.; & Eisenreich, S. J. (1994). "Seasonal variations in air-water exchange of polychlorinated biphenyls in Lake Superior." Environmental Science Technology 26 (8): 1491-1501.

Hintelmann, H; Douglas Evans, R.; & Villeneuve, J. Y. (1995). "Measurement of mercury methylation in sediments using enriched stable mercury isotopes combined with methylmercury determination by gas chromatography-inductively coupled plasma mass spectrometry." Journal of Analytical Atomic Spectrometry 10 (9): 619-624.

Hintelmann, H.; Keppel-Jones, K.; & Douglas Evans, D. (2000). "Constants of mercury methylation and demethylation rates in sediments and comparison of tracer and ambient mercury available." Environmental Toxicology and Chemistry (19): 2204-2211.

Hudson, R.J.M.; Gherini, S.A.; Watras, C.J.; & Porcella, D.B. (1994). "Modeling the biogeochemical cycle of mercury in lakes: the mercury cycling model (MCM) and its application to the MTL study lakes." Mercury Pollution: Integration and Synthesis. Lewis Publishers. Chapter 5.1.

Hurley, J.P.; Benoit, J.M.; Babiarz, C.L.; Shafer, M.M.; Andren, A.W.; Sullivan, J.R.; Hammond, R.; & Webb, D.A. (1995). "Influences of watershed characteristics on mercury levels in Wisconsin rivers." Environmental Science and Technology 29 (7): 1867-1875.

Hurley, J.P.; Cowell, S.E.; Shafer, M.M.; & Huges, P.E. (1998). "Tributary loading of mercury to Lake Michigan: importance of seasonal events and phase partitioning." The Science of the Total Environment 213: 129-137.

Iverfeldt, A.; & Lindqvist, O. (1986). "Atmospheric oxidation of elemental mercury by ozone in the aqueous phase." Atmospheric Environment 20 (8): 1567-1573.

Jeremiason, J.D.; Engstrom, D.R.; Swain, E.B.; Nater, E.A.; Johnson, B.M.; Almendinger, J.E.; Monson, B.A.; & Kolka, R.K. (2016). "Sulfate addition increases methylmercury production in an experimental wetland." Environmental Science and Technology 40 (12): 3800-3806.

Keeler, G. J. & Dvonch, T. J. (2005). "Atmospheric mercury: a decade of observations in the great lakes." Dynamics of Mercury Pollution on Regional and Global Scales. Springer. New York, NY.

Kerfoot, C. W.; Urban, N. R.; McDonald, C. P.; Rossman, R.; & Zhang, H. (2016). "Legacy mercury releases during copper mining near Lake Superior." Journal of Great Lakes Research 42: 50-61.

Kerfoot, W.; Urban, N.; McDonald, C.; Zhang, H.; Rossmann, R.; Perlinger, J.; Khan, T.; Hendricks, A.; Priyadarshini, M.; & Bolstad, M. (2018). "Mining Legacy Across a Wetland Landscape: High Mercury in Upper Peninsula (Michigan) Rivers, Lakes, and Fish." Environmental Sciences: Processes and Impacts

Kirillin, G.; Hochschild, J.; Mironov, D.; Terzhevik, A.; Golosov, S.; & Nützmann, G. 2011. "FLake-Global: Online lake model with worldwide coverage." Environmnetal Modelling & Software 26 (5): 683-684.

Knauer, D.; Pelkola, G.; Casey, S.; Krabbenhoft, D.; & DeWild, J. (2011). "The distribution of total and methyl mercury in Michigan's Upper Peninsula lakes." Michigan Department of Environmental Quality.

Knightes, C. D.; & Ambrose Jr., R. B. (2004). "Analysis of mercury in Vermont and New Hampshire lakes: evaluation of the regional mercury cycling model." U.S. Environmnetal Protection Agency, Ecosystems Research Division. Athens, GA. (EPA/600/R-04/080).

Knightes, C. D.; & Ambrose Jr., R. B. (2006a). "Development of an Ecological Risk Assessment Methodology for Assessing Wildlife Exposure Risk Associated with Mercury-Contaminated Sediments in Lake and River Systems." U.S. Environmental Protection Agency. Washington, DC. (EPA/600/R-06/073).

Knightes, C. D.; & Ambrose Jr., R. B. (2006b). "Evaluating regional predictive capacity of a process-based mercury exposure model, regional-mercury cycling model, applied to 91 Vermont and New Hampshire lakes and ponds, USA." Environmental Toxicology and Chemistry 26 (4): 807-815.

Knightes, C. D. (2008). “Development and test application of a screening-level mercury fate model and tool for evaluating wildlife for surface waters with mercury-contaminated sediments (SERAFM).” Environmental Modelling and Software 23 (4): 495-510.

Knightes, C.D.; Sunderland, E.M.; Barger, C.M.; Johnston, J.M.; & Ambrose Jr., R.B. (2009). “Application of ecosystem scale-fate and bioaccumulation models to predict fish mercury response times to changes in atmospheric deposition.” Environmental Toxicology and Chemistry 28 (4): 881-893.

Kolka, R. K.; Grigal, D. F.; Verry, E. S.; & Nater, E. A. (1999). “Mercury and organic carbon relationships in streams draining forested upland/peatland watersheds.” Journal of Environmental Quality 28 (3): 766-775.

Korthals, E.T.; & Winfrey, M.R. (1987). “Seasonal and spatial variations in mercury methylation and demethylation in an oligotrophic lake.” Applied and Environmental Microbiology 53: 2397-2404.

Kotnik, J.; Horvat, M.; Fajon, V.; & Logar, M. (2002a). “Mercury in small freshwater lakes: A case study: Lake Velenje, Slovenia.” Water, Air, and Soil Pollution 134 (1-4): 319-339.

Kotnik, J.; Horvat, M.; & Jereb, V. (2002b) “Modelling of mercury geochemical cycle in Lake Velenje, Slovenia.” Environmental Modelling and Software 17 (7): 593-611.

Kuss, J.; Holzmann, J.; & Ludwig, R. (2009). “An Elemental Mercury Diffusion Coefficient for Natural Waters Determined by Molecular Dynamics Simulation.” Environmental Science and Technology 43 (9): 3183-3186.

Lalonde, J.D.; Amyot, M.; Kraepiel, A.M.L.; & Morel, F.M.M. (2001) “Photooxidation of Hg(0) in artificial and natural waters.” Environmental Science and Technology 35 (7): 1367-1372.

Lalonde, J.D.; Amyot, M.; Orvoine, J.; Morel, F.M.M.; Auclair, J.C.; & Ariya, P.A. (2004). “Photoinduced oxidation of Hg-0 (aq) in the waters from the St. Lawrence estuary.” Environmental Science and Technology 38 (2): 508-514.

Lamborg, C. H.; Fitzgerald, W. F.; Vandal, G. M.; & Rolfus, K.R. (1995). “Atmospheric mercury in northern Wisconsin: sources and species.” Water, Air, and Soil Pollution: 80: 189-198.

Lamborg, C.H.; Rolfhus, K.R.; Fitzgerald, W.F.; & Kim, G. (1999). “The atmospheric cycling and air-sea exchange of mercury species in the South and equatorial Atlantic Ocean.” Deep-Sea Research Part II-Topical Studies in Oceanography 46 (5): 957-977.

Landis, M.S.; & Keeler, G.J. (2002). “Atmospheric mercury deposition to Lake Michigan during the Lake Michigan mass balance study.” Environmental Science and Technology 36 (21): 4518-4524.

Lehnherr, I.; St. Louis, V.L.; Hintelmann, H.; & Kirk, J.L. (2011) Methylation of inorganic mercury in polar marine waters.” Nature Geoscience 4 (5): 298-302.

Lessard, C. R.; Poulain, A. J.; Ridal, J.J.; & Blais, J.M. (2014). “Dynamic mass balance model for mercury in the St. Lawrence River near Cornwall, Ontario, Canada.” Science of the Total Environment 500-501: 131-138.

Lindberg, S.E.; & Zhang, H. (2000). “Air/water exchange of mercury in the Everglades II: measuring and modeling evasion of mercury from surface waters in the Everglades Nutrient Removal Project.” Science and the Total Environment 259 (1-3): 135-143.

Liu, Y. A. & Gupta, H. V. (2007). “Uncertainty in hydrologic modeling: toward an integrated data assimilation framework.” Water Resources Research 43 (7). 18 pp.

Lyon, B.F.; Ambrose, R.; Rice, G.; & Maxwell, C.J. (1997). “Calculation of soil-water and benthic sediment partition coefficients for mercury.” Chemosphere 35 (4): 791-808.

MacLeod, M.; Fraser, A. J.; & Mackay, D. (2002). Evaluating and expressing the propagation of uncertainty in chemical fate and bioaccumulation models. Environmental Toxicology and Chemistry 21 (4): 700-709.

MacLeod, M; Mckone, T.E.; & Mackay, D. (2005). “Mass balance for mercury in the San Francisco Bay area.” Environmental Science Technology 39 (17): 6721-6729.

Mackay, D. & Yeun, A. T. K. (1983). “Mass transfer coefficient correlations for volatilization of organic solutes from water.” Environmental Science Technology 17 (4): 211-217.

Manwell, J.F.; McGowan, J.G.; & Rogers, A.L. (2009) “Wind energy explained: theory, design, and application.” Chapter 2. Wind Characteristics and Resources. 2nd Ed. John Wiley & Sons. Chichester, United Kingdom.

Margossian, C.; & Gillespie, B. (2017). “Differential equations based models in Stan.”

Marvin-DiPasquale, M.C.; Agee, J.L.; Bouse, R.M.; & Jaffe, B.E. (2003). “Microbial cycling of mercury in contaminated pelagic and wetland sediments of San Pablo Bay, California.” Environmental Geology (43): 260-267.

Mason, R.P.; Fitzgerald, W.F.; Hurley, J.P.; Hanson Jr., A.K.; Donaghay, P.L. & Sieburth, J.M. (1993). “Mercury biogechemical cycling in a stratified estuary.” Limnology Oceanography 38 (6): 1227-1241.

Mason, R.P.; O'Donnell, J.; & Fitzgerald, W.F. (1994a). "Elemental mercury cycling within the mixed layer of the equatorial Pacific Ocean." Mercury Pollution: Integration and Synthesis. Lewis Publishers. Chapter 1.7.

Mason, R.P.; Fitzgerald, W.F.; & Morel, F.M.M. (1994b). "The biogeochemical cycling of elemental mercury: anthropogenic influences." Geochimica et Cosmochimica Acta 58 (15): 3191-3198.

Mason, R.P.; Morel, F.M.M.; & Hemond, H.F. (1995). "The role of microorganisms in elemental mercury formation in natural waters." Water, Air, and Soil Pollution 80: 775-787.

Mason, R.P.; Rolfus, K.R.; & Fitzgerald, W.F. (1998a) "Mercury in the North Atlantic." Marine Chemistry 61: 37-53.

Mason, R.P.; & Sullivan, K.A. (1998). "Mercury and methylmercury transport through an urban watershed." Water Resources 32 (2): 321-330.

Massey, A. (1970). "Biological Evaluation of Torch Lake, Houghton, Michigan." Michigan Water Resources Commission, Bureau of water Management, Department of Natural Resources. Lansing, MI. 13 pp.

Matilainen, T.; & Verta, M. (1995) "Mercury methylation and demethylation in aerobic surface waters." Canadian Journal of Fish and Aquatic Science 52: 1597-1608.

MathWorks (2018). "Choose an ODE solver." <https://www.mathworks.com/help/matlab/math/choose-an-ode-solver.html?requestedDomain=true#bu7wegm-1>.

McDonald, C.P.; & Urban, N.R. (2007). "Sediment radioisotope dating across a stratigraphic discontinuity in a mining-impacted lake." Journal of Environmental Radioactivity 92 (2): 80-95.

McDonald, C.P. & Urban, N.R. (2009). "Using a model selection criterion to identify appropriate complexity in aquatic biogeochemistry models." Ecological Modeling 221 (3): 428-432.

McDonald, C. P.; Urban, N. R.; Barkach, J. H.; & McCauley, D. (2010). "Copper profiles in the sediments of a mining-impacted lake." Journal of Soils and Sediments 10 (3): 343-348.

McDonald, C.P.; Bennington, V.; Urban, N.R.; & McKinely, G.A. (2012). "1-D test-bed calibration of a 3-D Lake Superior biogeochemical model." Ecological Modelling 225: 115-126.

Michigan Department of Environmental Quality. (2017). "Fish contaminant monitoring program." Surface Water Assessment Section. <http://www.michigan.gov/deq/0,4561,7-135-3313_3681_3686_3728-12600--,00.html>

Michigan Department of Environmental Quality (2013). "Michigan's water chemistry monitoring program, A report of statewide spatial patterns 2005-2009 and fixed station status and trends 1998-2008." Water Resources Department. (13/0005) pp. 71.

Michigan Department of Environmental Quality; Michigan Department of Natural Resources; & Department of Shared Solutions (2018). "Michigan surface water information management system." <http://www.mcgi.state.mi.us/miswims/>

Michigan Technological University Keweenaw Research Center (2017). "Archival Weather Data." <http://blizzard.mtukrc.org/~weather/>

Mironov, D. V. (2008). "Parameterization of lakes in numerical weather prediction. Description of a lake model". COSMO Technical Report, No. 11, Deutscher Wetterdienst, Offenbach am Main, Germany. 41 pp.

Mohseni, O.; Stefan, H. G.; & Erickson, T. R. (1998). "A nonlinear regression model for weekly stream temperatures." Water Resources Research 34 (10): 2685-2692.

Mohseni, O.; Stefan, H. G.; & Eaton, J. G. (2003). "Global warming and potential changes in fish habitat in U.S. streams." Climatic Change 59 (3): 389-409.

Monperrus, M; Tessier, E.; Amouroux, D.; Leynaert, A.; Huonnic, P.; & Dounard, O.F.X. (2007). "Mercury methylation, demethylation, and reduction rates, in coastal and marine surface waters of the Mediterranean Sea." Marine Chemistry 107: 49-63.

Morris, D. P.; Zagarese, H.; Williamson, C. E.; Balseiro, E. G.; Hargreaves, B. R.; Modenutti, B.; Moeller, R.; & Queimalinos, C. (1995). "The attenuation of solar UV radiation in lakes and the role of dissolved organic carbon." Limnology and Oceanography 40 (8): 1381-1391.

National Oceanic and Atmospheric Administration (2018a). "The Great Lakes dashboard." Great Lakes Environmental Research Laboratory. <https://www.glerl.noaa.gov//data/dashboard/GLD_HTML5.html>.

National Oceanic and Atmospheric Administration (2018b). "Great Lakes water level observations." Great Lakes Environmental Research Laboratory. <https://www.glerl.noaa.gov/data/wlevels/#observations>.

National Atmospheric Deposition Program (2017). "Mercury Deposition Network." NADP Program Office, Illinois State Water Survey. Champaign, IL. <http://nadp.sws.uiuc.edu/MDN/>.

Obrist, D.; Pearson, C.; Webster, J.; Kane, T.; Lin, C.; Aiken, G.R.; & Alpers, C.N. (2016). "A synthesis of terrestrial mercury in the western United States: spatial distribution defined by land cover and plant productivity." Science of the Total Environment 568: 522-535.

O'Driscoll, N.J.; Lean, D.R.S.; Loseto, L.L.; Carignan, R.; & Siciliano, S.D. (2004). "Effect of dissolved organic carbon on the photoproduction of dissolved gaseous mercury in lakes: potential impacts of forestry." Environmental Science and Technology 38 (9): 2664-2672.

Paterson, G. (2017). "The toxicokinetics of legacy and emerging pollutants." Environmental Engineering Seminar Series. Michigan Technological University. Houghton, MI.

Perlinger, J. A.; Urban, N. R.; Giang, A.; Selin, N.E.; Hendricks, A. N.; Zhang, H.; Kumar, A.; Wu, S.; Gagnon, V. S. Gorman, H. S., & Norman, E. S. (2018). "Responses of deposition and bioaccumulation in the Great Lakes region to policy and other large-scale drivers of mercury emissions." Environmental Science: Processes & Impacts 20 (1): 195-209.

Peretyazhko, T.; Charlet, L.; Muresan, B.; Kazimirov, V.; & Cossa, D. (2006) "Formation of dissolved gaseous mercury in a tropical lake (Petit-Saut reservoir, French Guiana)." Science of the Total Environment (364): 260-271.

Petersen, G.; Munthe, J.; Pleijel, K.; Bloxam, R.; & Vinod Kumar, A. (1998). "A comprehensive Eulerian modeling framework for airborne mercury species: development and testing of the tropospheric chemistry model (TCM)." Atmospheric Environment 32 (5): 829-843.

Plummer, M.; Best, N.; Cowles, K.; Vines, K.; Sarkar, D.; Bates, D., Almond, D.; & Magnusson, A. (2016). "Output Analysis and Diagnostics for MCMC." R Package version 0.19-1.

Poissant, L.; Amyot, M.; Pilote, M.; & Lean, D. (2000). "Mercury water-air exchange over the upper St. Lawrence River and Lake Ontario." Environmental Science Technology 34 (15): 3069-3078.

Poste, A.E.; Braaten, H.F.; de Wit, H.A.; Sørensen, K.; & Larssen, T. (2015). "Effects of photodemethylation on the methylmercury budget of boreal Norwegian lakes." Environmental Toxicology and Chemistry 34 (6): 1213-1223.

Poulain, A.J.; Lalonde, J.D.; Amyot, M.; Shead, J.A.; Raofie, F.; & Ariya, P.A. (2004). "Redox transformations of mercury in an Arctic snowpack at springtime." AE International – Polar Regions 38: 6763-6774.

Poulain, A.J.; Roy, V.; & Amyot, A. (2007). “Influence of temperate mixed and deciduous tree covers on Hg concentrations and photoredox transformations in snow.” Geochemica et Cosmochimica Acta 71: 2448-2462.

Priyadarshini, M. (2017). “Factors contributing to elevated concentrations of mercury and PCBs in fish in the inland lakes of Michigan’s Upper Peninsula and Lake Superior.” Master’s Thesis. Michigan Technological University. Houghton, MI.

Quershi, A.; MacLeod, M.; Scheringer, M.; & Hungerbühler, K. (2009). “Mercury cycling and species mass balances in four North American lakes.” Environmental Pollution 157 (2): 452-462.

R Core Team (2013). “R: A language and environment for statistical computing.” R Foundation for Statistical Computing, Vienna, Austria.

Rajar, R.; Žagar, D.; Četina, M; Akagi, H.; Yano, S.; Tomiyasu, T.; & Hovart, M. (2004). “Application of three-dimensional mercury cycling model to coastal seas.” Ecological Modelling 171: 139-155.

Rea, A. W.; Lindberg, S. E.; & Keeler, G. J. (2000). “Assessment of dry deposition and foliar leaching of mercury and selected trace elements based on washed foliar and surrogate surfaces.” Environmental Science and Technology 34 (12): 2418-2425.

Riley, G.A. (1956). “Oceanography of Long Island Sound 1952-1954.” II.Physical Oceanography. Bulletin Bingham Oceanography Collection 15. 438-463.

Ripley, B.; & Murdoch, D. (2017) “Building R for Windows.” <https://cran.r-project.org/bin/windows/Rtools/>

Rodriguez Martin-Doimeadios, R.C.; Tessier, E.; Amouroux, D.; Guyondeaud, R.; Duran, R.; Caumette, P.; & Donard, O.F.X. (2004). “Mercury methylation/demethylation and volatilization pathways in estuarine sediment slurries using species-specific enriched stable isotopes.” Marine Chemistry 90 (1-4): 107-123.

Rolfhus, K.R.; & Fitzgerald, W.F. (2004). “Mechanisms and temporal variability of dissolved gaseous mercury production in coastal seawater.” Marine Chemistry 90 (1-4): 125-136.

Rossmann, R. (2006) “Results of the Lake Michigan mass balance project: Polychlorinate Biphenyls modeling report.” U.S. Environmental Protection Agency. (EPA-600/R-04/167). 621 pp.

Salvagio Manta, S.; Bonsignore, M.; Oliveri, E.; Barra, M.; Tranchida, G.; Giaramita, L.; Mazzola, S.; Sprovieri, M. (2016). “Fluxes and the mass balance of mercury in Augusta Bay (Sicily, southern Italy).” Estuarine, Coastal, and Shelf Science 181: 134-143.

Sanemasa, I. (1975). “The solubility of elemental mercury vapor in water.” Bulletin of the Chemical Society of Japan 48 (6): 1795-1798.

Schäfer, J.; Castelle, S.; Blanc, G.; Dabrin, A.; Masson, M.; Lanceleur, L.; & Bossy, C. (2010). “Mercury methylation in the sediments of a macrotidal estuary (Gironde Estuary, south-west France).” Estuarine, Coastal, and Shelf Science 90 (2): 90-92.

Schwarzenbach, R.P.; Gschwend, P.M; & Imboden, D.M. (1993). “Environmental Organic Chemistry.” Wiley-Interscience. Chichester, UK.

Shampine, L. F. & Reichelt, M. W. (1997). “The MATLAB ODE suite.” SIAM Journal on Scientific Computing 18 (1): 1 - 22.

Shannon, J. D. & Voldner, E. C. (1995). “Modeling atmospheric concentrations of mercury and deposition to the Great Lakes.” Atmospheric Environment 29 (14): 1649-1661.

Sharif, A.; Monperrus, M.; Tessier, E.; Bouchet, S.; Pinaly, H.; Rodriguez-Gonzalez, P.; Maron, P.; & Amoureux, D. (2014). “Fate of mercury species in the coastal plume of the Adour River estuary (Bay of Biscay, SW France).” Science of the Total Environment 496: 701-713.

Smith, J.H.; Bomberger Jr., D.C.; & Haynes, D.L. (1980). “Prediction of the volatilization rates of high-volatility chemicals from natural water bodies.” Environmental Science and Technology 14 (11): 1332-1337.

Soetaert, K.; Petzoldt, T.; & Setzer, R. W. (2017). “Solvers for initial value problems of differential equations (‘ODE’, ‘DAE’, ‘DDE’).” R Package version 1.20.

Stan Development Team (2017). “Stan modeling language: user’s guide and reference manual.” Version 2.17.0.

State of Michigan (2005). “Michigan Counties V17.” Version 5a. <http://gis-michigan.opendata.arcgis.com/datasets/counties-v17a>.

State of Michigan (2017). “Lake Polygons.” <http://gis-michigan.opendata.arcgis.com/datasets/lake-polygons>.

Stordal, M.C.; & Gill, G.A. (1995) “Determination of mercury methylation rates using a 203-HG radiotracer technique.” Water, Air, and Soil Pollution 80 (1-4): 725-734.

Sun, R.; Wang, D.; Mao, W.; Zhao, S.; & Zhang, C. (2014). “Roles of chloride in photo-reduction/oxidation of mercury.” Chinese Science Bulletin 59 (27): 3390-3397.

Tsiros, L.X.; & Ambrose, R.B. (1998). “Environmental screening modeling of mercury in the upper everglades of South Florida.” Journal of Environmental Science and Health Part A-Toxic/Hazardous Substances and Environmental Engineering 33 (4): 497-525.

Urban, N.R. (unpub.) “Hypsographic curve for Torch Lake.”

Urban, N.R. (unpub.) “On going water quality sampling data for Torch Lake.”

U.S. Environmental Protection Agency. (2013). “2011 national listing of fish advisories.” (EPA-820-F-13-058).

U.S. Fish and Wildlife Service (2017). “National Wetlands Inventory: Download seamless wetlands data by state.” <https://www.fws.gov/wetlands/Data/State-Downloads.html>.

U.S. Geological Survey (2013a). “USGS NED n48w089 1/3 arc-second 2013 1 x 1 degree ArcGrid: U.S. Geological Survey.”

U.S. Geological Survey (2013b). “USGS NED n48w088 1/3 arc-second 2013 1 x 1 degree ArcGrid: U.S. Geological Survey.”

U.S. Geological Survey (2014). “NLCD 2011 Land Cover (2011 Edition, amended 2014), by State: NLCD2011_LC_Michigan: U.S. Geological Survey.”

U.S. Geological Survey (2014). “NLCD 2011 Percent Developed Imperviousness (2011 Edition, amended 2014), by State: NLCD2011_IMP_Michigan: U.S. Geological Survey.”

U.S. Geological Survey (2015). “USGS Surface-Water Daily Data for Michigan: USGS 04043050 Trap Rock River Near Lake Linden, MI.”

U.S. Geological Survey (2018). “USGS Surface-Water Daily Data for Michigan: USGS 04041500 Sturgeon River Near Alston, MI.”

U.S. Geological Survey (2017). “The National Map.” <https://viewer.nationalmap.gov/basic/>

U.S. Geological Survey, National Geospatial Program (2017). “USGS National Hydrography Dataset (NHD) Best Resolution 20170818 for Michigan State or Territory FileGDB 10.1.” Model Version 2.2.1: U.S. Geological Survey.

U.S. Naval Observatory (2015). “Sun or moon rise/set table for one year.” <http://aa.usno.navy.mil/data/docs/RS_OneYear.php>

Wang, M. (2016). “Introduction to Bayesian statistics.” Michigan Technological University. Houghton, MI.

Vandal, G.M.; Mason, R.P.; & Fitzgerald, W.F. (1991). “Cycling of volatile mercury in temperate lakes.” Water, Air, and Soil Pollution 56: 791-803.

Vandal, G.M.; Fitzgerald, W.F.; Rolfhus, K.R.; & Lamborg, C.H. (1995). “Modeling the elemental mercury cycle in Pallette Lake, Wisconsin, USA.” Water, Air, and Soil Pollution 80 (1-4): 529-538.

Vincent, A.C.; Mueller, D.R.; & Vincent, W.F. (2008). "Simulated Heat Storage in a Perennially Ice-covered High Arctic Lake: Sensitivity to Climate Change." Journal of Geophysical Research 113 (4).

Wang, M. (2016) “Bayesian Statistics.” Michigan Technological University. Houghton, MI.

Wanninkhof, R. (1992). “Relationship between wind speed and gas exchange over the ocean.” Journal of Geophysical Research: Oceans 97 (15): 7373-7382.

Wanninkhof, R. (2014). “Relationship between wind speed and gas exchange over the ocean revisited.” Limnology and Oceanography: Methods 12: 351-362.

Watras, C. J.; Bloom, N. S.; Hudson, R. J. M.; Gherini, S.; Munson, R.; Claas, S. A.; Morrison, K. A.; Hurley, J.; Wiener, J. G.; Fitzgerald, W. F.; Mason, R.; Vandal, G.; Powell, D.; Rada, R; Rislov, L.; Winfrey, W.; Elder, J.; Krabbenhoft, D.; Andren, A. W.; Babiarz, C.; Porcella, D. B.; & Huckabee, J. W. (1994). “Sources and fates of mercury and methylmercury in Wisconsin lakes.” Mercury Pollution: Integration and Synthesis. Lewis Publishers. Chelsea, MI. Section II, Chp. 3. 153-177.

Watras, C. J.; Morrison, K. A.; & Host, J. S. (1995). “Concentration of mercury species in relationship to other site-specific factors in the surface waters of northern Wisconsin lakes.” Limnology Oceanography 40 (3): 556-565.

Watras, C.J.; Back, R.C.; Halvorsen, S.; Hudson, R.J.M.; Morrison, K.A.; & Wente, S.P. (1998). “Bioaccumulation of mercury in pelagic freshwater food webs.” The Science of the Total Environment 219: 183-208.

Watras, C.J.; Morrison, K.A.; Regnell, O.; Kratz, & T.K. (2006). “The methylmercury cycle in Little Rock Lake during experimental acidification and recovery.” Limnology and Oceanography 51 (1): 257-270.

Watras, C.J.; Morrison, K.A.; Rubsam, J.L.; & Rodger, B. (2009). “Atmospheric mercury cycles in northern Wisconsin.” Atmospheric Environment 43: 4070-4077.

Weather Underground (2015). “Weather History for Lake Linden, MI for 01/01/2004 to 12/31/2013.”

Whalin, L.M.; & Mason, R.P. (2006) “A new method for the investigation of mercury redox chemistry in natural waters utilizing deflatable Teflon (R) bags and additions of isotopically labeled mercury.” Analytica Chimica Acta 558 (1-2): 211-221.

Whalin, L.; Kim, E.H.; & Mason, R. (2007). “Factors influencing the oxidation, reduction, methylation and demethylation of mercury species in coastal waters.” Marine Chemistry 107 (3): 278-294.

Whitman, W. G. (1923) “A preliminary experimental confirmation of the two-film theory of gas absorption.” Chemical and Metallurgical Engineering 29 (4): 146-148.

Wickham, H.; Chang, W.; & RStudio (2016). “Create elegant data visualisations using the grammar of graphics.” R Package version 2.2.1.

Wisconsin Department of Natural Resources (2017) “County Boundaries 24K.” Wisconsin Department of Natural Resources Open Data. <https://data-wi-dnr.opendata.arcgis.com/datasets/county-boundaries-24k?geometry=-104.657%2C42.025%2C-90.243%2C47.48>

Wurbs, R.A.; & James, W.P. (2014). “Water resources engineering.” Pearson Prentice Hall. Upper Saddle River, NJ. 828 pp.

Xia, X.; Li, Z.; Wang, P.; Cribb, M.; Chen, H.; & Zhao, Y. (2008). “Analysis of relationships between ultraviolet radiation (295–385 nm) and aerosols as well as shortwave radiation in North China Plain.” Atmospheric Geophysics 26: 2043-2052.

Yang, Y.; Leppäranta, M.; Cheng, B.; & Li, Z. (2012) "Numerical Modelling of Snow and Ice Thicknesses in Lake Vanajavesi, Finland." Tellus A: Dynamic Meteorology and Oceanography 64 (1): 17202.

Yu, X.; Driscoll, C. T.; Montesdeoca, M.; Evers, D.; Duron, M.; Williams, K.; Schoch, N.; & Kamman, N. C. (2011). “Spatial patterns of mercury in biota of Adirondack, New York lakes.” Ecotoxicology 20: 1543-1554.

Zhang, D.; Yin, Y.; Li, Y.; Cai, Y.; & Liu, J. (2017). “Critical role of natural organic matter in photodegradation of methylmercury in water: Molecular weight and interactive effects with other environmental factors.” Science of the Total Environment 578: 535-541.

Zhang, H.; & Lindberg, S.E. (2001) “Sunlight and iron(III)-induced photochemical production of dissolved gaseous mercury in freshwater.” Environmental Science and Technology 35 (2): 928-935.

Zhang, H.; Lindberg, S. E.; Marsik, F. J.’ & Keeler, G. J. (2001). “Mercury air/surface exchange kinetics of background soils of the Tahquamenon River watershed in the Michigan Upper Peninsula.” Water, Air, and Soil Pollution 126: 151-169.

Zhang, L.; Wright, L. P.; & Pierrette, B. (2009). “A review of current knowledge concerning dry deposition of atmospheric mercury.” Atmospheric Environment 43: 5853-5864.

Zhang, X.; Rygwelski, K. R.; Rossmann, R.; Pauer, J. J.; & Kreis Jr., R. G. (2008). “Model construct and calibration of an integrated water quality model (LM2-Toxic) for the Lake Michigan Mass Balance Project.” Ecological Modeling 219: 92-106.

Zhang, X.; Rygwelski, K. R.; Kreis Jr., R. G.; & Rossmann, R. (2014). “A mercury transport and fate model (LM2-Mercury) for mass budget assessment of mercury cycling in Lake Michigan.” Journal of Great Lakes Research 40 (2): 347-359.

Zheng, W.; Obrist, D.; Weis, D.; & Berquist, B.A. (2016). “Mercury isotope compositions across North American forests.” Global Biogeochemical Cycles 30: 1475-1492.

Zhu, S.; Zhang, Z.; & Liu, X. (2017). “Enhanced two dimensional hydrodynamic and water quality model (CE-QUAL-W2) for simulating mercury transport and cycling in water bodies.” Water 9 (643). 22 pp.

6 Appendix

Table 6.1. Model parameter values, description, units, and references.

Parameter	Description	Value	Units	Reference
A	Coefficient in total long wave radiation to lake surface calculation	0.5		Chapra 2014
a	Amplitude of DOC concentrations in the inflow to Torch Lake	2	mg L^{-1}	Urban (unpub.)
A[1]	Area of the lake surface	9730000	m^2	Hypsographic curve from Urban (unpub.)
A[2]	Area of the thermocline	8360000	m^2	Hypsographic curve from Urban (unpub.)
A[3]	Area of the surface sediments	8360000	m^2	Hypsographic curve from Urban (unpub.)
$Algae_{inflow}$	Algae concentration in the inflow to Torch Lake		mg L^{-1}	Urban (unpub.)
α[t]	Overall albedo	*		Calculated
α_0[t,n]	Coefficient for calculating light attenuation	*		Calculated; Chapra 2014
α_1[t,n]	Coefficient for calculating light attenuation	*		Calculated; Chapra 2014
α_{snow}	Albedo of ice	0.8		Feng and Stefan 1996
α_{ice}	Albedo of ice	0.75		Feng and Stefan 1996
α_{water}	Albedo of water	0.08		Feng and Stefan 1996
$A_{watershed}$	Area of the watershed (excludes surface area of lake)	188000000	m^2	Calculated using ArcGIS
b	Angular frequency of DOC concentrations in the inflow to Torch Lake	0.0172	day^{-1}	Urban (unpub.)

Parameter	Description	Value	Units	Reference
$BAF_{mixed\ feeders}[1]$	Bioaccumulation factor for mixed feeding fish, 5th percentile	$0.46 \cdot 10^6$	kg L^{-1}	Knightes & Ambrose, 2006a; Knightes 2008
$BAF_{mixed\ feeders}[2]$	Bioaccumulation factor for mixed feeding fish, 25th percentile	$0.95 \cdot 10^6$	kg L^{-1}	Knightes & Ambrose, 2006a; Knightes 2008
$BAF_{mixed\ feeders}[3]$	Bioaccumulation factor for mixed feeding fish, 50th percentile	$1.6 \cdot 10^6$	kg L^{-1}	Knightes & Ambrose, 2006a; Knightes 2008
$BAF_{mixed\ feeders}[4]$	Bioaccumulation factor for mixed feeding fish, 75th percentile	$2.6 \cdot 10^6$	kg L^{-1}	Knightes & Ambrose, 2006a; Knightes 2008
$BAF_{mixed\ feeders}[5]$	Bioaccumulation factor for mixed feeding fish, 95th percentile	$5.4 \cdot 10^6$	kg L^{-1}	Knightes & Ambrose, 2006a; Knightes 2008
$BAF_{piscivorous}[1]$	Bioaccumulation factor for piscivorous fish, 5th percentile	$3.3 \cdot 10^6$	kg L^{-1}	Knightes & Ambrose, 2006a; Knightes 2008
$BAF_{piscivorous}[2]$	Bioaccumulation factor for piscivorous fish, 25th percentile	$5.0 \cdot 10^6$	kg L^{-1}	Knightes & Ambrose, 2006a; Knightes 2008
$BAF_{piscivorous}[3]$	Bioaccumulation factor for piscivorous fish, 50th percentile	$6.8 \cdot 10^6$	kg L^{-1}	Knightes & Ambrose, 2006a; Knightes 2008
$BAF_{piscivorous}[4]$	Bioaccumulation factor for piscivorous fish, 75th percentile	$9.2 \cdot 10^6$	kg L^{-1}	Knightes & Ambrose, 2006a; Knightes 2008
$BAF_{piscivorous}[5]$	Bioaccumulation factor for piscivorous fish, 95th percentile	$14 \cdot 10^6$	kg L^{-1}	Knightes & Ambrose, 2006a; Knightes 2008
c	Phase shift of DOC concentrations in the inflow to Torch Lake	*		Calculated
c_1	Bowen coefficient	0.47	mmHg ^oC-1	Chapra 2014
C:Chla	Carbon to chlorophyll-a concentration in Torch Lake	40	mg C $(mg\ chla)^{-1}$	Urban (unpub.)

Parameter	Description	Value	Units	Reference
$C_{abiotic}[:, 1]$	Abiotic solids concentration in the epilimnion	0.3	mg L^{-1}	Urban (unpub.)
$C_{abiotic}[:, 2]$	Abiotic solids concentration in the hypolimnion	0.3	mg L^{-1}	Urban (unpub.)
$C_{abiotic}[:, 3]$	Abiotic solids concentration in the sediments	0	mg L^{-1}	Urban (unpub.)
$C_{algae}[:, 1]$	Algal (chlorophyll-a) concentrations in the epilimnion	*	mg L^{-1}	Calculated from the algal mass balance
$C_{algae}[:, 2]$	Algal (chlorophyll-a) concentrations in the epilimnion	*	mg L^{-1}	Calculated from the algal mass balance
$C_{algae}[:, 3]$	Algal (chlorophyll-a) concentrations in the epilimnion	0	mg L^{-1}	Urban (unpub.)
$C_{biotic}[:, 1]$	Biotic solids concentration in the epilimnion	*	mg L^{-1}	Calculated from the algal concentrations and the ratio of carbon to chlorophylla concentrations in Torch Lake
$C_{biotic}[:, 2]$	Biotic solids concentration in the hypolimnion	*	mg L^{-1}	Calculated from the algal concentrations and the ratio of carbon to chlorophylla concentrations in Torch Lake
$C_{biotic}[:, 3]$	Biotic solids concentration in the sediments	*	mg L^{-1}	Calculated from the algal concentrations and the ratio of carbon to chlorophylla concentrations in Torch Lake
$C_{DOC}[:, 1]$	DOC concentration in the epilimnion	*	mg L^{-1}	Calculated from the DOC mass balance
$C_{DOC}[:, 2]$	DOC concentration in the hypolimnion	*	mg L^{-1}	Calculated from the DOC mass balance

Parameter	Description	Value	Units	Reference
$C_{DOC}[:, 3]$	DOC concentration in the sediments	40	mg L^{-1}	Cusack & Mihelcic, 1999
C_{dpsed}	Sediment solids ratio in the deep sediments	1560000	mg L^{-1}	Calculated based on the porosity and bulk density
$C_{phosphorus}$	Phosphorus concentration in Torch Lake	5	µg L^{-1}	Mcdonald & Urban 2009; Massey 1970
$C_{sed}[:, 3]$	Sediment solids ratio in the surface sediments	111111	mg L^{-1}	Calculated based on the porosity and bulk density
$c_{p,w}$	Specific heat of water	4.184	J ^oC	
D	Detritus solids concentrations in Torch Lake	0.09	mg L^{-1}	Urban (unpub.)
$DOC_{inflow}[t]$	DOC concentration in the inflow to Torch Lake	*	mg L^{-1}	Calculated
DOC_{inflow}	Average DOC concentration in the inflow to Torch Lake	7	mg L^{-1}	Urban (unpub.)
dt	Time step	1	day	
$D_w[:, 1]$	Aqueous diffusivity coefficient for elemental mercury	*	cm^2 s^{-1}	Calculated; Kuss 2009
$D_w[:, 1]$	Aqueous diffusivity coefficient for elemental mercury	*	m^2 day^{-1}	Calculated by converting D'_w units
$D_w[:, 2]$	Aqueous diffusivity coefficient for divalent mercury	*	m^2 day^{-1}	Calculated by converting D'_w units
$D_w[:, 3]$	Aqueous diffusivity coefficient for methyl mercury	$5.27 \cdot 10^{-5}$	m^2 day^{-1}	Knightes & Ambrose, 2006a; Knightes 2008
$e_{air}[t]$	Vapor pressure of air	*	mmHg	Calculated; Chapra 2014
ϵ	Emissivity of water	0.97		Chapra 2014
$e_{sat}[t]$	Saturated vapor pressure	*	mmHg	Calculated; Chapra 2014
f[t]	Photoperiod (fraction of the day sunlight is present)	*		Calculated; Chapra 2014
$f_{abiotic}[t, :]$	Fraction of mercury partitioned to abiotic solids	*		Calculated

Parameter	Description	Value	Units	Reference
$f_{biotic}[t, :]$	Fraction of mercury partitioned to biotic solids	*		Calculated
$f_{ddp}[t]$	Coefficient for correction of dry deposition of mercury for accumulation on ice	*		Calibrated
$f_{dissolved}[t, :]$	Fraction of mercury dissolved	*		Calculated
$f_{DOC}[t, :]$	Fraction of mercury partitioned to DOC	*		Calculated
$f_{SW, PAR}$	PAR fraction of shortwave radiation	0.50		Xia et al. 2008
$f_{SW, UVB}$	PAR fraction of shortwave radiation	0.04		Xia et al. 2008
$f_{particulate}[t, :]$	Fraction of mercury partitioned to particulate solids	*		Calculated as the sum of abioitic and biotic partitioned mercury
$f_{THg,wdp}[1]$	Elemental mercury fraction of total mercury wet deposition	0		Baker and Bash 2012; Downs et al. 1998
$f_{THg,wdp}[2]$	Divalent mercury fraction of total mercury wet deposition	0.985		Hall et al., 2005
$f_{THg,wdp}[3]$	Methyl mercury fraction of total mercury wet deposition	0.015		Hall et al., 2005
$f_{watershed,wetland}$	Fraction of the watershed that is wetlands	0.1365		Calculated using ArcGIS
γ	Parameter describing the steepest slope of the relationship between air and inflow temperature	0.25		Mohseni et al. 1998; Mohseni et al. 2003
H[1]	Thickness of the Epilimnion layer in Torch Lake	10	m	Hypsographic curve from Urban (unpub.)
H[2]	Thickness of the Hypolimnion layer in Torch Lake	6.6	m	Hypsographic curve from Urban (unpub.)

Parameter	Description	Value	Units	Reference
H[3]	Thickness of the surface sediments layer	0.01	m	McDonald & Urban, 2007
$Hg_{atm}[1]$	Elemental mercury concentration in the atmosphere	$1.5 \cdot 10^{-9}$	mg L^{-1}	Zhang et al., 2001
$Hg_{atm}[2]$	Divalent mercury concentration in the atmosphere	$1.3 \cdot 10^{-11}$	mg L^{-1}	Zhu et al., 2016; Gustin & Jaffe, 2010
$Hg_{atm}[3]$	Methyl mercury concentration in the atmosphere	$2.0 \cdot 10^{-12}$	mg L^{-1}	Fitzgerald et al., 1991; Watras et al., 1994
$Hg_{atm}[4]$	Particulate mercury concentration in the atmosphere	$2.5 \cdot 10^{-11}$	mg L^{-1}	Zhu et al., 2016; Gustin & Jaffe, 2010
$Hg_{dpsed}[1]$	Elemental mercury concentration in the deep sediments	0	mg L^{-1}	Kerfoot et al., 2016
$Hg_{dpsed}[2]$	Divalent mercury concentration in the deep sediments	0.3	mg L^{-1}	Kerfoot et al., 2016
$Hg_{dpsed}[3]$	Methyl mercury concentration in the deep sediments	0.00056	mg L^{-1}	Kerfoot et al., 2016
Hg_{fish}	Mercury concentration in fish	*	ppm	Calculated; Knightes & Ambrose 2006a; Knightes 2008
$H_{precipitation}[t]$	Precipitation to Torch Lake	*	m^3 day^{-1}	Weather Underground
$I_0[t]$	Uncorrected radiation at the surface of the lake compartment	*	J m^{-2} day^{-1}	Michigan Technological University Keweenaw Research Center
$I_a[t,n]$	Average daylight intensity	*	J m^{-2} day^{-1}	Calculated
I_s	Saturated light intensity	4200000	J m^{-2} day^{-1}	Chapra 2014
$I_{surface}[t]$	Amount of radiation that is received through the surface to the lake water column	*	J m^{-2} day^{-1}	Calculated
J[t]	Total surface heat flux	*	J m^{-2} day^{-1}	Calculated; Chapra 2014

Parameter	Description	Value	Units	Reference
$J_{cond}[t]$	Surface heat flux from net conduction and convection	*	J m^{-2} day^{-1}	Calculated; Chapra 2014
$J_{evap}[t]$	Surface heat flux from net evaporation and condensation	*	J m^{-2} day^{-1}	Calculated; Chapra 2014
$J_{LW\ total}[t]$	Total incoming longwave radiation to the lake surface	*	J m^{-2} day^{-1}	Calculated; Chapra 2014
$J_{LW\ reflect}[t]$	Longwave radiation reflected back from the total longwave radiation to the lake surface	*	J m^{-2} day^{-1}	Calculated; Chapra 2014
$J_{SW}[t]$	Shortwave radiation	*	J m^{-2} day^{-1}	Michigan Technological University Keweenaw Research Center
K[t, :, :]	Overall process rate for mercury species	*	day^{-1}	Calculated
$K_{awxc}[t, :, :]$	Process rates for air-water exchange of mercury from the lake (volitalization)	*	day^{-1}	Calculated
$K_{bur}[t, :, :]$	Process rates for burial of mercury from the surface sediments to the deep sediments	*	day^{-1}	Calculated
$K_{d,abiotic}[1]$	Abiotic partitioning coefficient for elemental mercury	0	L mg^{-1}	Knightes & Ambrose, 2006a; Knightes 2008
$K_{d,abiotic}[2]$	Abiotic partitioning coefficient for divalent mercury	0.5	L mg^{-1}	Knightes & Ambrose, 2006a; Knightes 2008
$K_{d,abiotic}[3]$	Abiotic partitioning coefficient for methyl mercury	0.3	L mg^{-1}	Knightes & Ambrose, 2006a; Knightes 2008
$K_{d,biotic}[1]$	Biotic partitioning coefficient for elemental mercury	0	L mg^{-1}	Knightes & Ambrose, 2006a; Knightes 2008
$K_{d,biotic}[2]$	Biotic partitioning coefficient for divalent mercury	0.9	L mg^{-1}	Knightes & Ambrose, 2006a; Knightes 2008
$K_{d,biotic}[3]$	Biotic partitioning coefficient for methyl mercury	0.6	L mg^{-1}	Knightes & Ambrose, 2006a; Knightes 2008

Parameter	Description	Value	Units	Reference
$K_{d,DOC}[1]$	DOC partitioning coefficient for elemental mercury	0	L mg^{-1}	Knightes & Ambrose, 2006a; Knightes 2008
$K_{d,DOC}[2]$	DOC partitioning coefficient for divalent mercury	0.2	L mg^{-1}	Knightes & Ambrose, 2006a; Knightes 2008
$K_{d,DOC}[3]$	DOC partitioning coefficient for methyl mercury	0.1	L mg^{-1}	Knightes & Ambrose, 2006a; Knightes 2008
$K_{d,sed}[1]$	Sediment partitioning coefficient for elemental mercury	0	L mg^{-1}	Knightes & Ambrose, 2006a; Knightes 2008
$K_{d,sed}[2]$	Sediment partitioning coefficient for divalent mercury	0.08	L mg^{-1}	Knightes & Ambrose, 2006a; Knightes 2008
$K_{d,sed}[3]$	Sediment partitioning coefficient for methyl mercury	0.008	L mg^{-1}	Knightes & Ambrose, 2006a; Knightes 2008
$K_{dmth}[t, :, :]$	Process rates for demethylation of methyl to divalent mercury	*	day^{-1}	Calculated
$k_{dmth,ref}[1]$	Demethylation rate at reference temperature in the epilimnion	37.4	day^{-1}	Calibrated
$k_{dmth,ref}[2]$	Demethylation rate at reference temperature in the hypolimnion	37.4	day^{-1}	Calibrated
$k_{dmth,ref}[3]$	Demethylation rate at reference temperature in the sediments	13.2	day^{-1}	Calibrated
$K_{dpdf}[t, :, :]$	Process rates for mercuy from the surface to deep sediments due to sediment pore water diffusion	*	day^{-1}	Calculated
$k_e[t,n]$	Overall light extinction coefficient for the water column	*	m^{-1}	Calculated
$k_{e,ice}$	Light extinction coefficient from ice	1.5	m^{-1}	Feng and Stefan 1996

Parameter	Description	Value	Units	Reference
$k'_{e,PAR}[t,n]$	Overall light extinction coefficient for PAR in Torch Lake compartments without affects from algae in the water	*	m^{-1}	Calculated; Chapra 2014
$k_{e,PAR}[t,n]$	Overall light extinction coefficient for PAR in Torch Lake compartments	*	m^{-1}	Calculated; Chapra 2014
$k_{e,snow}$	Light extinction coefficient from snow	40	m^{-1}	Feng and Stefan 1996
$k_{e,UVB}[t,n]$	Overall light extinction coefficient for UVB in Torch Lake compartments	*	m^{-1}	Calculated; Morris et al. 1995
k_{ew}	Light extinction coefficient of particle free water and color	0.48	m^{-1}	Chapra 2014
$k_{growth,ref}$	Reference growth rate for algae	0.52	day^{-1}	Chapra 2014; McDonald & Urban 2009
$K'_{Henry}[t]$	Henry's law coefficient for mercury	*		Calculated; Gardfeldt 2003
$K_{Henry}[t]$	Henry's law coefficient for mercury	*	atm	Calculated; Sanemasa 1975
$K_{meth}[t, :, :]$	Process rates for methylation of divalent to methyl mercury	*	day^{-1}	Calculated
$k_{meth,ref}[1]$	Methylation rate at reference temperature in the epilimnion	4.66	day^{-1}	Calibrated
$k_{meth,ref}[2]$	Methylation rate at reference temperature in the hypolimnion	4.66	day^{-1}	Calibrated
$k_{meth,ref}[3]$	Methylation rate at reference temperature in the sediments	0.453	day^{-1}	Calibrated
$k_{mortality,ref}$	Reference mortality rate for algae	0.052	day^{-1}	Chapra 2014; McDonald & Urban 2009

Parameter	Description	Value	Units	Reference
$K_{outf}[t, :, :]$	Process rates for outflow of mercury from the lake	*	day^{-1}	Calculated
$K_{oxid}[t, :, :]$	Process rates for oxidation of elemental to divalent mercury	*	day^{-1}	Calculated
$k_{oxid,ref}[1]$	Oxidation rate at reference temperature in epilimnion	35	day^{-1}	Calibrated
$k_{oxid,ref}[2]$	Oxidation rate at reference temperature in hypolimnion	35	day^{-1}	Calibrated
$k_{oxid,ref}[3]$	Oxidation rate at reference temperature in sediments	65.2	day^{-1}	Calibrated
$K_{phdm}[t, :, :]$	Process rates for photodemethylation of methyl to elemental mercury	*	day^{-1}	Calculated
$k_{phdm,ref}[:]$	Photodemethylation rate at referenced light attenuation for PAR	$1.0 \cdot 10^{-9}$	$m^2\ J^{-1}\ day^{-1}$	Calibrated
$K_{redn}[t, :, :]$	Process rates for reduction of divalent to elemental mercury	*	day^{-1}	Calculated
$k_{redn,ref}[1]$	Reduction rate at reference temperature in epilimnion	1.99	day^{-1}	Calibrated
$k_{redn,ref}[2]$	Reduction rate at reference temperature in hypolimnion	1.99	day^{-1}	Calibrated
$k_{redn,ref}[3]$	Reduction rate at reference temperature in sediments	4.46	day^{-1}	Calibrated
$K_{resp}[t, :, :]$	Process rates for resuspension of mercury in the sediments to the hypolimnion	*	day^{-1}	Calculated

Parameter	Description	Value	Units	Reference
$K_{setl}[t, :, :]$	Process rates for settling of mercury in the epilimnion to hypolimnion and hypolimnion to sediments	*	day^{-1}	Calculated
$K_{SP,phosphorus}$	Half saturation constant for phosphorus	1	$\mu g\ L^{-1}$	Mcdonald & Urban 2009; Massey 1970
$K_{ssdf}[t, :, :]$	Process rates for mercury in the hypolimnion to and from the sediments due to sediment pore water diffusion	*	day^{-1}	Calculated
$K_{thdp}[t, :, :]$	Process rates for mercury in epilimnion to and from the hypolimnion due to thermocline dispersion	*	day^{-1}	Calculated
$L_e[t]$	Latent heat of water vaporization	*	$cal\ g^{-1}$	Calculated; Chapra 2014
$MeHg_{lake}$	Average annual methyl mercury concentration in the water column	*	$mg\ L^{-1}$	Calculated
$\mu_{H2O}[t]$	Dynamic viscosity of water	*	$g\ cm^{-1}\ s^{-1}$	Calculated; Crittenden et al. 2012
MW_{CO2}	Molecular weight of carbon dioxide	44.01	$g\ mol^{-1}$	
MW_{H2O}	Molecular weight of water	18.015	$g\ mol^{-1}$	
MW_{Hg0}	Molecular weight of elemental mercury	200.59	$g\ mol^{-1}$	
N	Non-volatile solids concentration in Torch Lake	0.47	$mg\ L^{-1}$	Urban (unpub.)
$Q_{inflow}[t]$	Runoff to Torch Lake	*	$m^3\ day^{-1}$	Calculated from Trap Rock River gauging station (USGS 2015)
$Q_{evaporation}[t]$	Evaporation from Torch Lake	*	$m^3\ day^{-1}$	Calculated; Chapra 2014
$Q_{outflow}[t]$	Outflow from Torch Lake	*	$m^3\ day^{-1}$	Calculated

Parameter	Description	Value	Units	Reference
$\Phi_{light}[t,n]$	Light attenuation	*	J m^{-2}	Calculated; Chapra 2014
$\Phi_{nutrients}$	Growth factor for algae due to nutrients	0.833		Calculated; Chapra 2014
$\Phi_{PAR}[t,n]$	Light attenuation for PAR	*	J m^{-2}	Calculated; Chapra 2014
ϕ_{ssed}	Porosity of the surface sediment layer	0.9		McDonald & Urban, 2007
ϕ_{dpsed}	Porosity of the deep sediment layer	0.5		McDonald & Urban, 2007
R	Ideal gas law constant	$8.21 \cdot 10^{-5}$	atm m^3 mol^{-1} K^{-1}	
$RC_{upland}[:]$	Upland runoff coefficient for all mercury species	0.05		Perlinger et al. 2018
$RC_{wetland}[2]$	Wetland runoff coefficient for methyl mercury	0.2		Knightes & Ambrose, 2006a; Knightes 2008
$RC_{wetland}[3]$	Wetland runoff coefficient for methyl mercury	4.9		Knightes & Ambrose, 2006a; Knightes 2008
ρ_{bulk}	Bulk density of the surface sediments	100000	mg L^{-1}	McDonald & Urban, 2007
$\rho_{H2O}[t]$	Density of water	*	g cm^{-3}	Calculated; Crittenden et al. 2012
ρ_w	Density of water	1	g cm^3	
R_L	Reflection coefficient of the lake surface	0.03		Chapra 2014
$SC_{Hg0}[t]$	Schmidt number for elemental mercury	*		Calculated; Wanninkhof 1992
$SC_{CO2}[t]$	Schmidt number for carbon dioxide	*		Calculated; Wanninkhof 2014
σ	Stefan-Boltzman constant	$4.9 \cdot 10^{-3}$	J m^{-2} day^{-1} K^{-4}	Chapra 2014
sw	Snow water equivalent	0.40		Urban (unpub.)
t	time	*	day	
T[t,1]	Temperature of the epilimnion	*	^oC	Calculated using the heat budget
T[t,2]	Temperature of the hypolimnion	*	^oC	Calculated using the heat budget

Parameter	Description	Value	Units	Reference
$T[t,3]$	Temperature of the sediments	*	^oC	Set equal to the temperature of the hypolimnion
θ	Temperature adjustment coefficient for mercury reaction rates	1.06		Calibrated; Mohseni et al., 1998; Mohseni et al., 2003
θ_g	Temperature adjustment coefficient for growth rate of algae	1.00		Calibrated
θ_m	Temperature adjustment coefficient for mortality rate of algae	1.07		Calibrated
$T_{air}[t]$	Temperature of the air	*	^oC	Weather Underground
$T_{air,inflect}[t]$	Temperature of the air at the inflection point of the inflow temperature as a function of the air temperature	10	^oC	Calibrated
$T_{dew\ pt}[t]$	Dew point temperature	*	^oC	Weather Underground
$t_{DOC\ peak}$	Day of the year for peak DOC concentrations	130	days	Calibrated
$T_{inflow}[t]$	Temperature of the inflow	*	^oC	Calculated; Mohseni et al. 1998; Mohseni et al. 2003
$T_{inflow,max}[t]$	Temperature of the inflow, minimum	0	^oC	Calibrated
$T_{inflow,min}[t]$	Temperature of the inflow, maximum	20	^oC	Calibrated
T_p	Daily period	24	hrs	
t_r	Time of the sunrise	*	hrs	U.S. Naval Observatory 2015
T_{ref}	Reference temperature for mercury reactions	20	^oC	Calibrated
$T_{ref,g}$	Reference temperature for growth of algae	20	^oC	Calibrated

Parameter	Description	Value	Units	Reference
$T_{ref,m}$	Reference temperature for mortality of algae	22	^{o}C	Calibrated
t_s	Time of the sunset	*	hrs	U.S. Naval Observatory 2015
$\nu_{H2O}[t]$	Kinematic viscosity of water	*	$cm^2\ s^{-1}$	Calculated as a ratio of the dynamic viscosity to density of water
$U_{w,7m}[t]$	Wind speed at 7 m above Torch Lake's surface	*	$m\ s^{-1}$	Calculated; Manwell et al. 2009
$U_{w,10m}[t]$	Wind speed at 10 m above Torch Lake's surface	*	$m\ s^{-1}$	Michigan Technological University Keweenaw Research Center
V[1]	Volume of the epilimnion	84600000	m^3	Hypsographic curve from Urban (unpub.)
V[2]	Volume of the hypolimnion	57800000	m^3	Hypsographic curve from Urban (unpub.)
V[3]	Volume of the surface sediments	83600	m^3	Hypsographic curve from Urban (unpub.)
$v_a[t]$	Air-side mass transfer velocity for elemental mercury	*	$m\ day^{-1}$	Calculated; Hornbuckle 1994; Smith 1980
$v_{a,H2O}[t]$	Air-side mass transfer velocity for water	*	$m\ day^{-1}$	Calculated; Hornbuckle 1994; Schwarzenbach 1993
$v_{awxc}[t]$	Air-water exchange velocity for elemental mercury	*	$m\ day^{-1}$	Calculated; Whitman 1923
v_{burl}	Burial velocity	$9.5 \cdot 10^{-7}$	$m\ day^{-1}$	Barkach & McCauely, 2006
$v_{ddeps}[1]$	Dry deposition velocity to the lake surface for elemental mercury (parameterized using air-water exchange instead)	0	$m\ day^{-1}$	Calibrated

Parameter	Description	Value	Units	Reference
$v_{ddeps}[2]$	Dry deposition velocity to the lake surface for divalent mercury	35	m day^{-1}	Calibrated
$v_{ddeps}[3]$	Dry deposition velocity to the lake surface for methyl mercury	1	m day^{-1}	Calibrated
$v_{ddeps}[4]$	Dry deposition velocity to the lake surface for particulate mercury	10	m day^{-1}	Calibrated
$v_{ddepc}[1]$	Dry deposition velocity to the watershed (vegetation) for elemental mercury	25	m day^{-1}	Zhang et al., 2009
$v_{ddepc}[2]$	Dry deposition velocity to the watershed (vegetation) for divalent mercury	350	m day^{-1}	Rea et al., 2000; Zhang et al., 2009
$v_{ddepc}[3]$	Dry deposition velocity to the watershed (vegetation) for methyl mercury	10	m day^{-1}	Rea et al., 2000; Zhang et al., 2009
$v_{ddepc}[4]$	Dry deposition velocity to the watershed (vegetation) for particulate mercury	100	m day^{-1}	Calibrated
v_{resp}	Resuspension velocity	$2.4 \cdot 10^{-7}$	m day^{-1}	Calculated from burial and settling velocity
v_{setl}	Settling velocity	0.9	m day^{-1}	Barkach & McCauely, 2006
$v_{setl,algae}$	Settling velocity for algae	0.5	m day^{-1}	Chapra 2014; McDonald & Urban 2009
v_{thdp}	Thermocline dispersion velocity	*	m day^{-1}	Calibrated
$v_w[t]$	Water-side mass transfer velocity for elemental mercury	*	m day^{-1}	Calculated; Hornbuckle 1994; Wanninkhoff 1992

Parameter	Description	Value	Units	Reference
$v_{w,CO2}[t]$	Water-side mass transfer velocity for carbon dioxide	*	m day^{-1}	Calculated; Hornbuckle 1994; Wanninkhoff 1992; Poissant 2000
W[t, :]	Total loading to mercury species	*	mg L^{-1} day^{-1}	Calculated
$W_{awxc}[t, :]$	Loading of mercury from air-water exchange	*	mg L^{-1} day^{-1}	Calculated
$W_{ddpc}[t, :]$	Loading of mercury from total dry deposition from watershed runoff to the lake	*	mg L^{-1} day^{-1}	Calculated
$W_{ddps}[t, :]$	Loading of mercury from total dry deposition to the lake surface	*	mg L^{-1} day^{-1}	Calculated
$W_{ddpT}[t, :]$	Loading of mercury from total dry deposition to the lake surface and from watershed runoff to the lake	*	mg L^{-1} day^{-1}	Calculated
$W_{dpdf}[t, :]$	Load of mercury to the surface sediments from the deep sediments due to sediment pore water diffusion	*	mg L^{-1} day^{-1}	Calculated
$W_{inflow}[t, :]$	Loading of mercury from inflow to Torch Lake	*	mg L^{-1} day^{-1}	Calculated
$W_{wdpc}[t, :]$	Loading of mercury from total wet deposition from watershed runoff to the lake	*	mg L^{-1} day^{-1}	Calculated
$W_{wdps}[t, :]$	Loading of mercury from total wet deposition to the lake surface	*	mg L^{-1} day^{-1}	Calculated

Parameter	Description	Value	Units	Reference
$W_{wdpT}[t, :]$	Loading of mercury from total wet deposition to the lake surface and from watershed runoff to the lake	*	mg L^{-1} day^{-1}	Calculated
z*	Surface roughness length over a lake with open water	0.001	m	Manwell et al. 2009
$z_{ice\ max}$	Maximum thickness of the ice	1	m	Calibrated
z_{snow}	Snow to Torch Lake	*	m	Calculated from precipitation and the snow water pack content
z_{ssed}	Thickness of the surface sediment diffusivity layer	0.005	m	McDonald & Urban, 2007
z_{dpsed}	Thickness of the deep sediment diffusivity layer	0.1	m	McDonald & Urban, 2007
$z_{water}[1]$	Depth to the bottom of the epilimion layer in Torch Lake	10	m	Hypsographic curve from Urban (unpub.)
$z_{water}[2]$	Depth to the bottom of the hypolimnion layer in Torch Lake	6.6	m	Hypsographic curve from Urban (unpub.)

*indicates a variable that changes with respect to time.

Table 6.2. Sensitivity results for all parameters expressed as the percent change in mercury concentrations.

Model Parameter	Change in Mercury Concentrations with Change in Model Parameter Value (%)								
	Hg0, Ep.	**Hg0, Hyp.**	**Hg0, Sed.**	**Hg2, Ep.**	**Hg2, Hyp.**	**Hg2, Sed.**	**MeHg, Ep.**	**MeHg, Hyp.**	**MeHg, Sed.**
Area of Watershed	7.0	6.8	5.8	7.0	6.8	5.8	7.0	6.8	6.2
Area of Lake Surface	-1.8	1.3	1.2	-1.7	1.3	1.2	-1.7	1.3	1.2
Area of Thermocline	-2.5	-4.6	3.3	-2.4	-4.6	3.3	-2.5	-4.6	3.6
Area of Sediments	0.7	0.9	-6.4	0.7	0.9	-5.9	0.7	0.9	-3.1
Volume of Epilimnion	0.3	-0.1	-0.2	0.3	-0.1	-0.2	0.3	-0.1	-0.1
Volume of Hypolimnion	0.1	-0.3	-0.3	0.1	-0.3	-0.3	0.1	-0.3	-0.3
Volume of Sediments	-0.3	-0.4	-0.4	-0.3	-0.4	-0.9	-0.3	-0.4	-4.0
Wetland to Watershed Ratio	2.3	2.2	1.9	2.3	2.2	1.9	2.3	2.2	2.0
Surface Sed. Diffusivity Layer Thickness	-1.7	-2.3	2.6	-1.7	-2.3	2.1	-1.7	-2.3	0.3
Deep Sed. Diffusivity Layer Thickness	0.0	0.0	0.1	0.0	0.0	0.1	0.0	0.0	0.1
Surface Sed. Porosity	1.8	2.4	-2.7	1.8	2.3	-2.2	1.8	2.3	-0.3
Deep Sed. Porosity	0.0	-0.1	-0.1	0.0	-0.1	-0.1	0.0	-0.1	-0.1
Burial Velocity	-1.2	-1.6	-3.4	-1.2	-1.6	-3.4	-1.2	-1.6	-2.7
Settling Velocity	-4.5	-2.7	5.1	-4.5	-2.7	5.2	-4.5	-2.7	5.5
Resuspension Velocity	0.2	0.3	-0.3	0.2	0.3	-0.3	0.2	0.3	-0.1
Hg2 Deep Sed. Conc.	0.0	0.1	0.1	0.0	0.1	0.1	0.0	0.1	0.1
MeHg Deep Sed. Conc.	0.0	0.0	0.0	0.0	0.0	0.0	0.0	0.0	0.0

Model Parameter	Change in Mercury Concentrations with Change in Model Parameter Value (%)								
	Hg0, Ep.	**Hg0, Hyp.**	**Hg0, Sed.**	**Hg2, Ep.**	**Hg2, Hyp.**	**Hg2, Sed.**	**MeHg, Ep.**	**MeHg, Hyp.**	**MeHg, Sed.**
Biotic Solids Conc., Ep.	-0.3	0.3	0.3	-0.2	0.3	0.3	-0.2	0.3	0.3
Biotic Solids Conc., Hyp.	-0.5	-0.8	0.5	-0.5	-0.7	0.5	-0.5	-0.7	0.6
Abiotic Solids Conc., Ep.	-1.5	1.2	1.1	-1.0	1.3	1.1	-1.0	1.3	1.1
Abiotic Solids Conc., Hyp.	-2.3	-3.7	3.0	-2.3	-3.1	3.0	-2.3	-3.2	3.3
DOC Conc., Ep.	-3.0	0.3	0.2	2.4	0.3	0.2	-3.2	0.3	0.2
DOC Conc., Hyp.	1.8	-2.5	-2.3	1.8	2.9	-2.3	1.8	-2.7	-4.0
DOC Conc., Sed.	0.0	0.0	0.0	0.0	0.0	0.0	0.0	0.0	-7.1
Solids Ratio in Surface Sed.	-2.0	-2.7	-6.5	-2.0	-2.7	2.8	-2.0	-2.7	4.4
Solids Ratio in Deep Sed.	0.0	-0.1	-0.1	0.0	-0.1	-0.1	0.0	-0.1	-0.1
Abiotic Partitioning Coef., Hg2	-3.7	-2.4	3.9	-3.1	-1.8	4.0	-3.7	-2.4	1.4
Abiotic Partitioning Coef., MeHg	-0.2	-0.1	0.2	-0.2	-0.1	0.2	0.3	0.4	3.2
Biotic Partitioning Coef., Hg2	-0.8	-0.4	0.8	-0.7	-0.3	0.8	-0.8	-0.4	0.3
Biotic Partitioning Coef., MeHg	0.0	0.0	0.0	0.0	0.0	0.0	0.1	0.1	0.6

Model Parameter	Change in Mercury Concentrations with Change in Model Parameter Value (%)								
	Hg0, Ep.	**Hg0, Hyp.**	**Hg0, Sed.**	**Hg2, Ep.**	**Hg2, Hyp.**	**Hg2, Sed.**	**MeHg, Ep.**	**MeHg, Hyp.**	**MeHg, Sed.**
DOC Partitioning Coef., Hg2	-1.3	-2.3	-2.0	4.2	3.1	-2.0	-1.3	-2.3	-2.1
DOC Partitioning Coef., MeHg	0.1	0.0	-0.1	0.1	0.0	-0.1	-0.2	-0.2	-8.7
Aqueous Diffusivity Coef., Hg2	0.7	1.4	-3.5	0.8	1.4	-3.0	0.8	1.4	-1.2
Aqueous Diffusivity Coef., MeHg	0.0	0.0	0.0	0.0	0.0	0.0	0.0	0.0	0.0
Atmospheric Conc., Hg0	4.2	4.2	3.6	4.2	4.2	3.6	4.2	4.2	3.8
Atmospheric Conc., Hg2	0.5	0.5	0.4	0.5	0.5	0.4	0.5	0.5	0.4
Atmospheric Conc., HgP	0.3	0.3	0.2	0.3	0.3	0.2	0.3	0.3	0.2
Atmospheric Conc., MeHg	0.0	0.0	0.0	0.0	0.0	0.0	0.0	0.0	0.0
Wet Dep., THg	4.1	3.9	3.3	4.1	3.9	3.3	4.1	3.9	3.5
MeHg to THg Ratio in Wet Dep.	0.3	0.3	0.2	0.3	0.3	0.2	0.3	0.3	0.3
Dry Dep. Velocity to Water, RGM	0.0	0.0	0.0	0.0	0.0	0.0	0.0	0.0	0.0
Dry Dep. Velocity to Water, HgP	0.0	0.0	0.0	0.0	0.0	0.0	0.0	0.0	0.0
Dry Dep. Velocity to Water, MeHg	0.0	0.0	0.0	0.0	0.0	0.0	0.0	0.0	0.0

Model Parameter	Change in Mercury Concentrations with Change in Model Parameter Value (%)								
	Hg0, Ep.	**Hg0, Hyp.**	**Hg0, Sed.**	**Hg2, Ep.**	**Hg2, Hyp.**	**Hg2, Sed.**	**MeHg, Ep.**	**MeHg, Hyp.**	**MeHg, Sed.**
Dry Dep. Velocity to Land, Hg0	3.8	3.7	3.2	3.8	3.7	3.2	3.8	3.7	3.4
Dry Dep. Velocity to Land, RGM	0.5	0.5	0.4	0.5	0.5	0.4	0.5	0.5	0.4
Dry Dep. Velocity to Land, HgP	0.3	0.2	0.2	0.3	0.2	0.2	0.3	0.2	0.2
Dry Dep. Velocity to Land, MeHg	0.0	0.0	0.0	0.0	0.0	0.0	0.0	0.0	0.0
Runoff Coef., Upland	4.1	4.0	3.4	4.1	4.0	3.4	4.1	4.0	3.6
Runoff Coef., Wetland Hg2	2.6	2.5	2.1	2.6	2.5	2.1	2.6	2.5	2.3
Runoff Coef., Wetland MeHg	0.3	0.3	0.3	0.3	0.3	0.3	0.3	0.3	0.3
Oxidation Rate, Water	-6.9	-7.1	1.7	2.3	2.2	1.8	2.3	2.2	1.9
Oxidation Rate, Sed.	-0.1	-0.2	-8.4	-0.1	-0.1	0.2	-0.1	-0.1	0.0
Reduction Rate, Water	7.3	7.4	-1.8	-2.4	-2.3	-1.9	-2.4	-2.3	-2.1
Reduction Rate, Sed.	0.1	0.2	9.7	0.1	0.2	-0.2	0.1	0.2	0.0
Methylation Rate, Water	-0.3	-0.3	0.0	-0.3	-0.3	0.0	9.6	9.6	3.9
Methylation Rate, Sed.	0.0	0.0	0.0	0.0	0.0	0.0	0.0	0.0	5.9
Demethylation Rate, Water	0.3	0.3	0.0	0.3	0.3	0.0	-8.8	-8.8	-3.6
Demethylation Rate, Sed.	0.0	0.0	0.0	0.0	0.0	0.0	0.0	0.0	-8.8
Photode-methylation Rate	0.0	0.0	0.0	0.0	0.0	0.0	0.0	0.0	0.0

Model Parameter	Change in Mercury Concentrations with Change in Model Parameter Value (%)								
	Hg0, Ep.	**Hg0, Hyp.**	**Hg0, Sed.**	**Hg2, Ep.**	**Hg2, Hyp.**	**Hg2, Sed.**	**MeHg, Ep.**	**MeHg, Hyp.**	**MeHg, Sed.**
Temp., Ep.	0.3	0.4	-0.6	0.3	0.4	-0.5	0.3	0.4	-0.1
Temp., Hyp.	0.0	0.0	0.0	0.0	0.0	0.0	0.0	0.0	0.0
Temp., Sed.	0.0	0.0	0.2	0.0	0.0	0.0	0.0	0.0	-1.1
Outflow	-3.4	-3.3	-2.8	-3.4	-3.3	-2.8	-3.4	-3.3	-3.0
Thermocline Dispersion Velcoity	0.6	-0.6	-0.5	0.6	-0.6	-0.5	0.6	-0.6	-0.5
Wind Speed	-3.2	-2.9	-2.4	-3.2	-2.9	-2.4	-3.2	-2.9	-2.6
PAR Attenuation, Ep.	0.0	0.0	0.0	0.0	0.0	0.0	0.0	0.0	0.0
PAR Attenuation, Hyp.	0.0	0.0	0.0	0.0	0.0	0.0	0.0	0.0	0.0

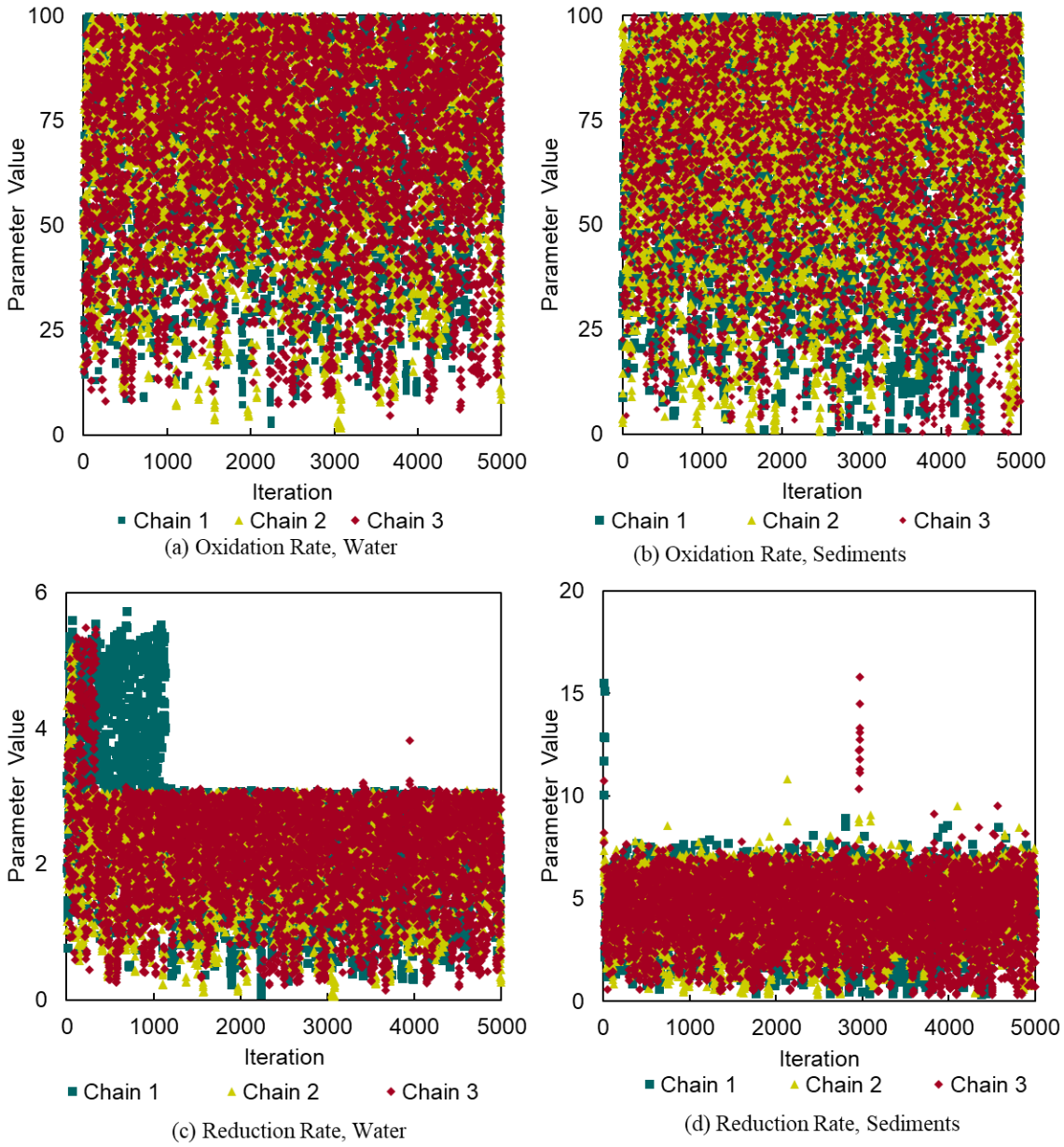

Figure 6.1. Trace plots for model parameters reduction and oxidation in the water and sediments as a function of the number of iterations.

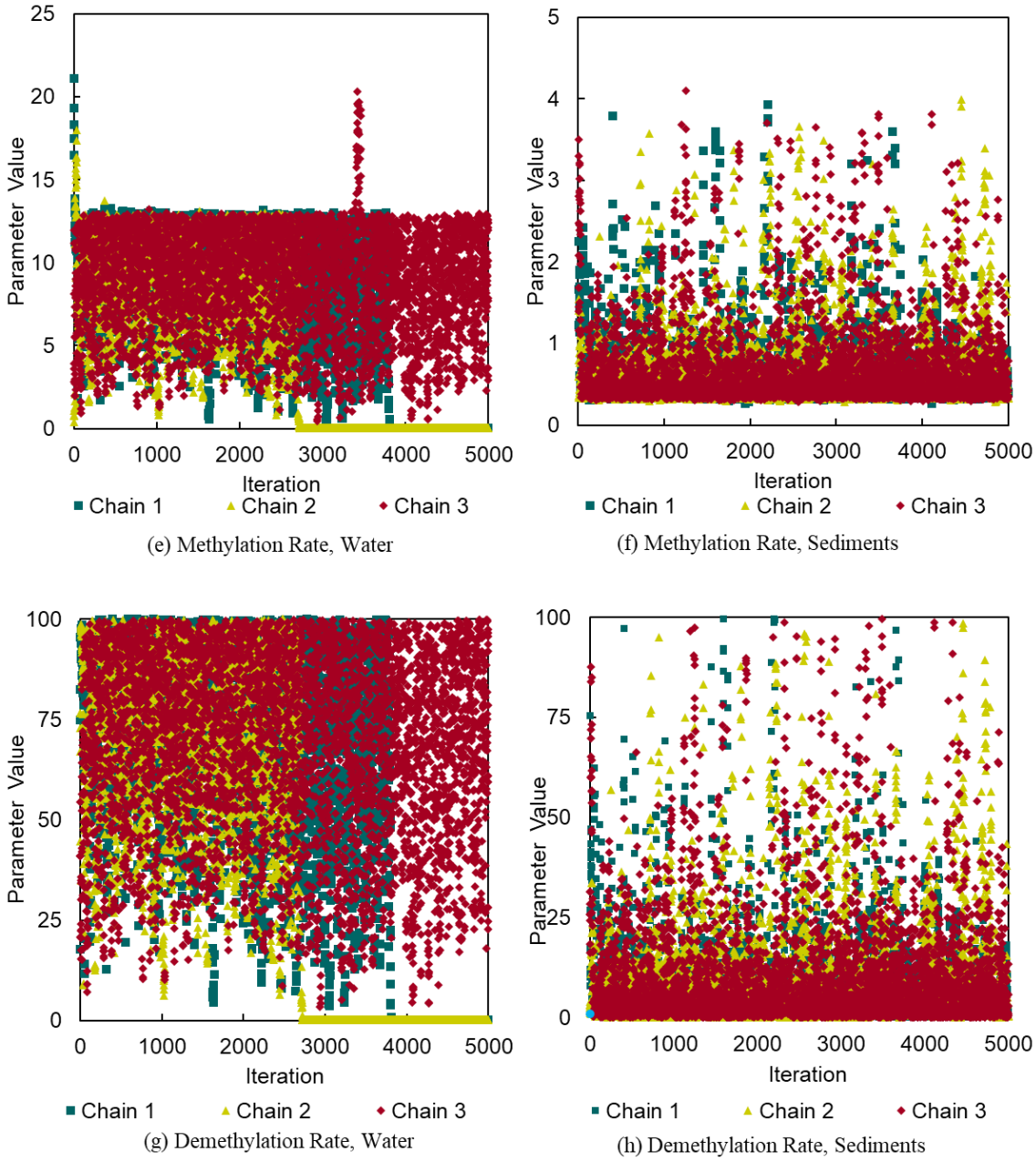

Figure 6.2. Trace plots for model parameters methylation and demethylation in water and sediments as a function of the number of iterations.